NUMERICAL STUDY OF DEFORMATION MECHANISMS IN HCP METALS

NUMERICAL STUDY OF DEFORMATION MECHANISMS IN HCP METALS

By HUA QIAO, M.ENG.

A Thesis

Submitted to the School of Graduate Studies

In Partial Fulfillment of the Requirements

For the degree

Doctor of Philosophy

McMaster University

Doctor of Philosophy in Mechanical Engineering (2016) McMaster University
(Mechanical Engineering) Hamilton, Ontario

TITLE: Numerical study of deformation mechanisms in HCP metals

AUTHOR: Hua Qiao, M.Eng.

SUPERVISOR: Professor P.D. WU

NUMBER OF PAGES: XVI, 158

Abstract

The operative deformation mechanisms which include both dislocation slip and twinning have a significant impact on the mechanical response of hexagonal close-packed (HCP) metals. Twinning plays an important role in accommodating plastic deformation due to the limited number of independent slip systems in HCP metals. The objective of this research is to study the deformation mechanisms associated with twinning in HCP metals (magnesium and zirconium alloys).

Heat treatments are often involved in the manufacturing of zirconium alloys. These alloys exhibit a strong thermal anisotropy with a thermal expansion coefficient along the c-axis nearly two times of that along a-direction. Therefore, residual stresses/strains are generated during the heat treatment process which influences the mechanical response (e.g. lattice evolution) under subsequent loading. The elastic viscoplastic self-consistent (EVPSC) model has been improved which includes thermal strain to study the behavior of a Zircaloy-2 slab under moderately large strains. Various self-consistent schemes (SCSs) of the EVPSC model are evaluated in terms of the deformation behavior of the material under different uniaxial strain paths. Numerical results show that the Affine and Meff=0.1 self-consistent models give much better performance for the Zircaloy-2 slab than the Secant and Tangent models.

The EVPSC-TDT model has been employed to mimic the twinning and detwinning behavior of extruded Mg alloy ZK60A under monotonic and cyclic loading. The model differentiates between the stress required to initiate twinning and that required to grow

(thicken) existing twins. This enables the model to simulate the unusual sharp yielding behavior during twinning as well as the gradual yielding associated with detwinning. It is demonstrated that this model gives a good prediction of the strength anisotropy, strength asymmetry, and strain hardening behavior along different directions, for cases in which the contribution of twinning is large, small and intermediate. For the first time, the lattice strain evolution is well predicted in an extruded magnesium alloy under cyclic loading which involves twinning and detwinning.

In all polycrystal models, an empirical equation for the termination of twinning in a grain is required. A new physics-based empirical equation for describing this phenomenon in magnesium alloys has been proposed in this study. It should be noted that the popular empirical equation currently used in all polycrystal models is applied at the grain level, while the new empirical equation is introduced at the twinning system level. The new description is represented by a single parameter while the commonly used empirical equation depends on two parameters. It is demonstrated that the proposed empirical equation is easily calibrated with the single parameter and is able to accurately simulate the experimentally observed rapid hardening associated with twinning exhaustion.

Acknowledgments

First, I greatly acknowledge my supervisor Dr. Peidong Wu for his instructive guidance, great patience and encouragement. Without his consistent instruction, the thesis could not be completed.

I would sincerely like to thank Dr. Sean R. Agnew (University of Virginia, USA), Dr. Mark Daymond (Queen's University, Canada) and Dr. Michael Gharghouri (Chalk River Laboratory, Canada) for their valuable contributions to this research.

Lastly, I would like to thank my parents for their support and understanding during my graduate studies. I would also like to give a special thanks to my wife Dongyan Huang whose encouragement and love have enabled me to complete the work. In addition, I would like to express my gratitude to my colleagues Dr. Xiaoqian Guo and Dr. Michael J. Nemcko for their help during the writing of this thesis.

This thesis is based on the following publications with permission:

Chapter 2. Qiao H., Wu P.D., Gharghouri M.A., Daymond M.R., 2015. Evaluation of elastic-viscoplastic self-consistent polycrystal plasticity models for zirconium alloys. International Journal of Solids and Structures 71, 308-322.

Chapter 3. Qiao H., Agnew S.R., Wu P.D., 2015. Modeling twinning and detwinning behavior of Mg alloy ZK60A during monotonic and cyclic loading. International Journal of Plasticity 65, 61-84.

Chapter 4. Qiao, H., Wu P.D., Guo X.Q. , Agnew S.R., 2016. A new empirical equation for termination of twinning in magnesium alloys. Scripta Materialia, accepted.

Author's contribution to publications:

All the three papers were written by the author and his co-workers. The following are the contributions by author in all publications:

(a) Prepare the numerical results and manuscript.

(b) Modify and validate the code.

(c) Act as a corresponding author for the two published papers.

Table of contents

List of figures

List of tables

Chapter 1. General introduction

1.1 Background

Magnesium has the lowest density of all structural metals. As a consequence, magnesium alloys have great potential in applications where weight reduction is essential. The automotive industry is particularly interested in magnesium and its alloys due to the pressure to reduce greenhouse gas emissions through vehicle weight reduction. Table 1.1 shows the physical properties of magnesium, aluminum and steel.

Table 1.1 Physical properties of Mg, Al and Iron (Kulekci, 2008)

Property	Magnesium	Aluminum	Iron
Crystal structure	HCP	FCC	BCC
Density at 20^{o}C (g/cm^{3})	1.74	2.70	7.86
Coefficient of thermal expansion 20-100 ^{o}C (10^{-6}/ ^{o}C)	25.2	23.6	11.7
Elastic modulus (GPa)	44.126	68.947	206.842
Tensile strength (MPa)	240 (for AZ91)	320 (for A380)	350
Melting point (^{o}C)	650	660	1.536

Other advantages of magnesium materials include high specific strength, good castability and weldability as well as improved corrosion resistance (Mordike and Ebert, 2001). However, the poor formability at room temperature and high cost during high-temperature manufacturing significantly restrict its use in a wide range of applications. The main reason for the poor ductility of magnesium is related to the low symmetry of the hexagonal-close-packed (HCP) crystal structure. In recent years, numerous studies have

been carried out by researchers from industrial and scientific communities with the objective to improve the ductility of these alloys (Kubota et al., 1999; Mukai et al., 2001; Agnew et al., 2004; Agnew et al., 2006a; Foley et al., 2011; Rosalie et al., 2012; Sandlöbes et al., 2014; Kumar et al., 2015). Nevertheless, the fundamental deformation mechanisms of magnesium alloys have not been clearly understood, so further efforts are required to advance magnesium technology.

Zirconium is known as a material with high corrosion-resistance and low neutron absorption. The corrosion-resistance of zirconium is directly related to the impurity content of the material. As the purity of zirconium based materials increases the corrosion-resistance decreases. With the development of nuclear industry, zirconium alloys (for example zircaloy-2, zircaloy-4) have become popular structural materials used in pressure tubes and thin-walled tubing. These alloys have excellent corrosion-resistance due to their compositions which consists of impurity elements such as tin, iron, chronium and nickel (Murty and Charit, 2006). The compositions of zircaloy-2 and zircaloy-4 are listed in Table 1.2. In addition, the zirconium alloy, Zr-2.5Nb, has been applied in medical applications such as knee and hip replacements due to its excellent wear resistance (Nomura, 2015).

Table 1.2 Compositions of zircaloy-2 and zircaloy-4

Alloy	Mean composition in weight %			
	Sn	Fe	Cr	Ni
Zircaloy-2	1.50	0.12	0.10	0.05
Zircaloy-4	1.50	0.22	0.10	N/A

Zirconium alloys also have a HCP crystal structure for a large range of temperatures, existing as an alpha phase which exhibits strong anisotropy in its thermal, elastic and plastic properties. The thermal expansion coefficient along the c-axis is nearly two times of that along a-direction, which makes it more sensitive to temperature variation than magnesium alloys. The elastic constants of zirconium alloys are often assumed to be the same as those of the single crystal. The anisotropy associated with the elastic properties of zirconium is more obvious than magnesium, which may be regarded as isotropic in many situations. Intensive studies on zirconium alloys have been found in literature due to its importance in the nuclear industry and its potential in medical applications (Zaimovskii, 1978; Northwood et al., 1975; Griffiths, 1988; Griffiths et al., 1995; Lee et al., 2001; Cox, 2005; Straumal et al., 2012; Sarkar et al., 2014; Trivedi et al., 2015). However, a thorough understanding of the deformation mechanisms for this alloy system has not been achieved due to the strong intrinsic anisotropy in elasticity, thermal expansion, and plasticity.

1.2 Deformation modes in HCP metals

Slip and deformation twinning are two major deformation modes which can accommodate plastic deformation in HCP metals. Slip can be considered as blocks of crystal sliding over one another along definite crystallographic planes (slip planes). Slip occurs when the resolved shear stress reaches a critical value in a specific slip system and the atomic displacements are often larger than the lattice spacing. The deformation induced by slip causes the lattice to reorient in a gradual manner.

Six types of slip systems have been observed in HCP metals, which are listed in Table 1.3. The first two types can provide four independent slip systems, which are equivalent as those offered by pyramidal <a> slip. These four independent slip systems are not enough to accommodate an arbitrary deformation according to the Von Misses criterion (Taylor, 1938). Thus, one of the <c> or <c+a> slip systems which can accommodate deformation along the c-axis is required to satisfy the Taylor criterion. However, these types of slip systems are very difficult to activate at room temperature due to their relatively high values of critical resolved shear stress (CRSS). In this case, tensile twinning is a significant alternative deformation mode in HCP metals to accommodate the deformation along the c-axis at room temperature.

Table 1.3 Independent slip systems in HCP metals (Partridge, 1967)

Slip system	Burgers vector	Slip direction	Slip plane	No. of slip systems	
				Total	Independent
1	a	$<11\bar{2}0>$	{0001}	3	2
2	a	$<11\bar{2}0>$	$\{10\bar{1}0\}$	3	2
3	a	$<11\bar{2}0>$	$\{10\bar{1}1\}$	6	4
4	$c+a$	$<11\bar{2}3>$	$\{11\bar{2}2\}$	6	5
5	c	<0001>	$\{10\bar{1}0\}$	3	2
6	c	<0001>	$\{11\bar{2}0\}$	3	2

Deformation twinning is caused by a small uniformly distributed shear component imposed on a specific plane, which causes a sudden reorientation of the parent lattice by atom displacements. The lattice in the twinned region is a mirror representation of that in the matrix.

A twin can be described by four elements (Figure 1.1): the first undistorted plane K_1, the direction of shear η_1, the second undistorted plane K_2, and η_2. The plane K_1 is the twin plane and remains unchanged during twinning, the shear direction of η_1 that lies in the plane K_1 is the direction where twinning occurs. The plane K_2 is displaced to $K_2^{'}$ by the twinning shear γ. η_2 and $\eta_2^{'}$ are the lines of intersection of the shear plane (normal to K_1 and K_2) with plane K_2 and $K_2^{'}$, respectively. A specific twinning mode will be defined when the four elements are fixed. The magnitude of the twinning shear γ is given by

$$\gamma = 2\cot(2\phi) \tag{1.2.1}$$

The magnitude of the twinning shear γ for a specific twinning mode is determined by the ratio c/a (Mathewson and Phillips, 1928). The most predominant twinning mode for most HCP materials at room temperature is $\{10\bar{1}2\}<10\bar{1}\bar{1}>$ twinning and the twinning shear γ for this mode can be written as

$$\gamma = \sqrt{3}a/c - c/\sqrt{3}a \tag{1.2.2}$$

For magnesium (zirconium) with c/a =1.624 (1.593), this type of twinning is called "extension" twinning which elongates the c-axis. The extension twinning results in a shear of 0.129 (0.168) and a lattice reorientation of approximately 86.3º (85.2º). It should be noted that if $c/a > \sqrt{3}$ as in cadmium and zinc, this twinning mode activates under a compressive stress along the c-axis and is named as "contraction" twinning. The

schematic representation for the shape changes produced by tensile twinning is illustrated in Figure 1.2.

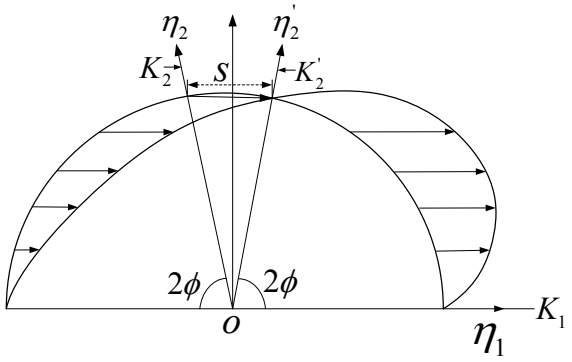

Figure 1.1 Crystallographic elements of twinning (Partridge, 1967)

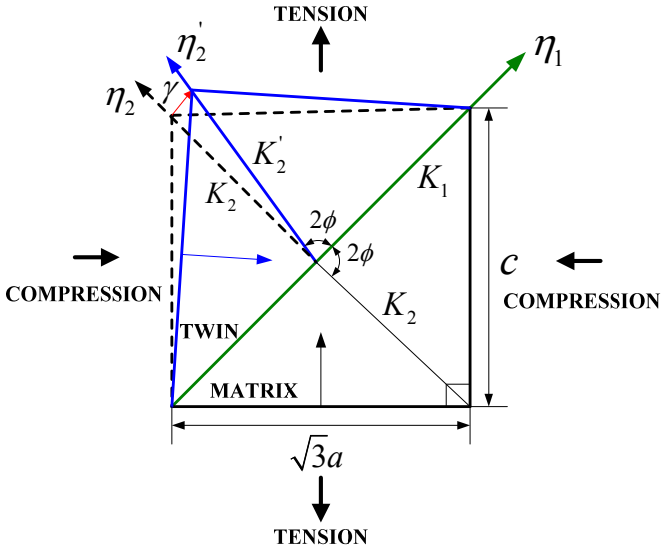

Figure 1.2 Shape changes produced by tensile twinning (Partridge, 1967)

The commonly observed deformation modes (Yoo, 1981; Partridge, 1967) in Magnesium at room temperature are: basal slip $\{0001\}<11\bar{2}0>$, prismatic $<a>$ ($\{10\bar{1}0\}<11\bar{2}0>$), pyramidal $<a>$ ($\{10\bar{1}1\}<11\bar{2}0>$), pyramidal $<c+a>$

($\{11\bar{2}2\}<11\bar{2}3>$) slips, and tensile twinning $\{10\bar{1}2\}<10\bar{1}1>$ as well as compressive twinning $\{10\bar{1}1\}<10\bar{1}2>$. The primary slip system of magnesium is the basal slip which is the glide along the closed-packed direction (<a>) and on the most closed-packed plane ((0002) plane) due to its lower CRSS than other slip systems. The compressive twinning and pyramidal $<c+a>$ slip are much harder than the basal slip and tensile twinning at room temperature. Ward Flynn et al (1961) concluded that the prismatic $<a>$ is more important than pyramidal $<a>$ slip. In addition, as pointed by Agnew et al. (2001), the deformations and crystallographic textures induced by pyramidal $<a>$ slip could be resulted from a combination of basal slip $<a>$ and prismatic $<a>$ slip. Therefore, pyramidal $<a>$ slip is often not included in the crystal-based plastic analysis. Figure 1.3 presents the frequently observed deformation modes in magnesium at room temperature.

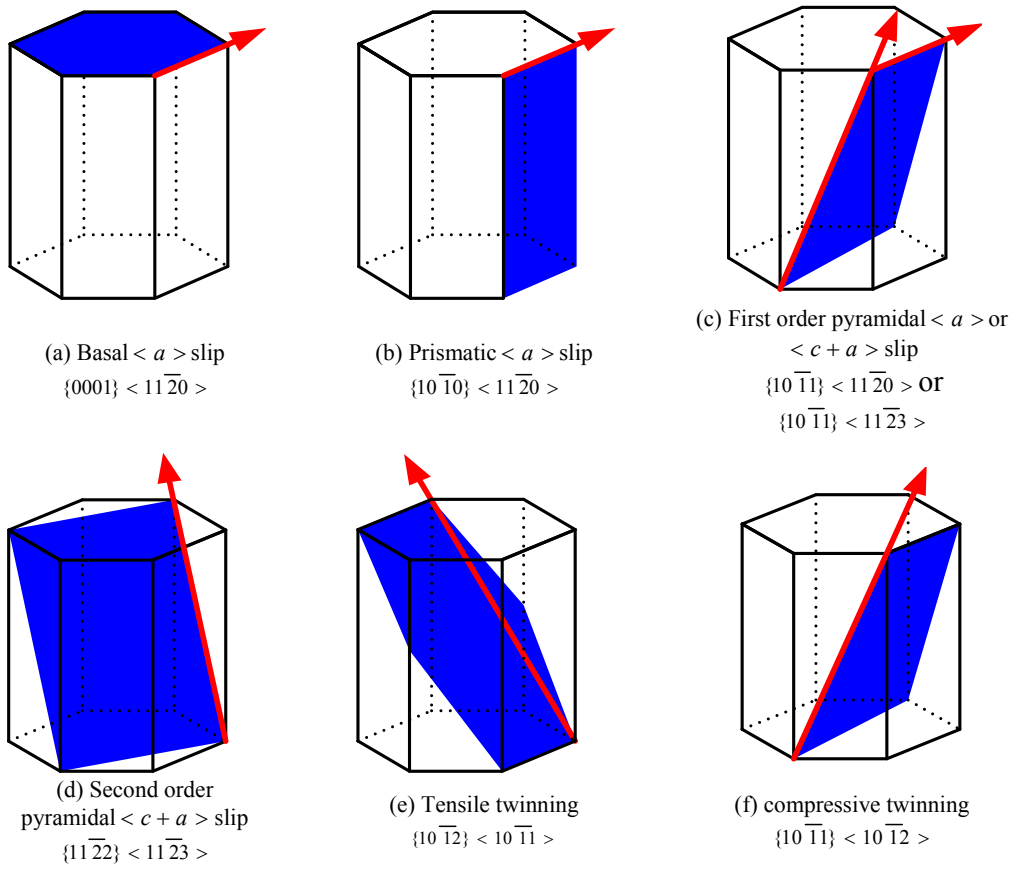

Figure 1.3 Frequently observed deformation modes in magnesium at room temperature (Partridge, 1967; Staroselsky, 1998)

For zirconium and its alloys, prismatic $<a>$ slip ($\{10\bar{1}0\}<11\bar{2}0>$) is the main deformation mechanism for a large range of temperatures (Akhtar, 1975; Rapperport and Hartley, 1960). Other observed deformation modes at room temperature include pyramidal <a> ($\{10\bar{1}1\}<11\bar{2}0>$), basal ($\{0001\}<11\bar{2}0>$), pyramidal <c+a> ($\{10\bar{1}1\}<11\bar{2}3>$ or $\{11\bar{2}2\}<11\bar{2}3>$), tensile twinning ($\{10\bar{1}2\}<10\bar{1}1>$ or $\{11\bar{2}1\}<11\bar{2}6>$), and compressive twinning ($\{10\bar{1}1\}<10\bar{1}2>$ or $\{11\bar{2}2\}<11\bar{2}3>$)

(Ballinger et al, 1984; Martin and Reed-Hill, 1964; Numakura et al, 1991; Rapperport and Hartley, 1960). Murty and Charit (2006) reported that the operable twinning modes are dependent on the type of loading: $\{10\bar{1}2\}<10\bar{1}1>$ twins are more likely to be activated than $\{11\bar{2}1\}<11\bar{2}6>$ twins under tension along the c-axis, $\{11\bar{2}2\}<11\bar{2}3>$ twins are dominant during compressive loading, and $\{10\bar{1}1\}<10\bar{1}2>$ twins are observed at high temperatures. A schematic of these twinning mechanisms is presented in Figure 1.4 (Tenckhoff, 1988). There are some disagreements in literature about the evidence of basal slip or pyramidal <a> slip at room temperature due to the difficulty in unambiguously identifying the slip plane by transmission electron microscopy observations. Martin and Reed-Hill (1964) reported slip markings near the basal plane trace in polycrystalline zirconium samples deformed at room temperature. Some researchers included basal slip as an active slip mode in crystal plasticity analysis of zirconium alloys (Castelnau et al, 2001; Francillette et al, 1998; Xu et al, 2008a), while Philippe et al (1988) and Tome et al (1991) preferred to include pyramidal <a> slip as an alternative in their analysis to basal slip in order to improve agreement with experimental data. Recently, Knezevic et al. (2013) revealed anomalous basal slip activity in zirconium under high strains and concluded that basal slip is an important deformation mechanism in Zr at room temperature under high to severe strain-deformation conditions. Table 1.4 lists the deformation modes employed by several typical research organizations for the numerical analyses of zirconium alloys based on different crystal plastic models.

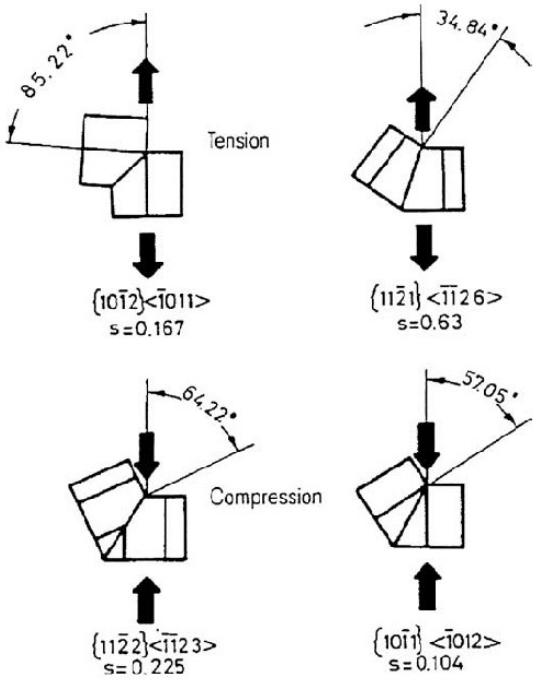

Figure 1.4 Schematic of twinning systems in zirconium (Tenckhoff, 1988)

Table 1.4 Deformation modes used for numerical simulation based on crystal plastic models at room temperature

	Prismatic $< a >$ $\{10\bar{1}0\} < 11\bar{2}0 >$	Basal $< a >$ $\{0001\} < 11\bar{2}0 >$	Pyramidal $< c+a >$ $\{10\bar{1}1\} < 11\bar{2}3 >$	Tens. twinning $\{10\bar{1}2\} < 10\bar{1}1 >$
LPMTM-CNRS, Universite Paris (a,b)	√	√	√	√
LANL(c,d)	√		√	√
Queen's University (e,f)	√	√	√	√

LANL, Los Alamos National Laboratory;
a. (Castelnau et al., 2001); b. (Francilliette et al., 1998) ; c. (Tome et al., 2001); d. (Proust et al., 2007); e. (Xu et al., 2008b) ;
f. (Mareau and Daymond, 2010)

1.3 CRSS for slip and twinning

The well-known Schmid law (Schmid, 1931) states that plastic deformation occurs when the shear stress on a specific slip system reaches a critical value. This value is called the critical resolved shear stress (CRSS) of the slip system. Considering a bar under uniaxial load with a given slip pane and slip direction (Figure 1.5), the resolved shear stress (RSS) on the plane along the direction can be given by;

$$\tau = \sigma \cos(\lambda)\cos(\varphi) \tag{1.3.1}$$

where λ is the angle between the tensile axis and the normal to the slip plane, φ is the angle between the tensile axis and the slip direction, and $\cos(\lambda)\cos(\varphi)$ is the so called Schmid factor. Therefore, the slip will occur when the RSS τ reaches the CRSS τ_c.

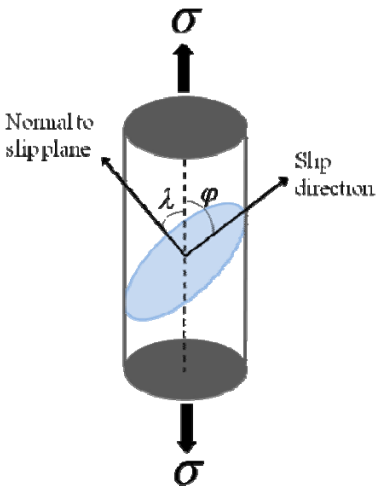

Figure 1.5 A uniaxial loaded bar with given slip plane and slip direction.

It is generally accepted that the CRSS criterion (Schmid law) is acceptable for dislocation slip in FCC and HCP metals, although a breakdown of the Schmid law has been reported for BCC metals (e.g. Duesbery and Vitek., 1998; ITO, 2001; Vitek et al.,

2004; Groger and Vitek, 2005). Furthermore, the Schmid law has introduced controversy in the literature related to twin nucleation. Bell and Cahn (1957) observed a large scatter in CRSS for zinc single crystals which suggested that there is no single CRSS existing for twinning. Some researchers reported evidence in support of the hypothesis that in metal crystals mechanical twinning starts when the resolved shear stress on the twinning plane along the twinning direction reaches a critical value (Thompson and Millard, 1952; Chin et al., 1969; Gharghouri et al, 1999). In general, the CRSS criterion has been used by researchers for most analytical/numerical studies on plastic deformation associated with slip and twinning in HCP metals.

CRSSs for polycrystals must be derived indirectly through polycrystalline modeling using an inverse approach (Agnew et al., 2006b; Herrera-Solaz et al., 2014), since the manufacturing of single crystals of many alloys to allow measurement of the CRSSs is either very difficult or in some cases impossible. Furthermore, the observed CRSSs required for polycrystals will be different from those found in a single crystal due to the interactions of the dislocations with grain boundaries (Xu et al., 2008a).

Lou et al. (2007) summarized CRSS values reported from Mg and its alloys containing aluminum and zinc solutes (Table 1.5). For Mg and Mg-Zn, the single-crystal data shows that basal slip has the lowest CRSS, twinning has a CRSS 2-4 times larger than basal slip, and prismatic slip has a relatively large CRSS. The CRSS values reported for polycrystalline AZ31 and AZ61 are fitted by polycrystal calculations in order to match the macroscopic response, or obtained using in situ neutron diffraction measurements (Gharghouri, 1997; Brown, 2005). Xu et al. (2008b) summarized CRSS

values for Zircaloy-2 and reported the approximate ranges for prismatic <a>, basal <a>, and pyramidal <c+a> slips as well as tensile twining: $90 \le \tau_0^{Pr} \le 120$ MPa, $120 \le \tau_0^{bas} \le 240$ MPa, $240 \le \tau_0^{Pyr} \le 340$ MPa, and $180 \le \tau_0^{tt} \le 280$ MPa. It is clear that the scatter is quite large for both Mg and Zirconium alloys.

Table 1.5 Critical resolved shear stresses (CRSS) reported for Mg and its Al-Zn alloy (Lou et al., 2007).

Metals	Conditions	$CRSS_{basal}$ (MPa)	$CRSS_{twin}$ (MPa)	$CRSS_{prism}$ (MPa)	$CRSS_{twin}/CRSS_{basal}$	$CRSS_{prism}/CRSS_{basal}$
Mg	SC	0.81[a];0.76[b]; 0.45[c];0.65[d]; 0.52[e]	2[f]	39.2[g]	2.5-4.4	48-87
Mg 0.5 at. Pct Zn	SC					
AZ31B	PC,VPSC,XRD	45[i]	15[i]	110[i]	0.33[i]	2.4[i]
	PC,EPSC,ND	10[j]	30[j]	55[j]	3[j]	5.5[j]
	PC,Taylor,XRD				2[k]	1-2.4[k]
	PC,TEM					1.1[l]
	PC,ND,Schmid factor		25-35[m]			
AZ61	PC,XRD					1.5-2[n]
Mg 7.7 at. Pct Al	PC,ND		65-75[o]			

SC, single crystal; PC, polycrystal; XRD, X-ray diffraction; ND, neutron diffraction; VPSC, visco-plastic self-consistent model; EPSC, elasto-plastic self-consistent model; Taylor, Taylor model.

a. Schmid (1931).
b. Bakarian and Mathewson (1943).
c. Burke and Hibbard (1952).
d. Hsu and Cullity (1954).
e. Conrad and Robertson (1957).
f. Reed-Hill and Robertson (1957a, b); Miura (2004).
g. Reed-Hill and Robertson (1957a, b).
h. Miura (2004).
i. Agnew (2002).
j. Agnew et al. (2003).
k. Styczynski et al. (2004).
l. Koike et al. (2003).
m. Brown et al. (2005).
n. Koike and Ohyama (2005).
o. Gharghouri (1997).

It is commonly accepted that a much higher local stress is needed to nucleate a twin than that for the twin to propagate and grow. The surface to volume ratio is very high when the twin is nucleated. A high surface to volume ratio will induce a high shear stress (Hosford, 1993). Thus, a fine grain size will result in a higher shear stress for nucleation. The interaction mechanisms between slip and twin modes as well as factors affecting the twinning stress have been thoroughly reviewed by Christian and Mahajan (1995).

1.4 Detwinning in HCP metals

In addition to slip and twinning, detwinning is another important deformation mechanism which accommodates plastic deformation in HCP metals. The phenomenon of detwinning has been known for many years (Obreimov and Startsev, 1959; Cooper, 1962). Indeed, detwinning of martensite is one of the key mechanisms upon which the shape memory phenomenon is built (see Miyazaki et al. 1989a, 1989b; Liu and Xie, 2003). In short, detwinning is actually twinning of the twinned region back into the orientation of the parent material from which it came. Twins can disappear or contract under reverse loading or unloading through detwinning. Figure 1.6 clearly shows the twinning and detwinning behavior in a Mg single crystal under cyclic tension and compression applied in the [0001] direction (Yu et al., 2011). In addition, intensive experimental studies on the deformation mechanisms associated with the twinning and detwinning behavior of magnesium alloys have been found in literature (Gharghouri et al., 1999; Cáceres et al., 2003; Kleiner and Uggowitzer, 2004; Brown et al., 2007; Lou et al., 2007; Wu et al., 2008a, 2008b; Proust et al., 2009; Hong et al., 2010b; Wu et al., 2012; Yu et al., 2012;

Chapuis et al., 2014a; Morrow et al., 2014a; Sarker and Chen, 2014). In contrast, for zirconium and its alloys, the experimental studies on detwinning behavior are sparse. Proust et al. (2010) observed the detwinning behavior in high purity Zr under reversal loading based on in-situ neutron diffraction experiments. Kapoor et al. (2014) studied the effect of strain rate on twinning in an extruded Zr alloy under uniaxial compression along extrusion direction and concluded that the decrease of twin volume fraction in Stage B with an increasing strain hardening rate may be caused by detwinning.

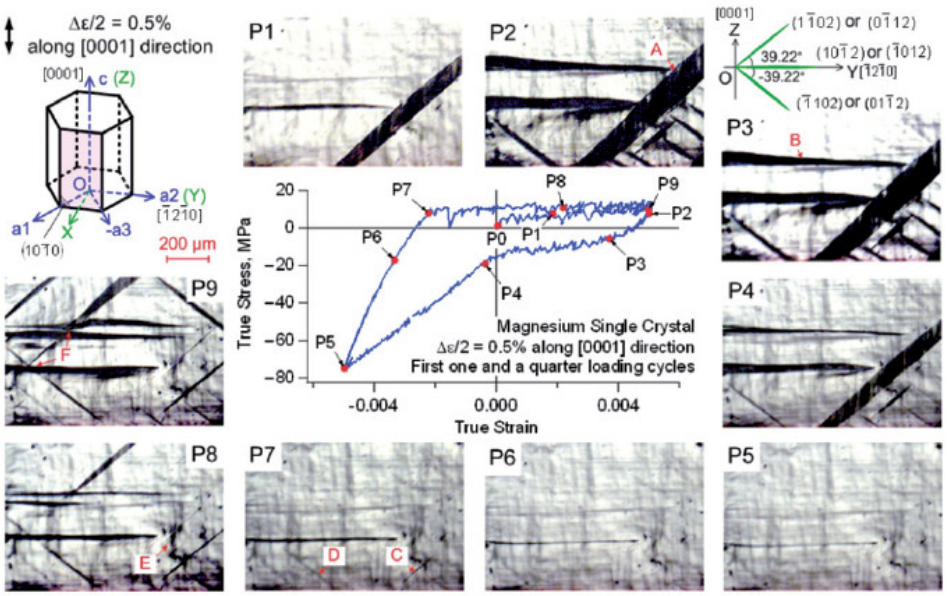

Figure 1.6 Stress-strain hysteresis loop and corresponding in-situ observation by light microscopy (Yu et al., 2011)

Partridge (1965) indicated that the stress required for detwinning is less than that for twinning nucleation and larger than that for twin growth during the study of cyclic twinning in HCP metals. Acoustic emission (AE) technology is used by material scientists to monitor the deformation process accompanied by plastic deformation,

fracture and phase transformations to provide further insights on these phenomena (Yudin and Ivanov, 1985). This technology has been used to study the deformation mechanisms of magnesium alloys (Chmelik et al., 2002; Bohlen et al., 2004; Lamark et al., 2004; Lou et al., 2007; Lu et al., 2008; Muránsky et al., 2010a). Two types of signals can be distinguished in AE analysis which consist of burst and continuous signals. A burst AE signal is associated with twin nucleation while a continuous one is related to dislocation slip. Lou et al. (2007) suggested that twinning required nucleation events detectable with AE signal while the shrinkage of twins (detwinning) was not accompanied by a significant AE signal. In addition, they established that the activation stress for twinning is larger than that for detwinning due to the need for nucleation. It has been demonstrated by (Muránsky et al., 2010a) that the coupled AE technique with in-situ neutron diffraction facilitates the distinction between twin nucleation and twin growth. These authors concluded that a sudden stress relaxation (stress drop) is associated with twin nucleation. Furthermore, they established that collaborative twin nucleation in many grains dominates yielding in fine-grained alloys, while twin nucleation is progressive over a larger strain range in coarse-grained alloys. Barnett and Muránsky and their coworkers have systematically studied the effects of grain size on the twinning process in wrought Mg alloys (Barnett et al., 2004, 2012, 2013; Muránsky et al., 2010a, 2010b).

To better characterize the deformation mechanisms associated with twinning, some researchers in the mechanics community have attempted to implement the effect of stress relaxation into crystal plasticity models. Beyerlein and Tomé (2010) and Mu et al. (2014) employed two different CRSSs for twin nucleation and growth with the CRSS for

nucleation being larger than the CRSS for growth. Clausen et al. (2008) incorporated the stress relaxation associated with twin propagation in the Elastic Plastic Self-Consistent (EPSC) model based on a Finite Initial Fraction (FIF) approach. In this research, the EVPSC-TDT model is used with different values between the stress required to initiate twinning and that required to grow (thicken) previously existing twins in order to mimic the deformation behavior of Mg alloy ZK60A under cyclic loading. It is also demonstrated that this enables the model to simulate the unusual stress-strain hysteresis behavior during twinning (e.g., sharp yielding behavior) as well as that of detwinning (characterized by quite gradual yielding). The CRSSs associated with twin nucleation, twin growth, and detwinning will also be discussed. These details will be reported in Chapter 3.

1.5 Constitutive models for polycrystalline materials

Plastic deformation behavior in metals is often modeled using two major approaches. One is polycrystal plasticity modeling which considers the polycrystalline material as a composite composed of many grains with different orientations; the other is phenomenological modeling which is based on the observed macroscopic deformation behavior. For the latter approach, the plastic deformation can be characterized by proposing an appropriate yield criteria, flow rule and hardening law. In this section, a polycrystal modeling approach based on the crystal plastic finite element method is included in an independent subsection 1.5.3. The equilibrium and compatibility

throughout the polycrystalline aggregate can be naturally accommodated in a weak finite element sense which is different from the other homogenized polycrystal models.

1.5.1 Phenomenological models

Crystallographic plasticity modelling is based on the microscopic deformation mechanisms of materials. With the initial crystallographic texture and hardening parameters set as inputs for the various deformation modes, the material anisotropy and yielding asymmetry are natural outputs. However, the so called phenomenological model is based on the observed macroscopic deformation behavior of materials and the plastic deformation can be characterized in terms of the stress/strain tensors as well as their invariants. The most common phenomenological theory for elastic-plastic deformation of metals is the Prandtl-Reuss flow theory with isotropic hardening based on the von Mises yield criterion. Based on such isotropic phenomenological models, various anisotropic phenomenological models have been proposed to describe the plastic anisotropy in cubic metals (Hill, 1948; Barlat et al., 1991; Barlat et al., 1997; Cazacu and Barlat, 2001, 2003). However, these models have been challenged by the strong strength differential (SD) effect observed in HCP metals where twinning is to be activated under favorable loading conditions and hence causes strong yielding asymmetry in tension and compression. To characterize the SD effect, the first method is to develop anisotropic continuum phenomenological models by adding stress invariants into the existing anisotropic yield functions. Hosford (1966) modified Hill's (1948) yield criterion by adding linear stress terms. A third invariant of stress deviator was added into an orthotropic yield surface by

Cazacu and Barlat (2004, 2006) and Plunkett et al. (2008). The other method is to introduce initial translation of yield surface by assuming a non-zero back stress in a combined isotropic-kinematic hardening model (Yoon et al., 1998; Li., 2006; Lee et al., 2008). Besides the yielding asymmetry and plastic anisotropy, unique hardening behavior associated with twinning and untwinning can be found in magnesium alloys under complex loading conditions such as reverse and cyclic loading. To mimic such unique hardening behavior, the two/multi-yield surface modeling approach has been proposed where separate hardening laws will be used for twinning, untwinning and slip modes (Lee et al., 2008; Li et al., 2010; Kim et al., 2013; Nguyen et al., 2013; Muhammad et al., 2015).

In summary, the phenomenological models are computationally time-efficient and easier to implement into commercial finite element software for industrial applications; however, these models could not track the texture evolution and correctly describe the microscopic mechanical responses in grain level.

1.5.2 Polycrystal models

Various polycrystal plasticity models have been developed in literature to describe the deformation mechanisms for polycrystalline materials. Among them, the most popular ones are the Taylor model (Taylor, 1938), the Sachs model (Sachs, 1928), and the Self-consistent model (Molinari et al., 1987; Lebensohn and Tomé, 1993; Turner and Tomé, 1994). The Taylor model assumes that all grains must accommodate the same plastic strain equal to the macroscopically imposed strain. With the iso-strain assumption, the

compatibility of deformation is satisfied while equilibrium amongst grains is violated which may cause unrealistic stress concentrations in some cases. The Taylor assumption is reasonable for materials with a mildly anisotropic plastic response. Therefore, it works well for face centered cubic (FCC) and body centered cubic (BCC) materials having high crystallographic symmetries. The Sachs model assumes that each grain in the polycrystalline aggregate is under a uniform stress and equal to the macroscopic stress. Under this assumption, adjacent grains in the aggregate will deform independently which will cause some gaps or overlaps at grain boundaries. The Sachs model is suitable for aggregates with soft grains and is commonly called the lower bound model in comparison to the upper bound Taylor model. The self-consistent approach (Kroner, 1958; Hill, 1965; Hutchinson, 1976) has proven to be more suitable than the classic Taylor model for modeling the mechanical behavior of HCP polycrystals (MacEwen et al., 1989; Wang et al., 2010b). In self-consistent models, all grains with the same orientation are treated as a single inclusion embedded in a Homogenous Effective Medium (HEM), which is the aggregate of all inclusions. Grain interaction is captured indirectly through the interactions of the inclusions with the HEM using the Eshelby inclusion formalism (Eshelby, 1957). The macroscopically imposed stress and strain coincide with the corresponding averages for the aggregate without imposing equal strains (or stresses) for all the grains.

Among the self-consistent models reported in the literature, the visco-plastic self-consistent (VPSC) model proposed by Molinari et al. (1987) and extended by Lebensohn and Tomé (1993) is the most popular one. The VPSC model has been employed to

investigate the deformation behavior of HCP materials (Lebensohn et al., 1996; Agnew and Duygulu, 2005; Jain and Agnew 2007; Proust et al., 2007, 2009; Xu et al., 2009; Wang et al., 2010b; Hutchinson et al., 2012; Steglich et al., 2012; EI Kadiri et al., 2013a; Oppedal et al., 2013; Kabirian et al., 2015). Turner and Tomé (1994) proposed an elasto-plastic self-consistent (EPSC) model. The EPSC model works only for small deformation and earlier EPSC models did not include texture evolution associated with slip or twinning. The model has been employed to investigate the deformation mechanisms of HCP metals via the interpretation of elastic lattice strain results (Agnew et al., 2003; Agnew et al., 2006b; Muransky et al., 2008; Xu et al., 2008b). Clausen et al. (2008) extended the EPSC model by including texture development and stress relaxation due to twinning, while Neil et al. (2010) developed a large strain EPSC model to approximately account for the kinematics of large strain, rigid body rotations, texture evolution and grain shape evolution. Mathis et al. (2015) employed such models to study the effect of loading mode on the evolution of the deformation mechanisms in randomly textured magnesium polycrystals. Recently, based on the framework of EPSC model, Zecevic et al. (2015) proposed a multi-scale EPSC model with hardening based on dislocation density, twinning and detwinning. However, the rate-insensitive character of the constitutive law upon which the EPSC model is based prevents us from addressing strain rate-sensitivity, and the experimentally observed stress relaxation and creep associated with finite hold times for acquisition of lattice-strain data.

Wang et al. (2010a) developed a finite strain Elasto-Viscoplastic Self-Consistent (EVPSC) model for polycrystalline materials. The proposed EVPSC model is a general

rate-sensitive self-consistent polycrystal plasticity model valid at arbitrarily large deformations. The EVPSC model has been successfully applied to analyze the deformation mechanisms of HCP metals (Wang et al., 2010b, 2010c, 2010d, 2011, 2012a; Guo et al., 2013; Qiao et al., 2015a). A twinning and detwinning model (TDT) has been proposed by Wang et al. (2012b, 2013a) and implemented into the EVPSC model, referred to as EVPSC-TDT. The EVPSC-TDT model has been applied to simulate the deformation mechanisms associated with the twinning/detwinning behavior for HCP metals under monotonic/cyclic loading (Wang et al., 2013c, 2015; Lee et al., 2014; Wu et al., 2014; Wang et al., 2015; Guo et al., 2015a, 2015b; Qiao et al., 2015b). Recently, Wu et al. (2015) proposed a new constitutive model to describe twin nucleation, propagation and growth (TNPG) for magnesium crystals. The TNPG model has been implemented into the EVPSC model and is able to capture key macroscopic features associated with twin nucleation, propagation and growth observed experimentally.

As mentioned above, the self-consistent scheme assumes each grain as an ellipsoidal inclusion embedded in a homogeneous effective medium. The Eshelby (1957) inclusion formulism is used to describe the interaction between the grain and aggregate. However, to apply the inclusion theory, it is necessary to linearize the elastic/visco-plastic constitutive response. Various SCSs have been evaluated by Wang et al. (2010b) through the study of the deformation behavior of a magnesium alloy AZ31B sheet under different uniaxial strain paths. The VPSC model was used to evaluate each scheme and the authors concluded that the Affine scheme gave the best overall performance among the self-consistent schemes (SCSs) examined for the AZ31B magnesium alloy. Due to the

differences in the operative deformation mechanisms between magnesium and zirconium alloys, one question arises: which self-consistent scheme is best for zirconium alloy (e.g. zircaloy-2). To answer the question, an evaluation of various SCSs for zirconium alloys will be one focus of this research and details will be reported in Chapter 2.

1.5.3 Crystal plasticity finite element method

Crystal plasticity finite element method (CPFEM) is another important alternative modeling method to investigate the deformation mechanisms of HCP metals, where both equilibrium and compatibility throughout the polycrystalline aggregate can be naturally accommodated in a weak finite element sense. In CPFEM simulations, the constitutive response at an integration point can be described by a single crystal or polycrystal constitutive model. The CPFE method using a polycrystal constitutive description at each integration point has been employed to study the deformation behaviour of HCP metals (see e.g., Tomé et al., 2001; Segurado et al., 2012; Herrera-Solaz et al., 2014). For the CPFE analysis with the single crystal constitutive model at each integration point, an element of the FE mesh represents a single crystal or a part of a single crystal. Based on the seminal work by Staroselsky and Anand (1998) and Kalidindi (1998), much of the progresses in the application of such CPFE models for the study of deformation mechanisms in HCP metals have been made in literature (Wu et al., 2007; Graff et al., 2007; Mayama et al., 2009; Choi et al., 2011; Hama and Takuda, 2011, 2012; Hama et al., 2013; Zhang and Joshi, 2012; Abdolvand and Daymond, 2011, 2012, 2013a, 2013b; Abdolvand et al., 2015).

1.6 Incorporation of twinning into crystal plasticity

An important aspect associated with various crystal plasticity models in the analyses for HCP materials is how to incorporate a reorientation scheme for deformation twinning into the constitutive model. Several methods for the incorporation of twinning have been proposed in literature (Van Houtte et al., 1978; Tomé et al., 1991; Kalidindi, 1998; Wang et al., 2012b, 2013a).

In Van Houtte's approach (Van Houtte et al., 1978), the decision to re-orient the grain was based on the increments of the twin volume fractions in a given time-step independent of the previous deformation history, such that the selected orientation may not be the most dominant one. Tomé et al. (1991) proposed a predominant twin reorientation (PTR) scheme which rectified the above deficiency of Van Houtte's approach. In the PTR scheme, twinning is treated as a pseudo slip and the evolution of twin volume fraction in a grain is tracked during the analysis. Once the accumulated twin volume fraction of all twin variants reaches a threshold, the grain will be reoriented according to the most predominant twin system. Kalidindi (1998) proposed a new approach to incorporate twinning as an additional mode of plastic deformation. The original multiplicative decomposition of the deformation gradient (Asaro and Rice, 1977) was utilized but the plastic part of the deformation gradient was extended to include deformation twinning. The same deformation gradient was applied on both the twinned and untwinned (matrix) regions. The orientation of all possible twins in the twinned region was determined according to the initial orientation of the untwinned region (matrix)

at the beginning of analysis. With further straining twinning volume fraction is transferred between the matrix and twins. The proposed TDT model (Wang et al., 2012b, 2013a) employed a similar twin reorientation scheme as the Kalidindi's approach. However, in the TDT model, twins are treated as new grains and there are no deformation constraints applied among the matrix and the twins.

In all of the approaches mentioned, a threshold value of twin volume fraction should be employed to prevent grains from twinning in their entirety, since this is rarely experimentally observed. Once the accumulated twin volume fraction of the grain reaches the threshold value, the grain will re-orientate itself (PTR scheme) or cease the transfer of twin volume fraction among matrix and twins (TDT and Kalidindi's approaches). In this research, a new physics-based empirical equation for the threshold value of twin volume fraction is proposed. The details will be reported in Chapter 4.

Chapter 2. Evaluation of elastic-viscoplastic self-consistent polycrystal plasticity models for zirconium alloys

2.1 Introduction

Due to the variety of slip and twinning systems typically active in Hexagonal-Close-Packed (HCP) crystals, aggregates of HCP crystals often show strong anisotropic mechanical behavior. As a result, the predicted overall mechanical response of a polycrystal depends strongly on how the various slip and twinning systems are activated and evolve with deformation in different grain orientations, and is thus very sensitive to the homogenization method used in the model. The wide variation in grain response in HCP metals such as zirconium and its alloys provides an excellent opportunity to evaluate various homogenization methods used in models of polycrystal plasticity.

Different homogenization schemes have been employed to model polycrystal plasticity. The self-consistent approach (Kroner, 1958; Hill, 1965; Hutchinson, 1976) has proven to be more suitable than the classic Taylor model (Taylor, 1938) for modeling mechanical behavior of HCP polycrystals (see e.g. MacEwen et al., 1989 and Wang et al., 2010a). In self-consistent models, all grains with the same orientation are treated as a single inclusion embedded in a Homogenous Effective Medium (HEM), which is the aggregate of all inclusions. Grain interaction is captured indirectly through the interactions of the inclusions with the HEM using the Eshelby inclusion formalism (Eshelby, 1957). The macroscopically imposed stress and strain coincide with the corresponding averages for the aggregate without imposing equal strains (or stresses) for

all the grains. Among the self-consistent plasticity models, the Elasto Plastic Self-Consistent (EPSC) model (Turner and Tomé, 1994), the Visco-Plastic Self-Consistent (VPSC) model (Molinari et al., 1987; Lebensohn and Tomé, 1993) and the Elastic-Viscoplastic Self-Consistent (EVPSC) model (Wang et al., 2010b) have been successfully employed to simulate the deformation behavior of HCP polycrystals (Agnew and Duygulu, 2005; Clausen et al., 2008; Hutchinson et al., 2012; Muránsky et al., 2008, 2009; Neil and Agnew, 2009; Oppedal et al., 2013; Xu et al., 2008b, 2009; Turner et al., 1995; Wang et al., 2010c, 2010d, 2011, 2012a, 2012b, 2013b, 2013c; Wu et al., 2012; Guo et al., 2013; Qiao et al., 2015b). It is now generally accepted that the numerical results are very sensitive to the stiffness of the grain-matrix interaction associated with different Self-Consistent Schemes (SCSs). Various SCSs have been evaluated by Wang et al. (2010b) through the study of the deformation behavior of a magnesium alloy AZ31B sheet under different uniaxial strain paths. It was found that the Affine self-consistent scheme gave the best overall performance among the SCSs examined.

In the nuclear industry, zirconium alloys (for example Zircaloy-2, Zircaloy-4 and Zr-2.5Nb) are used for pressure tubes and for thin-walled fuel cladding (Murty and Charit, 2006). Single phase zirconium alloys have an HCP crystal structure over a wide temperature range (alpha phase) and exhibit strong anisotropy in thermal, elastic and plastic properties. The thermal expansion coefficient along the *c*-axis is nearly twice that along the *a*-axis, resulting in strong thermal intergranular residual stresses after cooling from an elevated temperature. The elastic properties of alpha-zirconium are also anisotropic. The most readily activated slip mode in alpha-zirconium and its alloys over a

wide temperature range is prismatic $< a >$ slip $\{10\bar{1}0\} < 11\bar{2}0 >$. Zirconium alloys have been extensively studied experimentally in terms of stress-strain behavior, evolution of texture, and evolution of internal elastic strain (Francillette et al., 1998; Castelnau et al., 2001; Tomé et al., 2001; Proust et al., 2007; Xu et al., 2008b, 2008c, 2009).

For Zr alloys, the EPSC model is usually used to study lattice strain evolution at relatively small strains, while the VPSC model has been most frequently applied to study the stress-strain response, texture evolution and R-value. However, the EPSC model works only for small deformation and earlier EPSC models did not include texture evolution associated with slip or twinning reorientation. Clausen et al. (2008) extended the EPSC model by including texture development and stress relaxation due to twinning, while Neil et al. (2010) developed a large strain EPSC model to approximately account for the kinematics of large strain, rigid body rotations, texture evolution and grain shape evolution. However, the rate-insensitive character of the constitutive law upon which the EPSC model is based prevents us from addressing strain rate-sensitivity in general, and the experimentally observed stress relaxation and creep associated with finite hold times for acquisition of lattice-strain data. Such macroscopic relaxation and creep can only be accounted for using a rate-sensitive elastic-plastic model.

Mareau and Daymond (2010) proposed an Elasto-Viscoplastic Self-Consistent (EVPSC) model to study the development of lattice strains in a moderately textured Zircaloy-2 slab. However, their EVPSC model is applicable only to small deformations. The large strain EVPSC model developed by Wang et al. (2010a) is a completely general elastic-viscoplastic, fully anisotropic, self-consistent polycrystal plasticity model,

applicable to large strains and to any crystal symmetry. The EVPSC model has been used to study lattice strain evolution in magnesium alloys (Wang et al., 2012a) and stainless steels (Wang et al., 2013b). Very recently, Lee et al. (2014) applied the EVPSC model to understand the deformation mechanisms during loading and unloading under uniaxial tension in a solid-solution-strengthened extruded Mg-9wt.%Al alloy. Wu et al. (2014) employed the real-time in-situ neutron diffraction technique under continuous loading combined with numerical simulations using the EVPSC model to study the twinning and detwinning behavior of a wrought AZ31B Mg alloy.

In the present paper, various self-consistent polycrystal plasticity models for HCP polycrystals are evaluated by studying the strain behavior of a Zircaloy-2 slab under different deformation processes; strains up to 20% are considered, for which grain rotation is significant. In order to take into account the effects of thermal residual strains generated during the cooling process (from 898 K to 298 K) on the subsequent mechanical loading, the EVPSC model developed by Wang et al. (2010b) is extended by including the thermal strain effect. Values of the material parameters for the various models are fitted to experimental uniaxial tension and compression stress-strain curves along the normal direction (ND) and uniaxial tension along the rolling direction (RD). These values are then used to predict uniaxial tension and compression along other directions. An assessment of the predictive capability of the polycrystal plasticity models is made based on comparisons of the predicted and experimental stress responses, *R*-values, lattice strains, and texture coefficients. The experimental data are taken from Xu et al. (2008b, 2008c, 2009).

Though the mechanical behavior of Zr alloys under various deformation processes has been extensively studied, both experimentally and numerically (see e.g. Camposilvan et al., 2014; Gloaguen et al., 2014; Gurao et al., 2014; Kapoor et al., 2014; Keskar et al., 2014; Li et al., 2014; Morrow et al, 2014b; Mozzani et al., 2014; Muránsky et al., 2014; Padilla et al., 2012; Sattari et al., 2014; Knezevic et al., 2013; Yapici et al., 2009), the experiments performed on a Zircaloy-2 slab by Xu et al. (2008b, 2008c, 2009) represent the most extensive sets of currently available experimental data for a Zr polycrystal. We believe that the predictive capability of self-consistent plasticity models can be most efficiently assessed using the experimental data of Xu et al. (2008b, 2008c, 2009).

The Crystal Plasticity based Finite Element (CPFE) approach has also been used to study the large strain behavior of polycrystalline materials (see e.g. Abdolvand and Daymond, 2013a; Alharbi and Kalidindi, 2015; Choi et al., 2011; Fernandez et al., 2011; Hama et al., 2014; Ghosh and Anahid, 2013; Herrera-Solaz et al., 2014; Lim et al., 2014; Wu et al., 2004; Zhang et al., 2015). In CPFE simulations, an element of the finite element mesh represents either a single crystal or a part of a single crystal, and the constitutive response at an integration point is described by the single crystal constitutive model. This CPFE approach enforces both equilibrium and compatibility throughout the polycrystalline aggregate in the weak finite element sense (Anand and Kalidindi, 1994; Bronkhorst et al., 1992). Furthermore, the CPFE approach allows consideration of grain morphology and the modeling of deformation inhomogeneity within individual grains (Wu and Lloyd, 2004; Wu et al., 2007; Kanjarla et al., 2010). However, CPFEM

simulations are computationally much more intensive than the corresponding self-consistent polycrystal calculations.

The paper is organized as follows: In Section 2, we describe the theoretical basis for including thermal strains in the EVPSC model. The results of the simulations are presented, compared with the experimental data, and discussed in Section 3. Conclusions are presented in Section 4.

2.2 The EVPSC model

The total strain in a single crystal is composed of elastic strain, thermal strain and plastic strain. The elastic constitutive equation for a crystal is as follows:

$$\overset{\nabla^*}{\boldsymbol{\sigma}} = \mathscr{L} : \dot{\boldsymbol{\varepsilon}}^e - \boldsymbol{\sigma}\mathrm{tr}(\dot{\boldsymbol{\varepsilon}}^e + \dot{\boldsymbol{\varepsilon}}^T) \tag{2.2.1}$$

where $\mathscr{L}$ is the fourth order elastic stiffness tensor, $\dot{\boldsymbol{\varepsilon}}^e$ is the elastic strain rate tensor, $\dot{\boldsymbol{\varepsilon}}^T$ is the thermal strain rate tensor and $\overset{\nabla^*}{\boldsymbol{\sigma}}$ is the Jaumann rate of the Cauchy stress $\boldsymbol{\sigma}$ based on the lattice spin tensor $\boldsymbol{w}^e$.

The thermal strain rate $\dot{\boldsymbol{\varepsilon}}^T$ relates to the temperature rate $\dot{T}$

$$\dot{\boldsymbol{\varepsilon}}^T = \boldsymbol{\alpha}^T \dot{T} \tag{2.2.2}$$

in terms of the thermal dilation tensor $\boldsymbol{\alpha}^T$ defined as

$$\boldsymbol{\alpha}^T = \begin{bmatrix} \alpha_a & 0 & 0 \\ 0 & \alpha_a & 0 \\ 0 & 0 & \alpha_c \end{bmatrix} \tag{2.2.3}$$

where α_a and α_c are the single crystal thermal expansion coefficients along the *a*-axis and *c*-axis, respectively.

Due to the large thermal expansion anisotropy of zirconium, inclusion of thermal strains has previously been demonstrated by other authors to be required for the accurate modeling of internal strains; this is true for both self-consistent (Turner et al., 1995, Xu et al, 2008b, Mareau and Daymond, 2010) and finite element (Abdolvand et al., 2012) based crystal plasticity modeling approaches. It is worth mentioning that our approach of introducing the thermal strain effect is almost the same as the one developed by Turner et al. (1995) and used by Xu et al. (2008b). The only difference between our approach presented above and the one in Turner et al. (1995) is that we use the Jaumann rate of the Cauchy stress ($\overset{\nabla *}{\boldsymbol{\sigma}}$), while Turner et al. (1995) apply a simple rate of the Cauchy stress ($\dot{\boldsymbol{\sigma}}$). This is because the EVPSC model is valid for arbitrary large deformations and it is necessary to use an objective stress rate to accurately account for effects of large rotations in addition to large strains. However, for all the cases considered in the present paper, the thermal strains are relatively small and whether one uses the Jaumann rate of the Cauchy stress or not will have a negligible effect on the predicted results. Our numerical results have demonstrated that the difference in the predicted thermal strain effect between the present study and the one reported by Xu et al. (2008b) is negligible.

The plastic deformation of a crystal is assumed to be due to crystallographic slip and twinning on crystallographic systems $(\boldsymbol{s}^{\alpha}, \boldsymbol{n}^{\alpha})$. Here, $\boldsymbol{s}^{\alpha}$ and $\boldsymbol{n}^{\alpha}$ are, respectively, the slip/twinning direction and the normal to the slip/twinning plane for system α. The

following equation gives the grain (crystal) plastic strain rate $\dot{\boldsymbol{\varepsilon}}^p$ (see e.g., Asaro and Needleman, 1985):

$$\dot{\boldsymbol{\varepsilon}}^p = \sum_\alpha \dot{\gamma}^\alpha \boldsymbol{P}^\alpha \tag{2.2.4}$$

in terms of the shear rate $\dot{\gamma}^\alpha$ and the Schmid tensor $\boldsymbol{P}^\alpha = (\boldsymbol{s}^\alpha \boldsymbol{n}^\alpha + \boldsymbol{n}^\alpha \boldsymbol{s}^\alpha)$ for system α. For both slip and twinning, the driving force for shear rate $\dot{\gamma}^\alpha$ is the resolved shear stress $\tau^\alpha = \boldsymbol{\sigma} : \boldsymbol{P}^\alpha$, where $\boldsymbol{\sigma}$ is the Cauchy stress tensor.

For slip,

$$\dot{\gamma}^\alpha = \dot{\gamma}_0 \left| \tau^\alpha / \tau_{cr}^\alpha \right|^{\frac{1}{m}} \operatorname{sgn}(\tau^\alpha) \tag{2.2.5}$$

where $\dot{\gamma}_0$ is a reference shear rate, τ_{cr}^α is the critical resolved shear stress (CRSS), and m is the strain rate sensitivity. Due to its polar nature, the shear rate due to twinning is described by:

$$\dot{\gamma}^\alpha = \begin{cases} \dot{\gamma}_0 \left| \tau^\alpha / \tau_{cr}^\alpha \right|^{\frac{1}{m}} & \tau^\alpha > 0 \\ 0 & \tau^\alpha \le 0 \end{cases} \tag{2.2.6}$$

For both slip and twinning, the evolution of the critical resolved shear stress (CRSS) τ_{cr}^α as deformation proceeds is given by:

$$\dot{\tau}_{cr}^\alpha = \frac{d\hat{\tau}^\alpha}{d\gamma_{ac}} \sum_\beta h^{\alpha\beta} \dot{\gamma}^\beta \tag{2.2.7}$$

where γ_{ac} is the accumulated shear strain in the grain, and $h^{\alpha\beta}$ are the latent hardening coupling coefficients, which empirically account for the obstacles on system α

associated with system β. $\hat{\tau}^{\alpha}$ is the threshold stress, described here by an extended Voce law (Tomé et al., 1984):

$$\hat{\tau}_0^{\alpha} = \tau_0^{\alpha} + (\tau_1^{\alpha} + h_1^{\alpha}\gamma_{ac})(1 - \exp(-\frac{h_0^{\alpha}}{\tau_1^{\alpha}}\gamma_{ac})) \tag{2.2.8}$$

Here, τ_0, h_0, h_1 and $\tau_0 + \tau_1$ are the initial CRSS, the initial hardening rate, the asymptotic hardening rate, and the back-extrapolated CRSS, respectively.

The response of a polycrystal comprised of many grains is obtained using a self-consistent approach: each grain is treated as an ellipsoidal inclusion embedded in a Homogeneous Effective Medium (HEM), which represents the aggregate of all the grains. Interactions between each grain and the HEM are described using the Eshelby inclusion formalism (Eshelby, 1957). The behaviour of the inclusion (single crystal) and HEM (polycrystal) can be linearized as follows:

$$\dot{\boldsymbol{\varepsilon}} = \boldsymbol{M}^{e} : \dot{\boldsymbol{\sigma}} + \boldsymbol{M}^{v} : \boldsymbol{\sigma} + \boldsymbol{\alpha}^{T}\dot{T} + \dot{\boldsymbol{\varepsilon}}^{0} \tag{2.2.9}$$

$$\dot{\boldsymbol{E}} = \overline{\boldsymbol{M}}^{e} : \dot{\boldsymbol{\Sigma}} + \overline{\boldsymbol{M}}^{v} : \boldsymbol{\Sigma} + \overline{\boldsymbol{\alpha}}^{T}\dot{T} + \dot{\boldsymbol{E}}^{0} \tag{2.2.10}$$

Here, $\boldsymbol{M}^{e}$, $\boldsymbol{M}^{v}$, $\boldsymbol{\alpha}^{T}$, $\dot{\boldsymbol{\varepsilon}}$, $\boldsymbol{\sigma}$ and $\dot{\boldsymbol{\varepsilon}}^{0}$ are, respectively, the elastic compliance, the viscoplastic compliance, the thermal dilation tensor, the strain rate, the true stress, and the back-extrapolated strain rate for the grain. $\overline{\boldsymbol{M}}^{e}$, $\overline{\boldsymbol{M}}^{v}$, $\overline{\boldsymbol{\alpha}}^{T}$, $\dot{\boldsymbol{E}}$, $\boldsymbol{\Sigma}$ and $\dot{\boldsymbol{E}}^{0}$ are the corresponding terms for the HEM. The temperature rate $\dot{T}$ is assumed to be uniform across the polycrystal. Equations (9, 10) can be written in component form as follows:

$$\dot{\varepsilon}_{ij} = M^{e}_{ijkl}\dot{\sigma}_{kl} + M^{v}_{ijkl}\sigma_{kl} + \alpha^{T}_{ij}\dot{T} + \dot{\varepsilon}^{0}_{ij} \tag{2.2.9a}$$

$$\dot{E}_{ij} = \overline{M}^{\mathrm{e}}_{\mathrm{ijkl}} \dot{\Sigma}_{kl} + \overline{M}^{v}_{ijkl} \Sigma_{kl} + \overline{\alpha}^{T}_{ij} \dot{T} + \dot{E}^{0}_{ij} \tag{2.2.10a}$$

The grain-level stress and strain rates are related self-consistently to the corresponding values for the HEM (Turner and Tomé, 1994; Wang et al., 2010a):

$$(\dot{\boldsymbol{\varepsilon}} - \dot{\boldsymbol{E}}) = -\widetilde{\boldsymbol{M}}^{e} : (\dot{\boldsymbol{\sigma}} - \dot{\boldsymbol{\Sigma}}) - \widetilde{\boldsymbol{M}}^{v} : (\boldsymbol{\sigma} - \boldsymbol{\Sigma}) \tag{2.2.11}$$

where $\widetilde{\boldsymbol{M}}^{e}$ and $\widetilde{\boldsymbol{M}}^{v}$ are the interaction tensors that can be given by:

$$\widetilde{\boldsymbol{M}}^{e} = (\boldsymbol{I} - \boldsymbol{S}^{e})^{-1} : \boldsymbol{S}^{e} : \overline{\boldsymbol{M}}^{e}, \qquad \widetilde{\boldsymbol{M}}^{v} = (\boldsymbol{I} - \boldsymbol{S}^{v})^{-1} : \boldsymbol{S}^{v} : \overline{\boldsymbol{M}}^{v} \tag{2.2.12}$$

where $\boldsymbol{S}^{e}$ and $\boldsymbol{S}^{v}$ are the elastic and visco-plastic Eshelby tensors for a given grain, respectively, and $\boldsymbol{I}$ is the identity tensor. In the present study, we assume that the thermal residual strains are generated during the initial cooling process from a stress-free state at 898 K down to 298 K. The thermal deformation during cooling results in residual elastic strains and corresponding stresses, which bias subsequent plasticity. The overall thermal dilation tensor $\overline{\boldsymbol{\alpha}}^{T}$ relates self-consistently to the elastic terms (Turner and Tomé, 1994; Turner et al., 1995) as follows:

$$\overline{\boldsymbol{\alpha}}^{T} = \overline{\boldsymbol{M}}^{e} \left\langle \left(\boldsymbol{M}^{e^{-1}} + \widetilde{\boldsymbol{M}}^{e^{-1}} \right)^{-1} \right\rangle^{-1} \left\langle \left(\boldsymbol{M}^{e^{-1}} + \widetilde{\boldsymbol{M}}^{e^{-1}} \right)^{-1} \boldsymbol{M}^{e^{-1}} \boldsymbol{\alpha}^{T} \right\rangle \tag{2.2.13}$$

As discussed in (Wang et al., 2010a; 2010b), various linearization schemes can be used to solve Eq. (2.2.9). The Secant linearization scheme, proposed by Hutchinson (1976), can be written as:

$$\boldsymbol{M}^{v,\mathrm{sec}} = \dot{\gamma}_0 \sum_{\alpha} \left(\frac{\tau^{\alpha}}{\tau^{\alpha}_{cr}} \right)^{\frac{1}{m}-1} \frac{\boldsymbol{P}^{\alpha} \boldsymbol{P}^{\alpha}}{\tau^{\alpha}_{cr}}, \qquad \dot{\varepsilon}^{0,\mathrm{sec}} = 0 \tag{2.2.14}$$

The Tangent scheme, proposed by Lebensohn and Tomé (1993), is obtained by a first-order Taylor expansion of the plastic strain rate $\dot{\boldsymbol{\varepsilon}}^{p}$ around the grain stress; it can be written in terms of the Secant scheme as follows:

$$\boldsymbol{M}^{v,\tan} = \frac{1}{m}\boldsymbol{M}^{v,\sec}, \qquad \dot{\varepsilon}^{0,\tan} = 0 \tag{2.2.15}$$

The Secant and Tangent approaches lead to excessively stiff and soft interactions, respectively, which led Molinari and Toth (1994) and Tomé (1999) to propose a modified Tangent scheme by replacing m with an empirical adjustable parameter m^{eff} $(m < m^{\text{eff}} < 1)$. The so-called m^{eff} scheme is expressed as follows:

$$\boldsymbol{M}^{v,\text{meff}} = \frac{1}{m^{\text{eff}}}\boldsymbol{M}^{v,\sec}, \qquad \dot{\varepsilon}^{0,\text{eff}} = 0 \quad (m < m^{eff} < 1) \tag{2.2.16}$$

The Affine method (Masson et al., 2000; Lebensohn et al., 2004) employs the same formulation for the grain compliance as the Tangent method, but keeps the back extrapolated term in the local /global relation between strain rate and stress, which provides a harder inclusion/matrix interaction than the Tangent model as the rate sensitivity m decreases. The Affine method applies the following linearization:

$$\boldsymbol{M}^{v,aff} = \frac{\dot{\gamma}_0}{m}\sum_{\alpha}\left(\frac{\tau^{\alpha}}{\tau^{\alpha}_{cr}}\right)^{\frac{1}{m}-1}\frac{\boldsymbol{P}^{\alpha}\boldsymbol{P}^{\alpha}}{\tau^{\alpha}_{cr}}, \qquad \dot{\varepsilon}^{0,\text{aff}} = (1-\frac{1}{m})\dot{\varepsilon}^{p} \tag{2.2.17}$$

For details concerning the self-consistent equations associated with the different visco-plastic self-consistent algorithms, we refer to Lebensohn et al. (2007).

To model twinning, the Predominant Twin Reorientation (PTR) scheme proposed by Tomé et al. (1991) is used. PTR prevents grain reorientation by twinning until a threshold volume fraction A^{th1} is accumulated in any given system and rapidly raises the

threshold to a value around $A^{th1} + A^{th2}$. Secondary twinning is not allowed in the PTR model and grain size effects on twinning are not explicitly modelled.

2.3 Results and discussions

The material considered in the present paper is a Zircaloy-2 slab studied by Xu et al. (2008b, 2008c, 2009). The measured initial crystallographic texture is discretized to 1944 grains ($10^o \times 10^o \times 10^o$ grid in Euler space) with independent orientations and weights. This set of Euler angles is used in most of the simulations reported in the present paper. Following Xu et al. (2009), however, the initial texture with 15456 orientations ($5^o \times 5^o \times 5^o$ grid in Euler space) is employed to analyze the evolution of the texture coefficients. The {0002} and $\{10\bar{1}0\}$ pole figures of the texture with 1944 orientations are shown in Figure 2.1. The material exhibits a typical rolling texture, with a large number of grains having the basal pole aligned along the ND. The plastic deformation of Zircaloy-2 is assumed to be due to prismatic ($\{10\bar{1}0\} < 11\bar{2}0 >$), basal ($\{0001\} < 11\bar{2}0 >$) and pyramidal <c+a> ($\{10\bar{1}1\} < 11\bar{2}3 >$) slip as well as $\{10\bar{1}2\} < 10\bar{1}1 >$ tensile twinning.

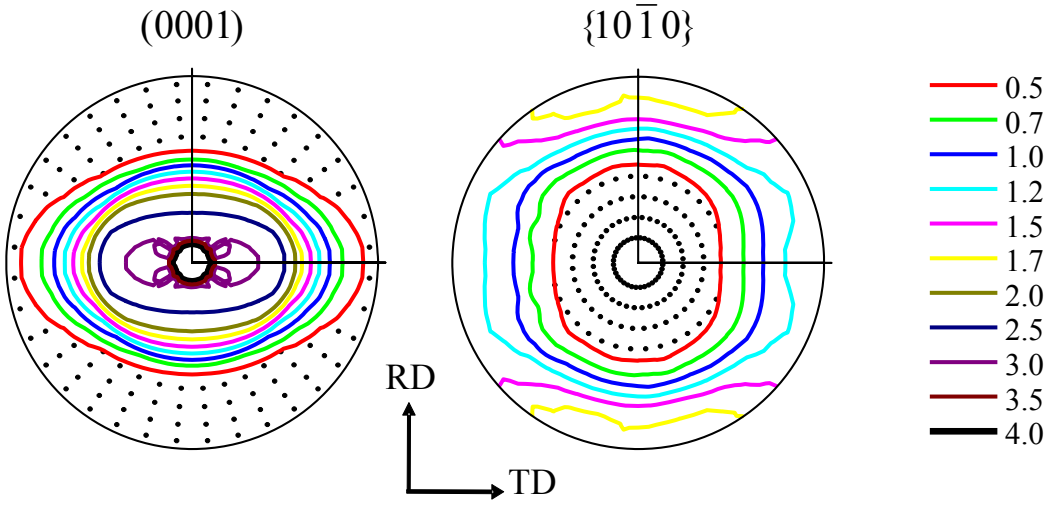

Figure 2.1 Initial texture of the Zircoaloy-2 slab represented in terms of the {0001} and {10$\bar{1}$0} pole distributions.

In all the simulations reported in the present paper, the reference slip/twinning rate, $\dot{\gamma}_0$, and the rate sensitivity, m, are prescribed to be the same for all the slip/twinning systems: $\dot{\gamma}_0 = 0.0001 s^{-1}$ and $m = 0.05$. The room temperature single crystal elastic constants of zirconium are taken to be $C_{11} = 143.5, C_{12} = 72.5, C_{13} = 65.4, C_{33} = 164.9$ and $C_{44} = 32.1$ (GPa). The thermal expansion coefficients are chosen as $\alpha_a = 5.3 \times 10^{-6} K^{-1}$ and $\alpha_c = 10.1 \times 10^{-6} K^{-1}$ (Xu et al., 2008b). The applied macroscopic strain rate is $\dot{\varepsilon} = 5.5 \times 10^{-5} s^{-1}$ for all tests considered in the present paper. Values of the hardening parameters for various SCSs are determined by curve-fitting numerical simulations of uniaxial tension and compression along the ND as well as uniaxial tension along the RD to the corresponding experimental data. For the initial texture considered, uniaxial tension along the RD is used to estimate the hardening parameters associated with basal and prismatic slip since little twinning is expected. The hardening parameters associated with

extension twinning are determined from uniaxial tension along the ND, for which twinning is expected to contribute significantly to the deformation. Uniaxial compression tests along the ND were used to determine the hardening parameters for pyramidal slip, since basal and prismatic slip, as well as twinning, are not expected to contribute significantly to the deformation. Table 2.1 lists values of the material parameters for the various self-consistent polycrystal plasticity schemes. These values are used in all the simulations reported in the present paper. The critical resolved shear stresses and the Voce hardening parameters for the Meff=0.1 model listed in Table 1 are very close to those used by Xu et al. (2008c) ,who used the VPSC model (Lebensohn and Tomé, 1993).

Table 2.1 List of material parameters for various self-consistent models. The parameter $h^{ss'}$ denotes latent hardening effect of the slip/twin mode s' upon the other deformation mode s.

Model	Mode	τ_0	τ_1	h_0	h_1	Latent h^{sPr}	Latent h^{sBa}	Latent h^{sPy}	Latent h^{sTw}	A^{th1}	A^{th2}
Affine	Prismatic	95	35	120	35	2	1	1	14		
	Basal	155	10	30	0	1	1	1	1		
	Pyramidal	310	70	2200	280	1	1	2	1		
	Tensile Twin	260	70	460	360	1	1	1	2	0.15	0.45
Meff	Prismatic	100	44	500	50	2	1	1	9		
	Basal	160	30	120	0	1	1	1	1		
	Pyramidal	320	110	2600	30	1	1	2	1		
	Tensile Twin	250	10	600	80	1	1	1	2	0.15	0.45
Secant	Prismatic	85	20	40	28	2	1	1	14		
	Basal	150	10	20	10	1	1	1	1		
	Pyramidal	300	80	960	145	1	1	2	1		
	Tensile Twin	250	100	500	400	1	1	1	2	0.15	0.45
Tangent	Prismatic	110	50	530	45	2	1	1	8		
	Basal	180	30	100	10	1	1	1	1		
	Pyramidal	310	200	5200	0	1	1	2	1		
	Tensile Twin	237	60	120	40	1	1	1	2	0.15	0.45

We start by focusing on the macroscopic behavior of the material in terms of the stress-strain responses and R-values under uniaxial tension/compression along different

directions. Figures 2.2-2.4 present the measured and fitted stress-strain curves, the predicted R-values, and the relative activities of the various deformation mechanisms under uniaxial tension and compression along the ND, and under uniaxial tension along the RD, respectively. Figure 2.2a shows that the experimental stress-strain curve under uniaxial tension along the ND is fitted well by all the SCSs (i.e. the Affine, Secant, Meff=0.1 and Tangent self-consistent schemes). The predicted R-values shown in Figure 2.2b are all in reasonable agreement with the experimental value. The predicted relative activities of the various deformation mechanisms for the different SCSs are shown in Figures. 2.2c-f. The relative activity of a given plastic deformation mode is defined as the ratio of the plastic shear rate due to this plastic mode to the total plastic shear rate from all the plastic deformation modes considered. It is clear that basal and prismatic slips are the most important deformation mechanisms under tension along the ND. Since the material exhibits a typical basal texture, extension twinning can be easily activated in uniaxial tension along the ND. Tension twinning is found to be very active initially but then decreases gradually with further deformation. The predicted maximum twin volume fraction based on the Secant model is about 30%, while all the other models give a maximum value of around 20%. Figure 2.2 shows that the activity of pyramidal <c+a> slip is significant only in the Secant model.

Figures 2.2c-f show that tensile twinning accounts for almost 100% of the plastic deformation at very small strains (relative activity ~100%). Twinning is activated before any other deformation mode at small strains because the cooling process generates tensile residual stress along the ND in the majority of grains, corresponding to the {0002}

reflection in Table 2.2. As a result, the large majority of grains experience a tensile stress parallel to the *c*-axis which favors tensile twinning in the early stages of deformation. At very small strains, only tensile twinning contributes to plastic deformation, resulting in a corresponding very high relative activity even though the macroscopic strain is negligible. Thus, activity plots must be interpreted carefully especially at very small strains or during an elastic-plastic transition stage.

Table 2.2 List of the predicted and experimental thermal residual strains of different families along the RD,TD, and ND induced by the cooling process.

	0002	10-10 (20-20)	10-11	10-12	11-20	11-22	20-21
RD	1241.6 (1170)	-116.1 (-108)	245.6 (207)	705.3 (598)	-113.4 (-106)	343.8 (271)	-1.8 (-20.5)
TD	1062.9 (990)	-328.1 (-322)	23.2 (6.6)	463.9 (411)	-328.1 (-322)	102.9 (71)	-217 (-230)
ND	463.9 (430)	-960.1 (-936)	-709.7 (-699)	-265.6 (-317)	-959.8 (-961)	-618.3 (-579)	-880.5 (-889)

(Note: the values in the brackets are the corresponding experimental data taken from Xu (2007))

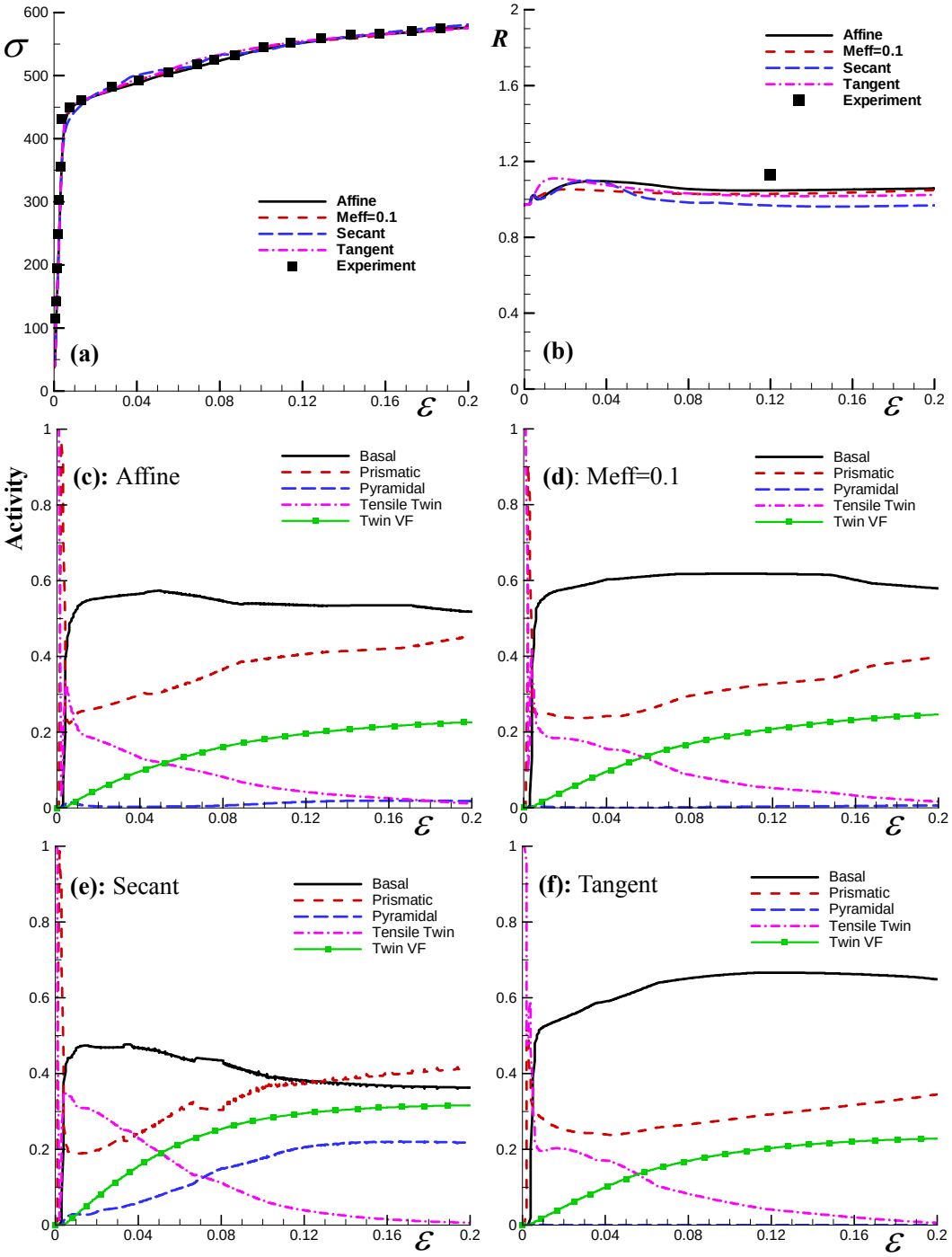

Figure 2.2 Fitted stress strain curves (a) and predicted R values (b) and activities (c-f) under tension along ND (NDT)

As shown in Figure 2.3a, the experimental stress-strain curve under uniaxial compression along the ND is fitted well by all the models. The predicted R-values agree well with the experiment, especially for the Affine model, which gives the best prediction (Figure 2.3b). The predicted relative activities of the various slip and twinning systems are presented in Figures 2.3c-f. Since the material has a typical basal texture, it is expected that extension twinning will contribute little during uniaxial compression along the ND. This trend is confirmed by all the models. The Affine and Meff=0.1 models exhibit quite similar relative activities: basal slip is the most active deformation mechanism during the entire deformation process; prismatic slip is also active but its activity decreases with continued straining, and the contribution of pyramidal slip increases gradually with loading. Basal slip (>80% at large strains), is predominant in the Tangent model, and the rest of the deformation is accommodated by prismatic slip. Almost no pyramidal slip is predicted up to a strain of 0.16. In contrast, the Secant model predicts that pyramidal slip is predominant. The activity of basal slip predicted by the Secant model is much less than predicted by the other models, especially the Tangent model.

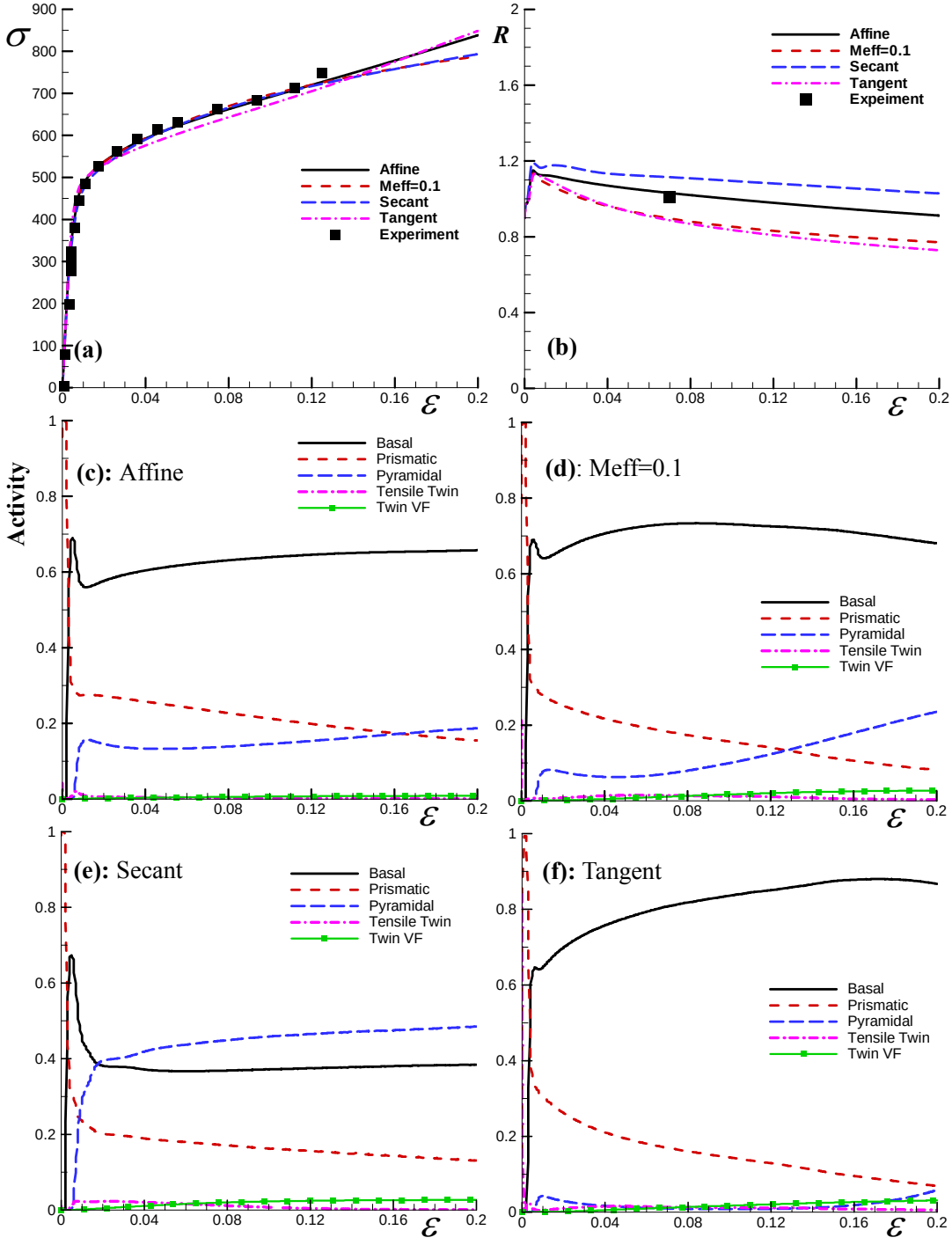

Figure 2.3 Fitted stress strain curves (a) and predicted R values (b) and activities (c-f) under compression along ND (NDC).

The measured and calculated macroscopic mechanical responses of the material under uniaxial tension along the RD are shown in Figure 2.4. All of the models capture the stress and strain curve well (Figure 2.4a). The measured R-value is in excellent agreement with the values obtained from the Meff=0.1 and Tangent models. The Affine model predicts the R-value reasonably well, but the Secant model significantly over-estimates the R-value. From Figures 2.4c-f, all the models predict that prismatic and basal slip are the primary and secondary deformation mechanisms, respectively, while tension twinning is inactive. Pyramidal slip contributes significantly in the Secant model but not in the other models.

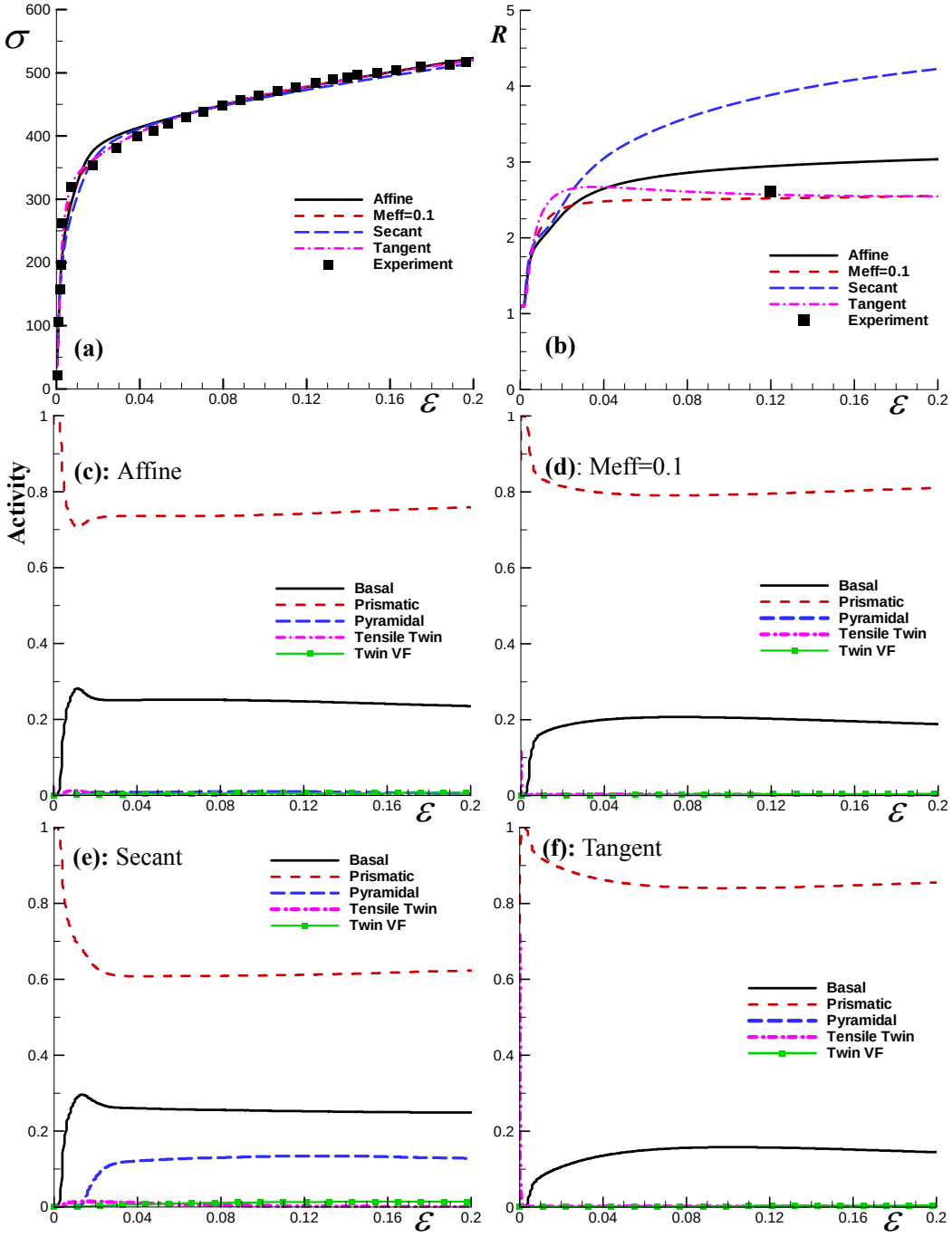

Figure 2.4 Fitted stress strain curves (a) and predicted R values (b) and activities (c-f) under tension along RD (RDT).

Figures 2.2-2.4 show that all the models fit the experimental flow curves reasonably well (Figures 2.2a, 2.3a and 2.4a). The Secant model gives the worst R-value prediction in the case of uniaxial tension along the RD, while the other models predict the measured R-values reasonably well.

Figure 2.5 shows the measured and predicted macroscopic stress-strain curves and R-values as well as the predicted relative activities of the various deformation mechanisms under uniaxial compression along the RD. The agreement between the predicted and measured macroscopic stress-strain curves is reasonable for all the models. However, all the models, especially the Secant model, significantly over-estimate the R-value. The predicted activities are found to be somewhat similar to those under uniaxial tension along the RD except that under uniaxial compression tension twinning becomes noticeable, especially in the Secant model.

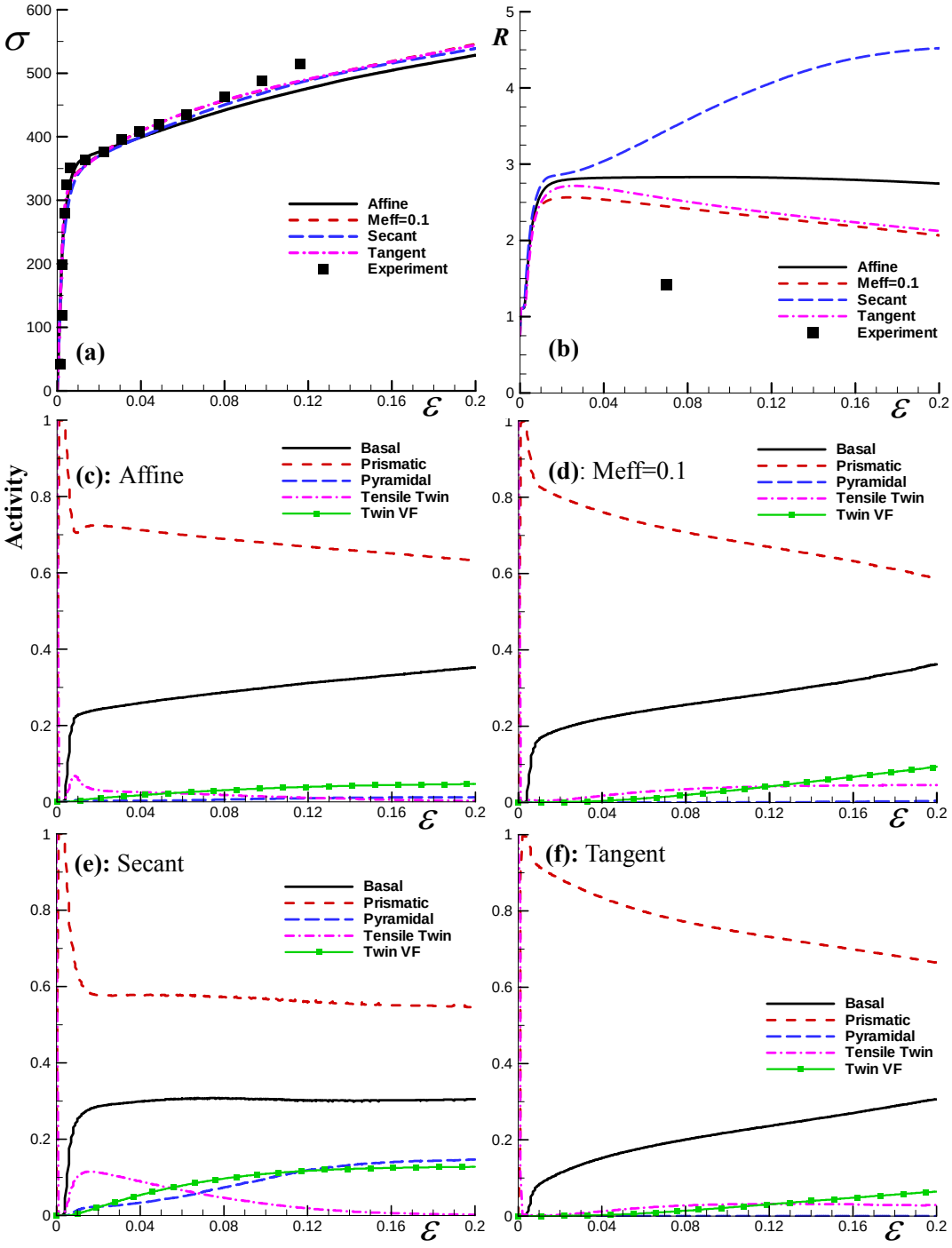

Figure 2.5 Predicted stress strain curves (a), R values (b) and activities (c-f) under compression along RD (RDC).

Figure 2.6 shows the measured and predicted stress-strain curves and R-values under uniaxial tension along the transverse direction (TD). The Meff=0.1 and Tangent models predict the flow curve well, while the Affine and Secant models noticeably under-estimate the flow curve. Under uniaxial tension along the TD, the Affine model predicts the R-value very well; the Meff=0.1 and Tangent models under-estimate the R-value, while the Secant model significantly over-estimates the R-value. The corresponding results for uniaxial compression along the TD are presented in Figure 2.7. All the models give similar flow curves and clearly over-estimate the flow curve beyond a strain ~0.08. The Tangent and Meff=0.1 models predict the R-value well, while the Affine and Secant models over-estimate the R-value, especially the Secant model. The predicted relative activities under uniaxial tension and compression along the TD are very similar to those under uniaxial tension and compression along the RD (see Figures 2.4 and 2.5), respectively, and thus are not presented here.

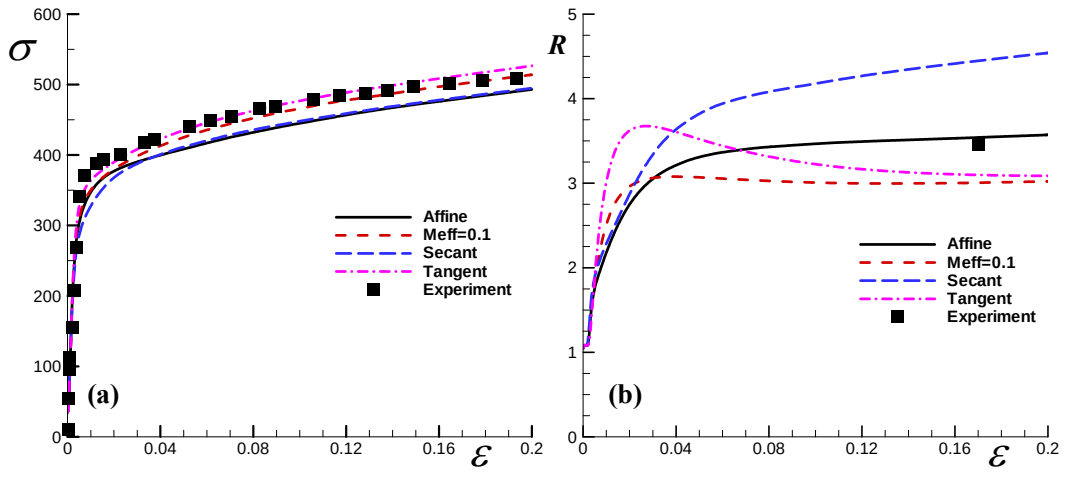

Figure 2.6 Predicted stress strain curves (a) and R values (b) under tension along TD (TDT).

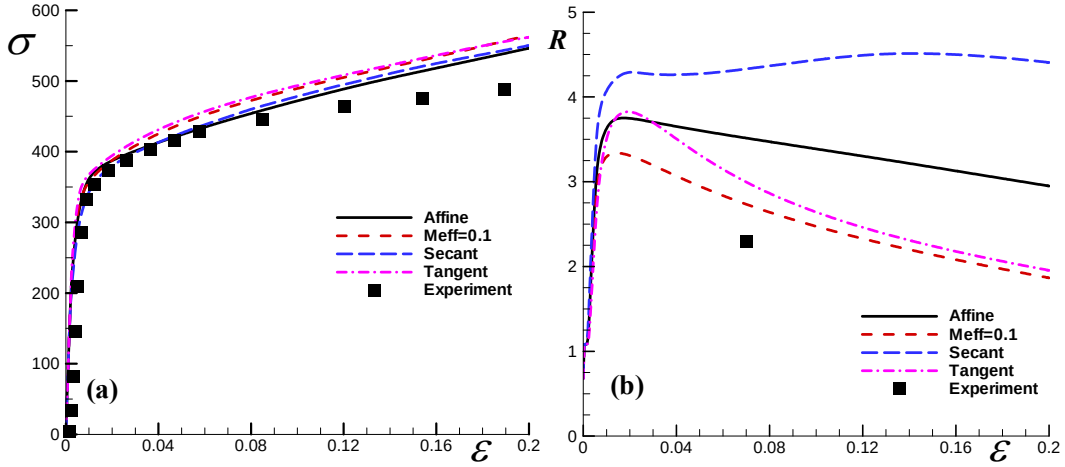

Figure 2.7 Predicted stress strain curves (a) and R values (b) under compression along TD (TDC)

Based on the flow curves and R-values shown in Figures 2.2-2.7, it is evident that the Secant model is significantly worse than the other models, and that it is difficult to distinguish between the Affine, Meff=0.1 and Tangent models. The evolution of the elastic lattice strains during loading in different grain orientations can be used as a very sensitive indicator of plastic deformation mechanisms at the microscopic level (see e.g., MacEwen et al., 1983, 1989; Gharghouri et al., 1999; Daymond and Priesmeyer, 2002; Xu et al., 2008b). Since the lattice strain evolution is sensitive to the constitutive model employed, it is expected that the choice of self-consistent scheme will have a significant influence on the predicted lattice strain evolution, hence providing a quantitative measure to evaluate self-consistent methodologies. We therefore use lattice strain data to evaluate the relative qualities of the Affine, Meff=0.1 and Tangent models. Our numerical lattice strain results for the Secant model are much worse than for the other models and are therefore not presented here. It is worth mentioning that lattice strain analyses are usually

preformed for various specific families of crystallographic planes. These grain families are used because they are the ones for which experimental lattice strain data are available.

The thermal residual strains induced during the cooling process have a great effect on the lattice strain evolution during subsequent loading. The thermal strain effect has been included in our EVPSC model to deal with the cooling process from 898 K to 298 K. The predicted thermal residual strains for different grain families along the RD, TD, and ND are listed in Table 2.2; the experimental data (Xu, 2007) are also provided for comparison. The unit of lattice strain in Table 2.2 and Figures 2.8-2.11 is microstrain (10^{-6}). The lattice strains in Figures 2.8-2.11 are reported relative to the residual strains in Table 2.2, and are thus shown with a starting value of zero.

Figure 2.8 compares the measured and predicted lattice strains during uniaxial tension along the ND (NDT). In Figure 2.8, the first index "NDT" in the notation "NDT/RD" indicates that the material is under uniaxial Tension along the ND, and the second index "RD" denotes that the lattice strains are along the RD. Similarly, the notation "RDC/TD" in Figure 2.11 is for lattice strains along the TD in the case of uniaxial Compression along the RD. Figure 2.8 shows that the material starts to deform plastically at a stress of ~250 MPa, as indicated by the deviations of the stress-lattice strain curves from linearity. However, the apparent yield stress from the macroscopic stress-strain curve is ~450MPa. This implies that at a stress of around 250 MPa some soft grains start to deform plastically, while other hard orientations are still elastic. This phenomenon is called micro-yielding. At a stress of about 450 MPa most of the grains deform plastically and the polycrystal is macroscopically in a plastic state.

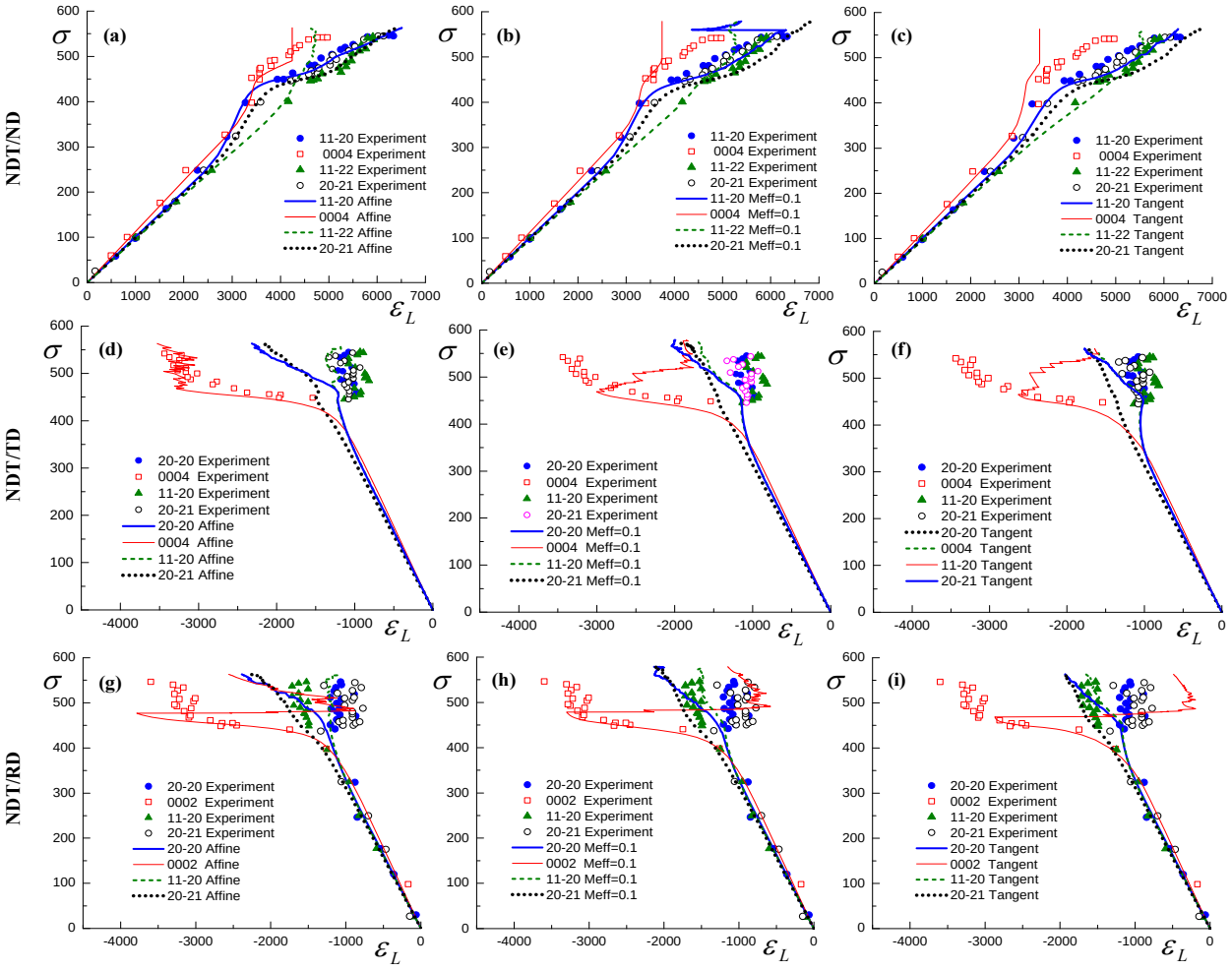

Figure 2.8 Predicted and experimental lattice strains along the ND, TD, and RD under uniaxial tension along ND (NDT).

Figures 2.8a-c show experimental and calculated lattice strains along the ND based on the Affine (Figure 2.8a), Meff=0.1 (Figure 2.8b) and Tangent (Figure 2.8c) models, respectively. Generally speaking, all the models successfully reproduce the trends in the lattice strain data. The response of the {0004} grain family is very well captured up to a stress of 500 MPa (a macroscopic strain of about 0.055), after which the predicted {0004} lattice strains cease to evolve because the models predict that the grains within this family

have been completely reoriented due to twinning. Beyond this strain, tensile twinning still contributes to plastic deformation in some of the other grain orientations modeled, as revealed in Figures 2.2c-f which show that tensile twinning activity is finite in the strain range $0.055 < \varepsilon < 0.120$. Indeed, though the {0004} grain family is the one most favorably oriented for tensile twinning, other grain families in which the *c*-axis is less than ~45° from the applied stress axis can also be expected to undergo twinning.

When considering uniaxial tension along the ND (NDT) but for lattice strains measured along the TD (NDT/TD; Figures 2.8d-f) and RD (NDT/RD; Figures 2.8g-i), the predicted lattice strain curves for the {0004} family show clear relaxation effects at a stress of ~470 MPa for all the models. This relaxation is caused by the sudden twinning-related reorientation of grains having the c-axis along the ND. Some reoriented grains align their c-axis in the RD or TD. The stress state in the twinned material becomes highly compressive with further straining along the ND. For all the models, the abrupt change in the {0004} family in the case of NDT/RD is more pronounced than for NDT/TD because initially there are more {0004} poles aligned along the TD than RD; as a result, more material is reoriented by twinning to the RD than the TD. This poor agreement between the simulations and experiments is mainly caused by the employed PTR twinning scheme, where the whole grain is suddenly reoriented once a threshold value of twin volume fraction is reached. Similarly, the poor agreement observed in the lattice strain evolution of the $\{20\bar{2}0\}$, $\{11\bar{2}0\}$, and $\{20\bar{2}1\}$ families is also due to the PTR twinning scheme applied in the present study. A much more gradual evolution of the lattice strain of the {0004} family was reported by Xu et al (2008b) for the same material.

However, the reorientation due to twinning was not accounted for in their study. Generally speaking, all the models give similar lattice strain results except that the Affine scheme does not show excessive relaxation in the NDT/TD curves.

Figure 2.9 presents the predicted and measured lattice strains under compression along the ND (NDC). For the NDC/ND lattice strains, it is clear that all the models fail to reproduce the lattice strain data for the $\{10\bar{1}0\}$ grain family. The volume fraction of these grains is very small at the start of the test due to the initial rolling texture, and can be expected to decrease further during the course of the test as a result of tensile twinning since they are compressed normal to the c-axis. These grains can thus be considered as isolated soft inclusions in a hard matrix since they are favorably oriented for tensile twinning while the majority of grains are unfavorably oriented for tensile twinning. As a result, the experimental data show strong relaxation effects as these grains twin and transfer their load to their hard neighbors at an applied stress of ~-300 MPa. All of the models incorrectly predict the applied stress at which these grains start to shed load, and also underpredict the extent of the relaxation associated with tensile twinning. Furthermore, at an applied stress of ~-500 MPa, all the models predict that these grains resume loading, in contrast to the trend exhibited by the experimental data. These poor simulation results occur because the models cannot handle strong local neighborhood effects which dominate the behavior of small grain families. Fortunately, since this grain family represents only a small component of the microstructure, failure to capture its behavior does not unduly affect the ability of the simulations to adequately capture the macroscopic flow behavior or the behavior of the other larger grain families. It is found

that the predicted results for the $\{0002\}$, $\{10\bar{1}2\}$ and $\{10\bar{1}1\}$ diffraction families by the Affine model are in good agreement with the experiments both qualitatively and quantitatively. On the other hand, the predictions of the Meff=0.1 and Tangent models are in poor agreement with the experiments, especially for the $\{10\bar{1}1\}$ family. For the lattice strains along the TD (NDC/TD; Figure 2.9d-f) and RD (NDC/RD; Figure 2.9g-i), the Meff=0.1 model gives the best prediction for the $\{0002\}$ family for NDC/TD, while the Affine model shows the worst prediction of this family. All models give reasonable agreement between the predictions and experiments for the other families. From Figure 2.9, it seems that the Tangent scheme gives the worst predictions.

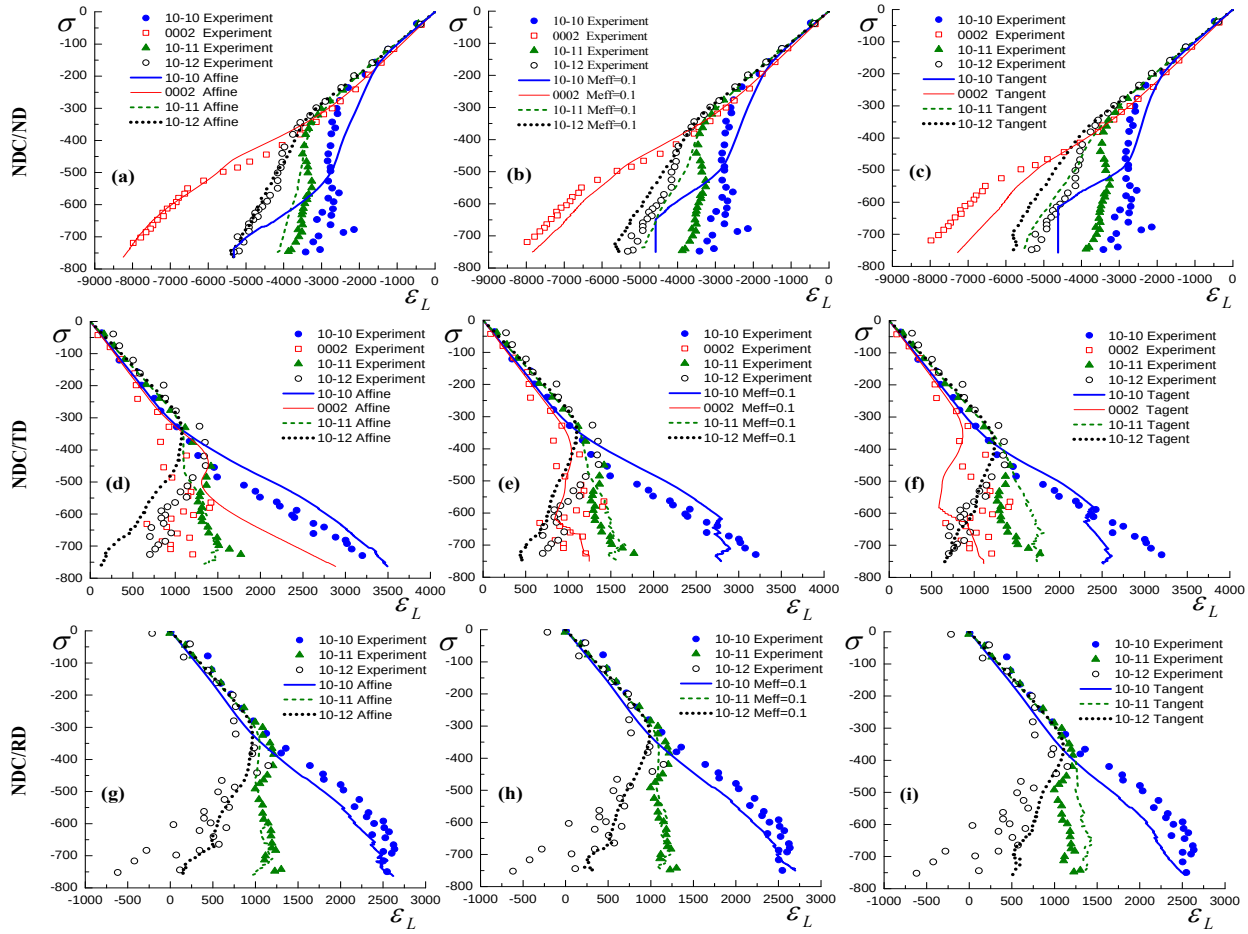

Figure 2.9 Predicted and experimental lattice strains along the ND, TD, and RD under uniaxial compression along ND (NDC).

The lattice strain evolution in the material under uniaxial tension (Figure 2.8) and compression (Figure 2.9) along the ND should correlate with the activities of deformation mechanisms shown in Figures 2.2 and 2.3, respectively. The activation of tensile twinning under uniaxial tension along the ND makes the {0004} family elongate plastically along the c-axis and therefore the {0004} family carries less ND lattice strain than the other families. Under uniaxial compression along the ND, the {0004} family carries more ND lattice strain due to the polar nature of twinning, and the fact that the critical resolved

shear stress for pyramidal slip is quite high. In addition, during compression along the ND, the $\{10\bar{1}1\}$ and $\{10\bar{1}2\}$ families can plastically accommodate the deformation along the ND through the activation of the basal and prismatic slip, which results in these families carrying less ND lattice strain than the {0004} family.

Figure 2.10 shows the predicted and measured lattice strains under tension along the RD (RDT). Along the loading direction of RD (RDT/RD; Figure 2.10a-c), the lattice strain variations for the different diffraction families can be reproduced by all the models. Along the two lateral directions (Figures 2.10d-i), the Affine model gives the best prediction. The Meff=0.1 and Tangent models clearly underestimate the load bearing of the {0002} family in the RDT/TD, and also depart from the positive shifts exhibited by the lattice strain in the $\{11\bar{2}0\}$, $\{20\bar{2}1\}$ and $\{11\bar{2}2\}$ families. The $\{20\bar{2}0\}$, $\{11\bar{2}0\}$, $\{11\bar{2}2\}$ and $\{20\bar{2}1\}$ grain families, corresponding to lattice strains measured along the loading direction, have orientations for which it is easy to activate either prismatic or basal slip and therefore their lattice strains do not depart much from simple linear behavior. For TD/ND, the {0002}/{0004} family is the hardest one because pyramidal slip and twinning are difficult to activate and thus contribute very little. These observations are consistent with the predicted activities of the various deformation mechanisms in Figures 2.4c, 2.4d and 2.4f.

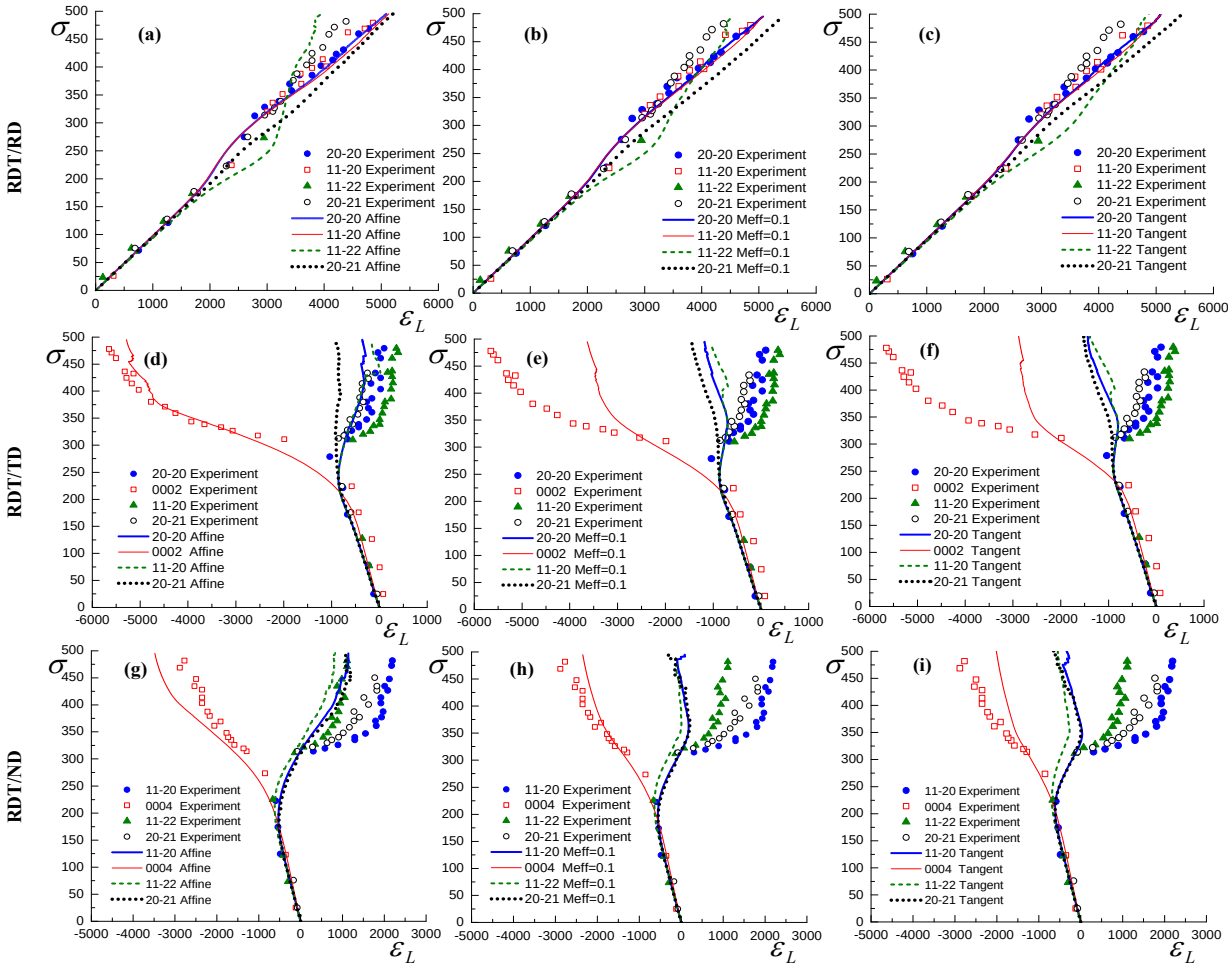

Figure 2.10 Predicted and experimental lattice strains along the RD, TD, and ND under uniaxial tension along RD (RDT).

Figure 2.11 compares the predicted lattice strain developments under compression along the RD (RDC) to the experimental ones. Along the loading direction (RDC/RD), the sudden increase in lattice strain in the {0002} family at an applied stress of ~370 MPa (strain ~0.02) in the experiment is due to grain reorientation by twinning. The Affine model gives a good agreement between predictions and experiments after stress ~400 MPa, where some grains are reoriented to the {0002} family by the PTR twin scheme,

although the relative intensity is small. The Meff=0.1 and Tangent models predict the general trends too but with a less good agreement. In addition, the Affine model shows the best agreement with the experiment for the $\{10\bar{1}1\}$ family. All models predict well the lattice strain of the $\{10\bar{1}0\}$ family before the macroscopic yield stress ~350 MPa (strain ~0.01). Beyond this applied stress, the lattice strains in the $\{10\bar{1}0\}$ family are overestimated by all the models. As shown in Figures 2.5c-f, a decrease in prismatic activity and an increase in basal activity were predicted by all the models. Therefore, the $\{10\bar{1}0\}$ family, relaxing through prismatic slip, should become plastically harder and exhibit larger lattice strains under further straining. Also, the $\{10\bar{1}1\}$ and $\{10\bar{1}2\}$ families which undergo increased basal activities should become softer and exhibit smaller lattice strain. In the TD and ND directions (Figures 2.11d-i), the Meff=0.1 model gives a much better prediction than the Affine and Tangent models for all examined families. From Figure 2.11, it seems that the Meff=0.1 model gives the best predictions.

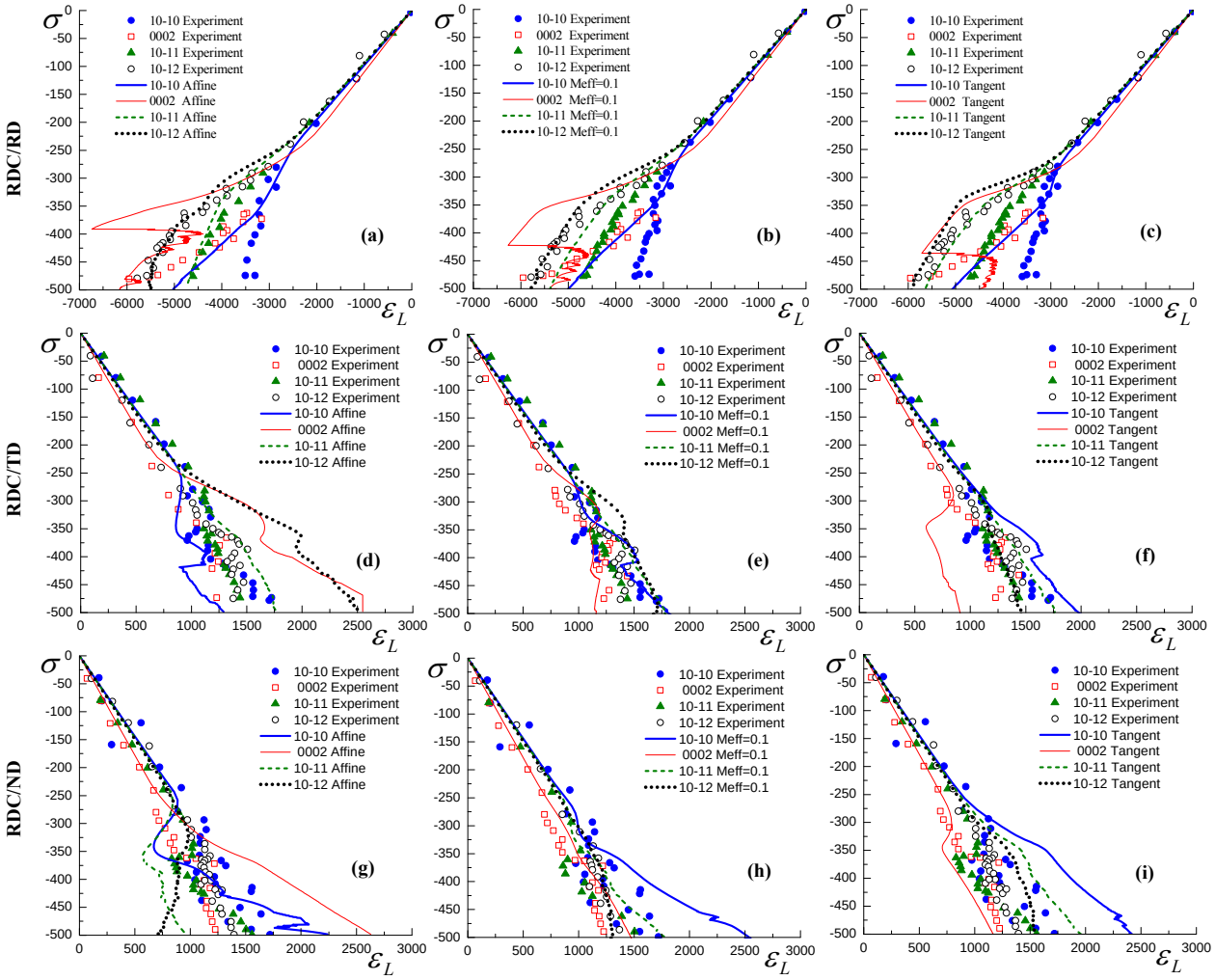

Figure 2.11 Predicted and experimental lattice strains along the RD, TD, and ND under uniaxial compression along RD (RDC).

As mentioned by Xu et al. (2009), the VPSC model does not capture the development of texture coefficients for some of the basal and prismatic planes when significant twinning occurs. Therefore, we have further evaluated the models in terms of the evolution of texture coefficients in the material under uniaxial tension along the ND and uniaxial compression along the RD. However, our numerical results indicated that

there was no clear evidence that showed one model was better than the others in predicting the evolution of texture coefficients.

Based on the above discussion in terms of stress-strain curves, R-values, and evolutions of lattice strains and texture coefficients, we can conclude that the Affine and Meff=0.1 models give much better performance than the Secant and Tangent models. However, there is no clear evidence to show which is best among all the models. This finding is not consistent with the previous studies on magnesium alloys (Wang et al., 2010b; Askari et al., 2013). Wang et al. (2010b) concluded that the Affine self-consistent scheme gave the best overall performance among the SCSs examined, while Askari et al. (2013) preferred to employ the Tangent self-consistent approach. Note that the lattice strain evolution of the same material has been simulated by Xu et al. (2008a) using the EPSC model, by Mareau and Daymond (2010) using their EVPSC model, and by Abdolvand et al. (2011) and Abdolvand and Daymond (2012) based on CPFEM. Although the main purpose of this study is to evaluate the various self-consistent schemes (SCSs), it is found that the predictions based on the EVPSC model with the Affine and Meff=0.1 schemes are at least not worse than those based on the above mentioned models for the Zircaloy-2 slab.

2.4 Conclusions

In this study, the EVPSC model proposed by Wang et al. (2010b) has been improved by incorporating the thermal deformation effect to account for the effects of thermal residual strains generated during initial cooling process on subsequent mechanical loading of a Zircaloy-2 slab. Various self-consistent schemes used in the

modified EVPSC model have been evaluated in terms of the quality of predictions of the macroscopic behaviors of stress-strain curves and R-values and the microscopic behaviors of evolution of lattice strains and texture coefficients. The deformation mechanisms of prismatic, basal, first order pyramidal <c+a> slips and tensile twinning are chosen to accommodate the plastic deformation. The material parameters involved in the Voce-law hardening and latent hardening are obtained by adjusting to fit three sets of experimental stress strain curves (tension/compression along the ND and tension along the RD). It has been demonstrated that, among the models examined, the EVPSC model with the Affine and Meff=0.1 self-consistent schemes give much better performance for the Zircaloy-2 slab than the Secant and Tangent SCSs.

The main purpose of this study is to evaluate the quality of various homogenization methods for polycrystalline materials. The effect of the behavior of the single crystal is eliminated as much as possible by using the same single crystal description. More specifically, the slip/twinning hardening is described by (7) and (8) and twinning is characterized by the PTR model. Of course, the evaluation made in the present paper depends on the single crystal plasticity linearization employed. The mismatch between predictions and experiments in the cases where twinning is significant strongly suggests that a more realistic and accurate twinning model is required. Wang et al. (2012b, 2013a) have recently proposed a physically based twinning and detwinning (TDT) model. The TDT model, together with the EVPSC model, has been successfully used to study the twinning behaviors of Mg alloys under various monotonic and strain-path changes (see Guo et al., 2013; Lee et al., 2014; Qiao et al., 2015b; Wang et al., 2013c; Wu et al., 2014).

We have very recently applied the EVPSC-TDT model to study the mechanical behavior of Zr alloys. Our preliminary results seem to be very promising. This work is in progress and will be reported elsewhere.

Chapter 3. Modeling twinning and detwinning behavior of Mg alloy ZK60A during monotonic and cyclic loading

3.1 Introduction

The phenomenon of detwinning has been known for many years (Obreimov and Startsev, 1959; Cooper, 1962). Indeed, detwinning of martensite is one of the key mechanisms upon which the shape memory phenomenon is built (e.g., Miyazaki et al. 1989a, 1989b; Liu and Xie, 2003). In short, detwinning is actually twinning of the twinned crystal back into the orientation of the parent material from which it came. In some cases, this process involves reverse motion of the boundaries which surround the original twin, denoted stage C in the presently employed Twinning-DeTwinning (TDT) model (Wang et al., 2012b, 2013a, 2013c). In other cases, it actually involves the nucleation of a new twin (with the parent orientation) within the original twin (denoted stage D in the TDT model, Wang et al., 2012b, 2013a, 2013c).

In the context of Mg alloys, it was the recent work of Cáceres et al. (2003) which made the research community pick up this topic again. Cáceres et al. (2003) were interested in the pseudoelastic behavior of cast alloy AZ91. Shortly thereafter, Kleiner and Uggowitzer (2004) showed that the phenomenon was not strictly limited to anelastic loading/unloading conditions at low strains. They showed that a rather unique stress-strain response during reverse loading was observed in textured alloy AZ61 subjected to larger strains which induced twinning. The work of Lou et al. (2007) generated a great deal of interest, both from materials scientists interested in measuring the phenomenon in-

situ (Muransky et al., 2008; Jain et al., 2007; Wu et al., 2008a, 2008b) and from members of the mechanics community which became interested in constitutive modeling (discussed below). The work of Lou et al. (2007) is experimentally significant for two reasons: first, because it made use of novel testing equipment, permitting relatively thin sheets to be tested in in-plane compression to considerable levels of strain without buckling (Boger et al., 2005) and second, because it employed acoustic emission (AE) which provided clues about the relation between the twinning-detwinning phenomenon and nucleation events. Later research coupled the AE technique with in-situ neutron diffraction (ND) so that both twin nucleation and growth could be monitored simultaneously (Muransky et al., 2010a).

The constitutive modeling efforts have followed two main streams. One stream developed analytical phenomenological models (e.g., Lee et al., 2008; Li et al., 2010; Kim et al., 2013) which are easier to implement within finite element modeling codes. The other stream took a crystal plasticity modeling approach: Proust et al. (2009) and Guillemer et al. (2011) employed self-consistent approaches, Hama and Takuda (2012) employ a finite element crystal plasticity-based approach, and Gu et al. (2014) recently employed a full-constraints Taylor-Lin model. A consistent feature of these models is a failure to capture the significant distinction in the shape of the flow curve during twinning- and detwinning-dominated flow. In the former case, yielding can be rather abrupt (approaching elastic-perfectly plastic). Recent authors have associated the yield plateau observed during testing of textured Mg alloys along certain directions with Lüders banding (Muransky et al., 2010b; Barnett et al., 2012). While the phenomenological

models often capture this sharp yielding behavior, most crystal plasticity models fail to capture sharp initial yielding phenomenon. Additionally, even when initial yielding by twinning is experimentally observed to be abrupt, the reverse-yielding due to detwinning is often observed to be quite gradual. In some respects, it is reminiscent of a classic Bauschinger (1886) effect. However, both types of model generally fail to capture the very gradual reverse yielding phenomenon.

As was recently introduced by Beyerlein and Tomé (2008) and subsequently employed in work which additionally stressed the stochastic nature of twin nucleation (e.g., Capolungo et al., 2009; Beyerlein and Tomé, 2010; Niezgoda et al., 2014), the present study employs a lower critical resolved shear stress for twin boundary motion (twinning or detwinning) relative to twin nucleation provides. We show that this provides a good description for the behavior observed experimentally using the in-situ neutron diffraction technique. Notably, it enables modeling of the sharp yielding behavior during initial twinning and the comparatively gradual yielding behavior during detwinning. Further, favorable comparison is made with the intensity changes and internal strain evolution observed in-situ. The intensity changes provide a measure of the volume fraction of twinning and the internal strain developments provide another constraint for the selection of model parameters governing the various deformation mechanisms. There are outstanding features in the data, which have yet to be modeled, and these opportunities for further improvement are highlighted.

3.2 Modeling Approach

3.2.1 Crystal plasticity

The polycrystal is modeled using a mean-field micromechanical homogenization approach which involves self-consistently determining the responses of both the aggregate and the large number of discrete volume weighted "grains" from which it is composed. The orientations and weights of the individual grains are selected to model an experimentally measured crystallographic texture using the POLE8 software (Tomé, 2007). As such, there is no knowledge of the immediate neighborhood of individual grains, nor is there any attempt to model the neighborhood dependence of the response. Rather, the interaction between the individual grain and the surrounding homogeneous effective medium is regarded as adequate to capture the constitutive response of interest.

The details of the particular elasto-viscoplastic self-consistent (EVPSC) approach employed have recently been published in detail (see Wang et al., 2010a). In short, the approach of Molinari and coworkers (Kouddane et al., 1993; Molinari et al., 1997; Mercier and Molinari, 2009) and Li and Weng, (1997, 1998a, 1998b) is employed to additively decompose the elastic and viscoplastic portions of the deformation rate tensor, $\boldsymbol{d}$. The elastic portion, $\boldsymbol{d}^e$, is linked with the Cauchy stress rate via the elastic compliance tensor, $\boldsymbol{M}^e$, while the viscoplastic portion, $\boldsymbol{d}^{vp}$, is linked to the Cauchy stress itself via an instantaneous (linearized) viscoplastic compliance tensor, $\boldsymbol{M}^{vp}$.

$$\boldsymbol{d} = \boldsymbol{d}^e + \boldsymbol{d}^{vp} = \boldsymbol{M}^e : \dot{\boldsymbol{\sigma}} + \boldsymbol{M}^{vp} : \boldsymbol{\sigma} + \boldsymbol{d}_0 \tag{3.2.1}$$

with $\boldsymbol{d}_0$ being back extrapolated term. One can link the grain-level response to that of the surrounding homogeneous (anisotropic) matrix separately, for each of these portions (elastic and viscoplastic). The homogenization of the viscoplastic portion follows the approach of Molinari et al. (1987) and Lebensohn and Tomé (1993), while the elastic problem follows the approach of Nemat-Nasser and Obata (1986).

$$\boldsymbol{d} - \boldsymbol{D} = -\widetilde{\boldsymbol{M}}^{e} : \left(\dot{\boldsymbol{\sigma}} - \dot{\boldsymbol{\Sigma}}\right) - \widetilde{\boldsymbol{M}}^{vp} : \left(\boldsymbol{\sigma} - \boldsymbol{\Sigma}\right) \tag{3.2.2}$$

where $\boldsymbol{D}$ and $\boldsymbol{\Sigma}$ are the strain rate and the Cauchy stress for the effective medium, respectively. $\widetilde{\boldsymbol{M}}^{e}$ is the so-called elastic interaction tensor, which is a function of the surrounding medium elastic compliance and the ellipsoidal shape of the inclusion. Similarly, $\widetilde{\boldsymbol{M}}^{vp}$ is the linearized viscoplastic interaction tensor, which is a function of the medium viscoplastic compliance and the shape of the inclusion. This combined elasto-viscoplastic interaction equation is the same as that developed by Turner et al. (1994) and shown to be valid for the case of a linear elastic-linear (Newtonian) viscoplastic material, i.e. the Maxwell solid. For the present, we assume that this equation remains valid for the non-linear (high power law exponent) viscoplastic response used to model low temperature behavior of metals. This permits the following independent self-consistent equations for the homogeneous elastic ($\overline{\boldsymbol{M}}^{e}$), viscoplastic ($\overline{\boldsymbol{M}}^{vp}$) compliances, and back-extrapolated term ($\boldsymbol{D}^{0}$) to be developed:

$$\overline{\boldsymbol{M}}^{e} = < \boldsymbol{M}^{e} \boldsymbol{B}^{e} > \tag{3.2.3a}$$

$$\overline{\boldsymbol{M}}^{vp} = < \boldsymbol{M}^{vp} \boldsymbol{B}^{vp} > \tag{3.2.3b}$$

$$\boldsymbol{D}^{0} = < \boldsymbol{M}^{vp} \boldsymbol{b} + \boldsymbol{d}^{0} > \tag{3.2.3c}$$

where $\boldsymbol{B}^e$ and $\boldsymbol{B}^{vp}$ (and $\boldsymbol{b}$) are the elastic and viscoplastic concentration tensors which relate the medium stress rate and stress to the inclusion stress rate and stress, respectively.

3.2.2 Grain level response

The kinematics of slip-based crystal plasticity have been published many times (e.g. Asaro and Needleman, 1985), so only the highlights are given here. The plastic deformation rate, $\boldsymbol{d}^p$, within a given crystal is the sum of that due to each of the individual slip systems, α.

$$\boldsymbol{d}^p = \sum_{\alpha} \dot{\gamma}^{\alpha} \boldsymbol{P}^{\alpha} \tag{3.2.4}$$

where $\boldsymbol{P}^{\alpha}$ is the Schmid tensor, corresponding to shear rate, $\dot{\gamma}^{\alpha}$, on a given crystallographic plane in a given crystallographic direction. The power-law viscoplastic constitutive rule provides a relationship between the resolved shear stress within the crystal.

$$\tau^{\alpha} = \boldsymbol{P}^{\alpha} : \boldsymbol{\sigma}^c \tag{3.2.5}$$

and the resulting shear rate $\dot{\gamma}^{\alpha}$ ($\boldsymbol{\sigma}^c$ is the Cauchy true stress acting on the crystal.)

$$\dot{\gamma}^{\alpha} = \dot{\gamma}_0 \left| \tau^{\alpha} / \tau_{cr}^{\alpha} \right|^{\frac{1}{m}} \operatorname{sgn}\left(\tau^{\alpha}\right) \tag{3.2.6}$$

The constants $\dot{\gamma}_0$ and τ_{cr}^{α} are the reference shear rate and critical resolved shear stress for the slip system α. The sgn operation simply determines the direction of straining with respect to the stressing direction. This seemingly innocuous final point will be critical as concerns twinning. The rate sensitive approach is used for expediency, rather than

attributing physical meaning to the particular value of the rate sensitivity employed. As highlighted by many previous authors (e.g., Asaro and Needleman, 1985), the power law relation provides a solution to the so-called ambiguity problem by offering a unique relationship between the stress and the straining direction. Using high power law exponents, as required for describing room temperature behavior of most metals, causes numerical problems (i.e., very stiff matrices as noted by Bronkhorst et al., 1992). A possible solution to this conundrum was proposed by Kok et al. (2002) and by ascribing the imposed strain rate in the test to the reference rate constant, $\dot{\gamma}_0$, they effectively eliminate the overall rate sensitivity implied by the relationship.

During each straining step, initial guesses are made for the elastic and viscoplastic compliances of the homogeneous matrix and then self-consistency is solved iteratively (per Eq. 3.2.3). The initial guesses for each straining step are the converged results of the previous straining step except the very first straining step, for which we employ the upper bound, Voigt estimate, for elasticity and a value close to zero (e.g. 1×10^{-10}) for viscoplasticity. The latter assumption is good for any of the common linearization strategies employed in self-consistent codes (e.g. tangent, secant, or affine) and power law viscoplasticity (Eq. 3.2.6).

3.2.3 Twinning model*

* The model was developed to describe phenomena associated with {10.2} tension twinning in HCP crystals. However, the principles are expected to be applicable to deformation twinning more generally, particularly those cases for which twin boundary migration is easy.

In the present TDT model, the deformation processes of twinning and de-twinning can take place by four operations as illustrated in Figure 3.1:

A. twin initiation (which here comprises nucleation and propagation phases),

B. twin growth,

C. twin shrinkage, and

D. re-twinning (initiation of a twin with the parent orientation within the twin.)

Note that operation D is actually a subset of a broader class of secondary twinning operations, which include twinning of all possible variants within the twins.

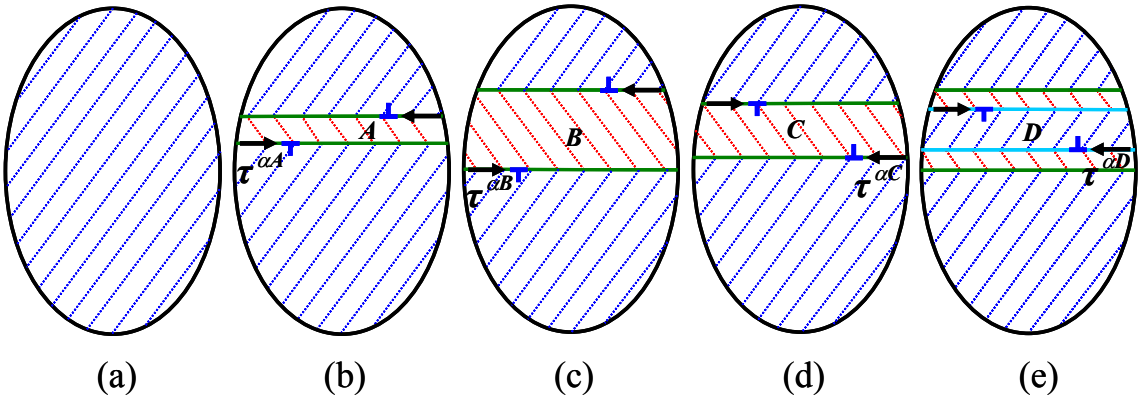

Figure 3.1 Schematic representation of twinning and detwinning in a grain, after Wang et al. (2012b). (a) The grain is twin-free and is called the matrix in the text. (b) The grain undergoes twin initiation (Operation A) resulting in a twin band (called twin). Solid green lines represent twin boundaries (TBs). Lattices in the matrix (represented by blue lines) and twin (red lines) are crystallographic mirrors of one another. (c) Operation B is growth of the twin, thereby consuming the matrix. (d) Operation C is the reverse of operation B, involving propagation of the TBs back into the twin, causing growth of the matrix. (e) Operation D is another means of shrinking the twinned region through twin nucleation within the existing twin back into the orientation of the original matrix (hence the blue dotted lines).

Starting with a twin-free grain (referred to as 'matrix') in Figure 3.1a, the grain starts twinning on variant α (Figure 3.1b) when the resolved shear stress (RSS) in the matrix,

equals the critical resolved shear stress (CRSS) for operation A (τ_A). The grain is then split into a twinned domain (twin) and an un-twinned domain (matrix). The corresponding crystallographic lattices are mirrored across the twin boundary (TB) plane. When it is stated that a grain is "split," note that an entirely new "grain" is introduced into the self-consistent formulation to represent each twin variant that is activated, with a volume fraction corresponding to the amount of shear that has been accumulated during that straining step. Note further that the newly formed twin grains are free to undergo slip according to the same laws as the matrix grains. At this point, secondary twinning (twinning within the twins) is not accounted for, since this would lead to a proliferation of grains. The stress level in the newly formed grains is determined by the self-consistent algorithm and requires no assumptions. The accumulated shear strain (or strain hardening state) within the twin domain reset to zero.

Due to the polar nature of twinning, the initial twinning event can only produce shear in the forward (twinning) direction. It is clear that the Cauchy stress acting on the matrix must be used to calculate the RSS of twin initiation because the twin is not born yet. The RSS acting on the twinning system is calculated in the same way as for slip Eq. (3.2.4), and must be positive for twin nucleation to take place. In the present modeling scheme, no differentiation is made between twin nucleation and the rapid propagation (presumably at speeds approaching the speed of sound) across the matrix grain; this is denoted operation A. After this operation, twin growth (thickening) will occur when the RSS on the twinning system exceeds τ_B, the CRSS for twin growth, termed operation B. It is generally understood that the CRSS for twin growth is less than or equal to that required

for initiation (Venables 1964; Partridge 1967; Christian and Mahajan, 1995; Christian, 2002).

A key feature of the TDT model is an acknowledgement that the driving force for twin growth is provided by stresses acting on the twin boundary (TB) and the strategy employed is designed to approximate this reality. "Because the model is implemented within an effective medium approximation, it does not provide the local stresses at the TB, only the average stress in the ellipsoids that represent matrix and twin." (Wang et al. 2012b) Thus, the Cauchy stress acting on the matrix grain and that acting on the new twin grain are both interrogated to assess the level of twin growth which may occur within a given straining increment. This is a key feature, which permits the model to describe the strain hardening plateau that is often observed when twinning is the primary strain accommodation mechanism. Other modeling strategies have not succeeded in predicting a strain hardening plateau without resorting to ad hoc solutions, such as delaying the reorientation associated with twinning until after the plateau is complete (e.g. Agnew et al., 2001) or adopting a very low CRSS value for prismatic slip when twinning is the dominant mechanism (Clausen et al., 2008; Muransky et al, 2009). The former is known to be a poor representation, given all of the in-situ (and ex-situ) data which has been developed for twin volume fraction, f^{tw}, as a function of strain (e.g., Brown et al., 2005; Muransky et al., 2009; Lou et al., 2007). These data have unequivocally shown that f^{tw} is rapidly increasing throughout the plateau region. The suggestion of Clausen et al. (2008), that prismatic slip in Mg is strongly sensitive to the applied pressure (such that

tensile and compressive responses would be so asymmetric), has failed to develop experimental support.

The lowering of the parameter describing prismatic slip strength during compression testing adopted by Clausen et al. (2008) has since been proven unnecessary by Wang et al. (2013a), though a number of recent papers have repeated this error as they reanalyzed the data published by Clausen et al. (2008) by employing the low value for prismatic slip strength for modeling ED compression (see Abdolvand and Daymond, 2012 and Juan et al., 2014). In addition, there are examples of FE-based crystal plasticity models in which no reorientation is accounted for at all (Graff et al., 2007). In such case, the appearance of a plateau and subsequent rapid hardening are entirely phenomenological and should not be viewed as physically based.

Twin growth (operation B shown in Figure 3.1c) occurs when the sign of the resolved shear stress is positive. When the sense of the stress is negative, detwinning (operation C) can occur. This simply means that the twin boundary retreats from the matrix into the twin. Hence, the twin volume fraction f^{tw} decreases. To some readers, this may initially seem like a violation of the twin polarity introduced above. However, the aforementioned polarity of twinning only applies to the creation of a twin. Stresses in the anti-twinning direction will never result in twin nucleation, but once the twin is created, there is nothing to prevent the reverse motion of the TB, thereby accommodating twinning shear in the reverse sense. In the present model, no discrimination is made between the CRSS values of twin growth τ_B and twin shrinkage τ_C; i.e., it is imagined that the twin boundaries can move with equal ease in the forward and reverse directions.

This is contrary to the conclusion of Lou et al. (2007), that twinning is somewhat more difficult than detwinning, so this item will be discussed later in the paper.

Finally, operation D is introduced for the sake of completeness. The critical stress conditions for this nucleation event could be less than, equal to, or greater than that of the initial nucleation event. However, we do not discriminate between operations C and D in the present analysis. (Consider the possibility that nucleation D requires a higher critical stress than boundary motion, C. In such a case, operation D would never occur in the present mean-field formulation. Discriminating between these two mechanisms will require a full-field approach such as the crystal plasticity finite element method with many elements per grain or molecular dynamics.) In summary, we assume $\tau_A > \tau_B = \tau_C = \tau_D$, and there is no distinction made between operations C and D in the present code. As such, operation D will not be discussed further.

In mathematical terms, the following criterion is polled within the parent crystals for all possible twin variants, α.

$$\dot{\gamma}_A^\alpha = \begin{cases} \dot{\gamma}_0 \left| \tau^\alpha / \tau_A \right|^{\frac{1}{m}} & \tau^\alpha > 0 \\ 0 & \tau^\alpha \le 0 \end{cases} \tag{3.2.7}$$

A- twin initiation (nucleation and initial propagation across matrix grain)

This expression explicitly accounts for the polarity of twinning. The power law form is identical to that employed for slip (Eq. 3.2.6). As mentioned earlier, this is for mathematical convenience and does not reflect a belief that twinning is similarly rate sensitive to slip. On the contrary, the authors acknowledge that {10.2} extension twinning in Mg alloys is apparently rate insensitive over a wide range of temperatures and strain

rates (Livescu et al., 2006; Jain and Agnew, 2007; Tucker et al., 2009; Ulacia et al., 2011; Agnew et al., 2014b). Future work is planned to investigate modeling this aspect of twinning phenomenon as well. The volume fraction of twin produced is directly proportional to the twin shear accommodated and the characteristic shear of the twinning mode in question.

$$\dot{f}_A^\alpha = \left|\dot{\gamma}_A^\alpha\right| / \gamma^{tw} \tag{3.2.8}$$

Once twins have been created and a critical level of twin strain γ_{cr}^{tw} (f_{cr}^{tw}) accommodated, the stress for continued growth drops to τ_B. The concept of discriminating between the stress required to initiate twins τ_A and that required to grow them τ_B was introduced previously by Wang et al. (2012b; 2013a). However, it was not to this point exploited. Here, it is shown that the concept makes it possible to describe the sudden yielding and the yield plateau observed in materials where twinning is the main strain accommodation mechanism responsible for yield. This is a simplified model and further work on the issue of transition between nucleation, propagation and growth is merited.

The criterion for twin growth is examined within both the matrix and the twin. This is a key distinction between the present model and that proposed by prior authors (Van Houtte, 1978; Tomé et al., 1991; Kalidindi, 1998; Clausen et al., 2008; Levesque et al., 2010) which reflects the authors' desire to approximate the fact that twin growth is actually governed by stresses applied on the TB interface itself.

$$\dot{\gamma}_{BM}^\alpha = \begin{cases} \dot{\gamma}_0 \left|\tau^\alpha / \tau_B\right|^{\frac{1}{m}} & \tau^\alpha > 0 \\ 0 & \tau^\alpha \le 0 \end{cases} \tag{3.2.9a}$$

B- twin growth (due to reaching the critical stress level within the matrix, M)

$$\dot{\gamma}_{BT}^{\alpha} = \begin{cases} -\dot{\gamma}_0 \left| \tau^{\alpha} / \tau_B \right|^{\frac{1}{m}} & \tau^{\alpha} < 0 \\ 0 & \tau^{\alpha} \geq 0 \end{cases} \tag{3.2.9b}$$

B-twin growth (due to reaching the critical stress level within the twin, T)

The negative sign in equation (3.2.9b), relative to equations (3.2.7&3.2.9a) is not a violation of the polarity of twinning, rather it reflects the fact that the sense of stress within the twin which drives the outward motion of the twin boundary is of opposite sign. Consideration of the crystallography and geometry of the problem will make this requirement obvious. It is important to note that the resolved shear stress τ^{α} in (3.2.9a) is calculated from the true stress tensor $\boldsymbol{\sigma}$ of the matrix and the Schmid tensor $\boldsymbol{P}^{\alpha}$ associated with the lattice of the matrix for system α, while the one in (3.2.9b) from those of the twin. The volume fraction change $\dot{f}_B^{\alpha}$ during the growth phase is the sum of that due to (3.2.9a) and (3.2.9b).

$$\dot{f}_B^{\alpha} = \left| \dot{\gamma}_{BM}^{\alpha} \right| / \gamma^{tw} + \left| \dot{\gamma}_{BT}^{\alpha} \right| / \gamma^{tw} \tag{3.2.10}$$

Similar to the situation described by equations (3.2.9a&3.2.9b) for twin growth, the possibility of twin shrinkage (Operation C) is probed within the matrix (Eq. 3.2.11a), as well as the twin itself (Eq. 3.2.11b).

$$\dot{\gamma}_{CM}^{\alpha} = \begin{cases} -\dot{\gamma}_0 \left| \tau^{\alpha} / \tau_C \right|^{\frac{1}{m}} & \tau^{\alpha} < 0 \\ 0 & \tau^{\alpha} \geq 0 \end{cases} \tag{3.2.11a}$$

C- twin shrinkage (due to reaching the critical stress level within the matrix, M)

$$\dot{\gamma}^{\alpha}_{CT} = \begin{cases} \dot{\gamma}_0 \left| \tau^{\alpha} / \tau_C \right|^{\frac{1}{m}} & \tau^{\alpha} > 0 \\ 0 & \tau^{\alpha} \leq 0 \end{cases} \tag{3.2.11b}$$

C- twin shrinkage (due to reaching the critical stress level within the twin, T)

Again, these equations (3.2.11a) and (3.2.11b) do not reflect a violation of the polarity of twinning. If no twin is present, then only one sense of stress can create a twin, per equation (3.2.7). However, once a twin is created, a stress in the anti-twinning direction can drive the twin boundary in the reverse direction. Similar to the description of equation (3.2.9), the resolved shear stresses in (3.2.11a) and (3.2.11b) are calculated from the true stresses and the Schmid tensors in the matrix and twin, respectively. The volume transfer $\dot{f}^{\alpha}_{C}$ during this "detwinning" is governed by an equation of the same form as equation (3.2.10)

$$\dot{f}^{\alpha}_{C} = -\left| \dot{\gamma}^{\alpha}_{CM} \right| / \gamma^{tw} - \left| \dot{\gamma}^{\alpha}_{CT} \right| / \gamma^{tw} \tag{3.2.12}$$

At the risk of redundancy, it is reiterated that the only coupling between the twin and matrix are the common critical resolved shear stress values for twinning and the volume fraction transfers (Eqs. 3.2.10 & 3.2.12). The stress states in the matrix and twin grains are computed independently, via the self-consistent algorithm, which employs linearized versions of the single crystal constitutive law such that the respective orientations of the twin and matrix are naturally taken into account.

The final element of this crystal plasticity model is a threshold approach which is employed to prevent grains from twinning in their entirety, since this is rarely observed experimentally. When the volume fraction of twins in a given grain exceeds a threshold

value, V^{th}, that grain ceases being able to twin. Two empirical parameters, B_1 and B_2, are employed to control this aspect of the response.

$$V^{th} = \min\left(1.0,\ B_1 + B_2 \frac{V^{eff}}{V^{acc}}\right) \tag{3.2.13}$$

The total accumulated twin volume fraction in the polycrystal is denoted as V^{acc}, and the volume fraction of grains which have ceased twinning is denoted as V^{eff}. B_1 essentially controls the level of strain (volume fraction) which a grain can undergo prior to the twinning mechanism beginning to undergo exhaustion. B_2, on the other hand, essentially controls the rate at which this exhaustion takes place once it has begun. Eventually, the capacity to twin is completely exhausted and additional straining within the twins (and surrounding matrix grains) will rely on other means of straining. Since the alternatives involve deforming by basal slip (low critical stress, but poorly oriented) or non-basal slip (well oriented, but high critical stresses), the applied stress on the grain must be high in order for it to continue straining. As such, the combination of B_1 and B_2 control the length of the plateau and the steepness of the subsequent strain hardening. Note that the present model is completely empirical at this time. However, it provides twin exhaustion as the basis for rapid hardening, which is alternative to the Hall-Petch effect, such as employed by previous modelers (CG model, e.g. Proust et al., 2007, 2009; Levesque et al., 2010). Further, it will be shown unnecessary to employ a special latent hardening effects associated with twinning, though previous modeling attempts using VPSC have required it (e.g., Jain and Agnew, 2007; Oppedal et al., 2012). The former group employed a high

value of the latent hardening of slip modes by twinning, while the latter employed a high value of a transmutation storage parameter to induce a high dislocation density (hence high Taylor hardening) within the twins (Niewczas, 2010). While it has been proposed that dislocations may be transmuted, based upon crystallographic relationships, there is conflicting evidence that suggests twins may actually sweep the matrix of preexisting dislocations (Rampton et al. 2012).

For both slip and twinning, the evolution of the CRSS values, τ_{cr}^{α}, is potentially controlled by an empirically determined latent hardening matrix, $h^{\alpha\beta}$.

$$\dot{\tau}_{cr}^{\alpha} = \frac{d\hat{\tau}^{\alpha}}{d\Gamma} \sum_{\beta} h^{\alpha\beta} \left| \dot{\gamma}^{\beta} \right| \tag{3.2.14}$$

where Γ is the total accumulated shear strain within the grain due to all slip and twinning systems; $\dot{\gamma}^{\beta}$ is the shear on a specific slip or twinning system, β; and $\hat{\tau}^{\alpha}$ is an empirical Voce hardening law (with an initial CRSS value τ_0, an initial hardening rate h_0, and a saturation stress ($\tau_0 + \tau_1$). Note, however, that the twins do not appear to undergo strain hardening in the present work. The strain hardening behavior of twinning appears to be a function of grain size, as pointed out in recent work of Barnett et al. (2012). In the present work, all components of the latent hardening matrix are assumed to be equal to 1, due to a lack of available theoretical or experimental data to justify alternative values. The area of latent hardening within hexagonal close packed metals appears to be an open topic, with very little work to date on the subject (e.g., Lavrentev and Pokhil, 1975 and Hiura, 2010).

3.2.4 Comparison with experiments

For comparison with experimentally measured in-situ neutron diffraction data, subsets of grains are identified which would satisfy the Bragg diffraction conditions for a given set of crystallographic $\{hk.l\}$ planes. The experimental spectrometer (described previously by Bourke et al., 2002) has a detector with a central square region having an angle of 13º. Within the EVPSC simulation code, all grains which have $\{hk.l\}$ normal vectors which fall within this acceptance angle are added to subset. The volume fraction of these grains is directly proportional to the diffracted intensity, and so it may be compared with experimentally measured, normalized intensity. Similarly, the predicted stress level within each grain permits the normal component of the elastic strain parallel to the diffraction vector (i.e. the $\{hk.l\}$ normal vector) to be calculated via generalized Hooke's law and the known elastic constants for Mg single crystals. A volume weighted average of this strain over the subset of grains, denoted $\{hk.l\}$, permits direct comparison with experimentally measured lattice strain, which is computed as the normalized difference between the lattice plane spacing under load and at zero load as follows:

$$\varepsilon^{\{hk.l\}} = \frac{d^{\{hk.l\}} - d_0^{\{hk.l\}}}{d_0^{\{hk.l\}}} \tag{3.2.15}$$

3.3 Results

The initial texture of the material was modeled as 2,160 or 15,552 discrete orientations (grains) having volume fractions selected to well-represent the experimentally measured (neutron diffraction) texture of the extruded alloy, ZK60A, plate

measured using synchrotron X-ray diffraction and published by Wu (2009). The smaller grain set was used for rapid initial parameterization, and the larger grain set was employed for final simulations in order to improve statistics of the intensity and internal strain predictions. Contour plot pole figures of the discretized texture generating using POLE8 (Tomé, 2007) are presented in Figure 3.2. Note that this extruded plate essentially exhibits the <10.0> || the extrusion direction (ED) texture typical of axis-symmetric extrusions, but the {00.2} pole figure exhibits the strongest intensity parallel to the plate transverse direction (TD). Note also that this texture is distinct from the one published with the original in-situ neutron diffraction study of cyclic deformation (Wu et al.; 2008b). That prior texture measurement was made using a laboratory X-ray diffractometer and deviates from numerous synchrotron measurements made later on the same plate. It is suggested that the texture published by Wu et al. (2008b) was collected from the surface of the extrusion, which is characterized by heavy shear and not representative of the bulk of the extrusion.

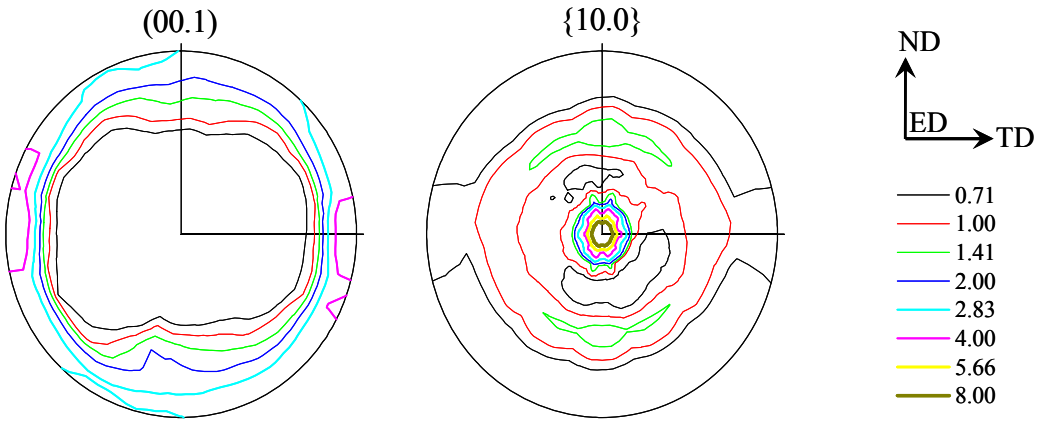

Figure 3.2 Initial texture of the ZK60A plate represented in terms of the {00.1} and {10.0} pole figures.

3.3.1 Parameterizing the model with data from monotonic straining along the ED

Uniaxial tension and compression curves (Figure 3.3) and in-situ neutron diffraction (Figure 3.4) published by Wu et al. (2008a) were used to develop the initial guesses for the crystal plasticity model parameters. These initial guesses are then tuned manually to obtain the best fit to the flow curves, internal strain data, and texture evolution. In the present study, we consider three types of slip systems: Basal <*a*> ($\{0001\}<11\bar{2}0>$), Prismatic <*a*> ($\{10\bar{1}0\}<11\bar{2}0>$) and Pyramidal <*c*+*a*> ($\{\bar{1}\,\bar{1}22\}<\bar{1}\,\bar{1}23>$), and one twinning mode: the $\{10\bar{1}2\}<\bar{1}011>$ extension twin system. The reference slip/twinning rate $\dot{\gamma}_0$ and the rate sensitivity m are prescribed to be the same for all slip/twinning systems: $\dot{\gamma}_0 = 0.001\,s^{-1}$ and $m = 0.05$, respectively. Wang et al. (2010b) have evaluated several self-consistent approaches by studying the large strain behaviour of magnesium alloy AZ31B sheet under tension and compression along different directions. It has been demonstrated that, of the approaches examined, the Affine self-consistent scheme gives the best overall performance. Therefore, all the simulations reported in the present paper are based on the Affine self-consistent scheme. The internal strains are simulated based on the numerical procedure described by Wang et al. (2012a, 2013b) and recently used by Lee et al. (2014).

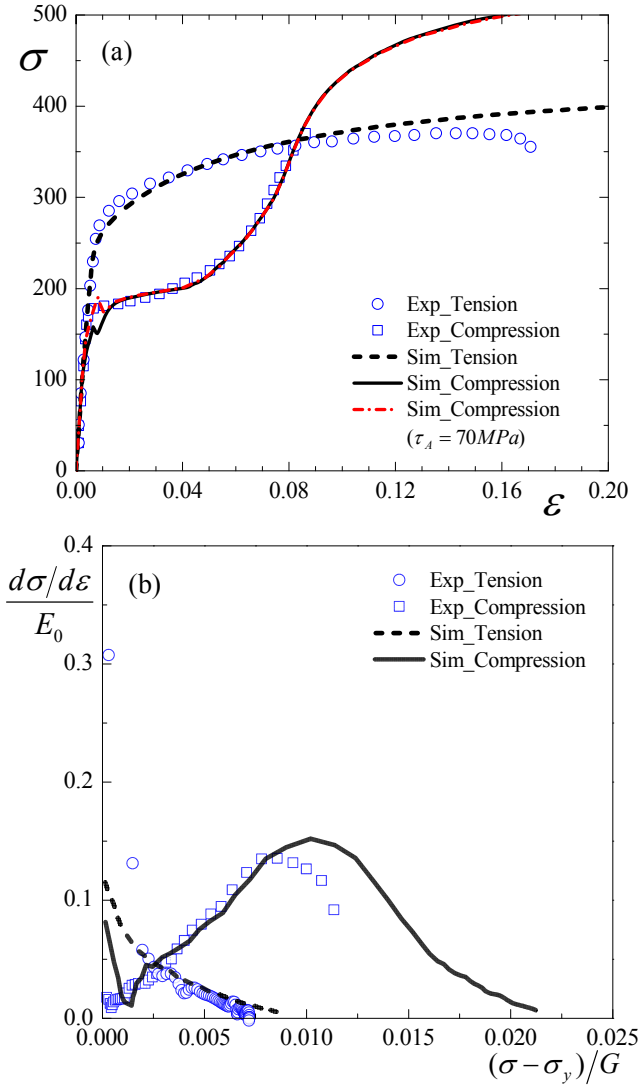

Figure 3.3 (a) Measured and simulated (fit parameters in Table 3.1) stress-strain responses in monotonic, uniaxial tension/compression along the ED. The dash-dot curve illustrates that quite sudden yielding can be predicted for twinning-dominated response, if high values of the twin activation stress, τ_A = 70 MPa, and the threshold volume fraction, f_{cr}^{tw} = 0.045, are employed. (b) The Kocks-Mecking plot (Kocks and Mecking, 2003) of the normalized strain hardening rate versus the flow stress minus the yield stress, where E_0 (45GPa)and G (16.3GPa) are the Young's modulus and shear modulus, respectively.

The internal strain data obtained from in situ diffraction are particularly useful for determining the parameters which describe the behavior of the various slip and twinning

systems. At first, all of the grain orientations strain similarly and this is a reflection of the near elastic isotropy of Mg alloys (Figure 3.4). The room temperature elastic constants of the Mg-Zn alloy are assumed to be close to those of pure Mg: $C_{11} = C_{22} = 58.0$; $C_{33} = 61.2$; $C_{12} = 25.0$; $C_{13} = C_{23} = 20.8$; $C_{44} = C_{55} = 16.6$; and $C_{66} = 16.5$ GPa (Simmons and Wang, 1971), though the possible role of a stiffer (Xie et al., 2013) Mg-Zn intermetallic phase is discussed later in the paper. The first subset of grains to undergo yielding (during both tension and compression) of Mg alloy, ZK60A, are those with {10.2} poles parallel to the stress axis (Agnew et al., 2014a). The {10.1} are the first grains to yield in the present data set of Wu et al. (2008a), since the {10.2} data were not presented (Figure 3.4). The {10.1} grains begin to slow their accumulation of elastic strain at an applied stress level of ~ 100 MPa. Simultaneously the {10.0} and {11.0} oriented grains begin load sharing a greater fraction of the imposed load. Because all grains are deforming similarly at this point in the deformation, it is reasonable to employ the Schmid law (Eq. 3.2.5), and the macroscopically imposed stress to define an initial estimate of the critical resolved shear stress for basal slip of 36 MPa (Schmid factor ~ 0.36).

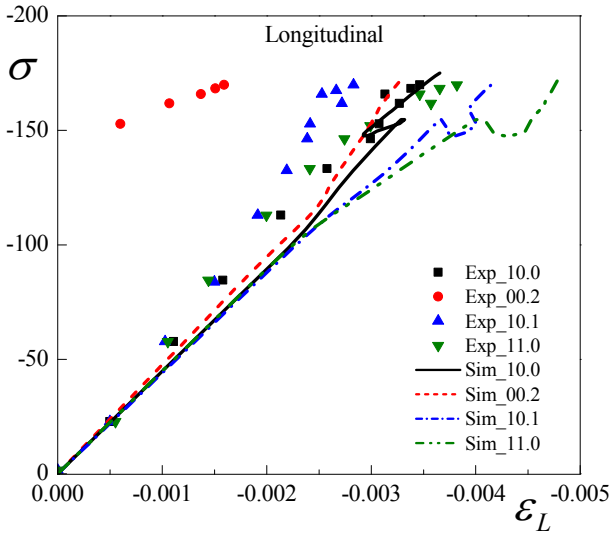

Figure 3.4 Measured and simulated (fitted) internal strain during the first quarter cycle (compressive strain to 1.2%) of in situ cyclic deformation. Predicted strain levels within the {00.2} grains should be ignored up to the point at which twinning begins, (~150 MPa) since there is an initially low volume fraction of grains with this orientation, making estimation of an internal strain impossible.

The next major event during compressive loading is the sudden yielding at 150-175 MPa (depending upon the sample), and which has already been associated with {10.2} extension twinning. In particular, the intensity of the {00.2} diffraction peak begins to increase in intensity at ~150 MPa, due to the reorientation of portions of grains which were previously oriented to have their {10.0} poles parallel to the extrusion axis (discussed in more detail below). These {10.0} grains are perfectly oriented to undergo extension twinning (i.e. the Schmid factor is close to 0.5). These facts permit setting the CRSS for the initiation of twinning (τ_A) in the vicinity of 75 MPa. For those who may object to the use of the macroscopic (polycrystalline) stress in the Schmid relation to determine the CRSS for application in a grain-level model, it is emphasized that the internal stress levels within various {*hk.l*} subsets of grains are still not so different at this stage in the deformation (see the lattice strain values at 150 MPa, Figure 3.4).

The comparison of measured and predicted internal strains reveals three important points. First, the purely elastic loading portion (up to 25 MPa) correlates well between simulation and experiment. However, once the slightest bit of microplasticity occurs, the experimental data deviate from the simulated. This signifies that there is a load sharing effect due to the presence of a hard elastic phase. In a previous study, including an appropriate phase fraction of elastic second phase inclusions provided a sufficient level of load sharing to explain the observation (Agnew et al., 2013). In the present study, simulation trials with including hard elastic inclusions failed to immediately correct this deficiency and further consideration will be required to overcome this deviation between model and experiment. Second, it is emphasized that the {00.2} grains should be ignored up to the point at which twinning begins, (~150 MPa) since there is an initially low volume fraction of grains with this orientation, making estimation of an internal strain impossible. Once twinning has initiated, the new grain orientations appear, which are unloaded with respect to the matrix grains. This strong relaxation phenomenon has been previously modeled by Clausen et al. (2008), but this effect is not accounted for in the present work. Third, the major inflections observed in the internal strain evolution (such as the deviation of {10.0} and {10.1}) do occur at similar applied stress levels. The oscillations in the predictions correspond with the predicted yield point peak associated with twinning.

The final aspects which can be readily determined from the experimental compression are the empirical parameters which govern the rate at which grains cease twinning (see Eq. 3.2.13). The regime of rapid strain hardening begins at a strain of about

0.04. This enables fixing parameter B_1, the volume fraction when continued twinning begins to become more difficult. Since the majority of the strain throughout the plateau region has been associated with twinning (Brown et al., 2005), the majority grains have a Schmid factor for twinning of near 0.5, and the characteristic shear for {10.2} twinning is ~0.13, we can invoke relation (3.2.8) to estimate $B_1 \sim 0.04/(0.5 \cdot 0.13) \sim 0.6$. As mentioned earlier, the rate of strain hardening beyond this point is governed by the empirical parameter B_2, which determines the rate at which grains cease twinning.

Examination of the tensile test data shows that monotonic, macroscopic yielding occurs at ~260-275 MPa. In-situ neutron diffraction data obtained from similar, extruded ZK60A, material (Agnew et al., 2014a) shows microyielding due to basal slip at the same stress level as during compression. On the other hand, the macroscopic yielding of such textured extrusions has previously been shown via in-situ neutron diffraction and polycrystal plasticity modeling to be due to the slip of <a> dislocations on prismatic planes. These prior works were performed on distinct extruded alloys, AZ31B (Agnew et al., 2006; Wang et al., 2012a) and ZM20 (Muransky et al., 2010b), which demonstrates the broad applicability of the notion that prismatic slip is responsible for the yielding of extrusions in tension. An initial estimate for the CRSS of prismatic slip of 115 MPa is given by again assuming that the stress within the relevant grains is similar to that imposed on the aggregate (something confirmed by in-situ measurements, Agnew et al, 2014a) and invoking the Schmid factor of the majority <10.0> oriented grains, Schmid factor = 0.43.

The present monotonic data do not permit fixing the CRSS for <c+a> pyramidal slip; it would require knowing the flow stress at higher levels of compressive strain. However, results from in-situ monotonic compression data from similar extruded ZK60A material (Agnew et al., 2014a) show that the grains oriented for <c+a> slip, i.e. the {00.2} grains, undergo an inflection in lattice strain development in the vicinity of 8000 με (close to 340 MPa, assuming isotropy). The Schmid factor for <c+a> slip in these grains is also in the vicinity of 0.43. As such, the CRSS for <c+a> slip may be estimated as in the vicinity of 145 MPa within alloy ZK60A, though the present alloy samples are somewhat stronger than those tested by Agnew et al. (2014a).

The initial CRSS values and hardening responses were adjusted to best-fit the experimentally observed flow curves (first the monotonic and then the cyclic ED data, discussed below). The resulting parameters are presented in Table 3.1. Concerning the strain hardening of the individual deformation modes, the basal slip system has been shown to harden very little in recent crystal plasticity modeling studies of magnesium alloys (Clausen et al., 2008; Agnew et al., 2013, Wang et al., 2012a, 2012b). Consistent with the suggestion of Jain et al. (2012), we employ a value for the initial hardening rate of basal slip, in the vicinity of μ/100, given μ ~ 16.3 GPa. The twinning mode has been shown to exhibit very little strain hardening; many current studies assume no hardening at all (Wang et al., 2010b, 2012a). The fact that the present material has a dramatic strain hardening plateau is particularly suggestive of low strain hardening behavior. Thus, the strain hardening of the aggregate is largely associated with strain hardening of the non-basal slip modes. Notably, we employ a higher level of strain hardening to the non-basal

slip modes than Jain et al. (2012), but consistent with prior studies of the present authors. This empirical result again suggests that the fundamental mechanisms of strain hardening (i.e. dislocation interactions) within hexagonal close packed metals remain an open topic. Works like that of Capolungo et al. (2010) and Bertin et al. (2014) represent a start in this direction.

Table 3.1 List of material parameters for slip and twin systems used in the EVPSC model. (All latent hardening parameters are 1.)

Mode	$\boldsymbol{\tau_0}$(MPa)	τ_1(MPa)	h_0(MPa)	$f_{cr}^{tw}(\gamma_{cr}^{tw})$	B_1	B_2
Basal	40	15	150			
Prismatic	115	15	800			
Pyramidal	125	160	1200			
Extension twin	A(56) B=C=D (32)	0	0	0.035(0.0046)	0.56	0.70

The resulting model can be used to map out the slip and twinning mode activities predicted to occur during monotonic deformation (Figure 3.5). The basal slip mode is the most active at low stresses, below the macroscopic yield point. From the macroscopic yield stress and beyond, other mechanisms are similarly important. During tension along the extrusion axis, it is the non-basal (prismatic) slip of <a> dislocations which becomes most prominent. During compression along the extrusion axis, the {10.2} extension twinning mode is a dominant mechanism until it is exhausted at a compressive strain, ε ~ 0.1. The sharp oscillation between twinning and basal slip at low strains is due to the simplistic model presently employed to transition from twin nucleation to twin growth.

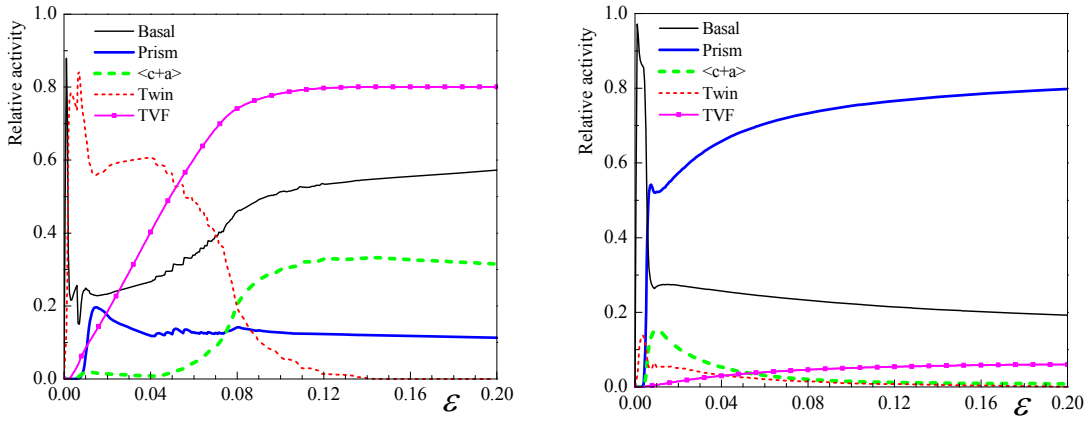

Figure 3.5 The relative deformation mode activities under uniaxial (a) compression and (b) tension along the extrusion direction (ED).

The total predicted twin volume fraction f^{Tot} reaches ~80% at the strain ~0.1, where twinning is almost exhausted. The relative contributions of twinning driven by stresses within the matrix f^{Mat} and within the twin f^{Twin}, respectively, are presented in Figure 3.6. At the low strain levels, the twin growth is mainly driven by the stress within the matrix and gradually taken over by the driving force within the twin itself with further straining. The cross-over when twinning driven by stresses within the twin itself begins to exceed twinning driven by the stresses within the matrix occurs at a strain of ~0.04 (Figure 3.6b), the same strain level at which the strain hardening rate starts to increase dramatically.

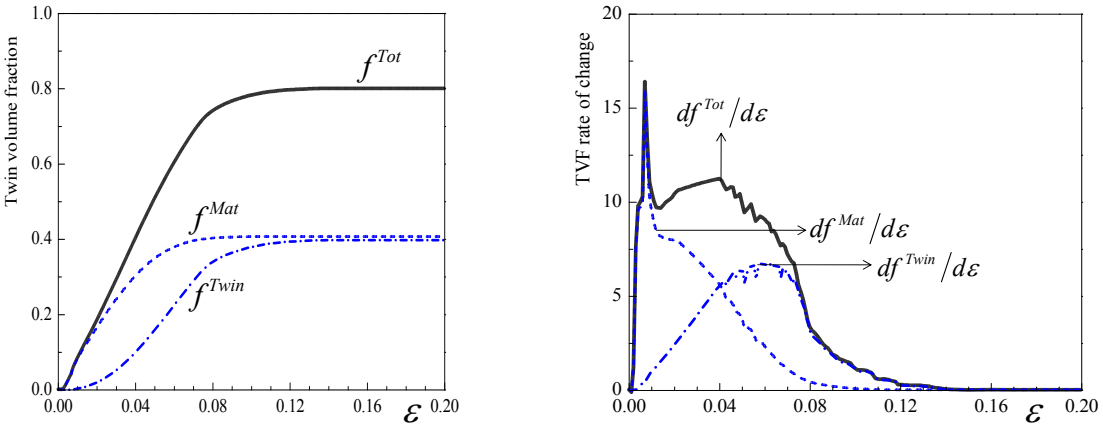

(a) **(b)**

Figure 3.6 (a) Predicted twin volume fraction and (b) the derivative of the same, as a function of macroscopic strain under uniaxial compression along the ED. Note the cross-over when twinning driven by stresses within the twin itself begins to exceed twinning driven by the stresses within the matrix occurs at a strain of ~0.04, the same strain level at which the strain hardening rate starts to increase dramatically.

3.3.2 Cyclic deformation along the ED

The stress-strain response during the first 2 ¼ cycles of deformation provides a direct means of refining the model parameters obtained from the monotonic data by comparing the simulation predictions and experiment. The initial loading in compression activates twinning*, which gives rise to a sudden yield (even a slight yield point peak in the simulation results) followed by a relative strain hardening plateau. In comparison, the yielding upon compressive unloading and reloading in tension is very gradual. The response is well-captured by the EVPSC-TDT model, and this may be attributed to the lower CRSS value employed for twinning operation C ("ungrowing") relative to operation A ("initiation") (see Table 3.1). The correlation of the stress strain response and

* The ED compressive yield point was significantly different between the monotonic and cyclic test data published by Wu et al. (2008a). Hence, the critical stress for twinning was adjusted downward only after comparing the predictions with the cyclic test data.

the twinning behavior can be made by examining Figures 3.7-3.9. Recall that the critical stress for operation C is set equal to that of twin thickening (operation B) in the present model. Twin thickening or thinning correspond to motion of the same boundary in the forward or reverse direction. Without strong evidence to the contrary, it seemed most prudent to assume that the critical stress to drive such interfacial motion is independent of direction, and the present results provide evidence to support this assumption. Rapid hardening occurs during the tensile straining cycles, once the detwinning operation is complete. Note that the model which controls the exhaustion of twinning (Eq. 3.2.13) and associated parameters B_1 and B_2 are not used to govern detwinning behavior. However, there may be a small *residual* twin volume fraction left after detwinning which has been observed experimentally (Hama et al., 2012). Such a parameter could be important for larger strain cycles and/or larger numbers of cycles. For the present case, it was not essential (values between $f_{residual}^{tw}$ = 0 and 0.005 were explored and shown to give similar results.)

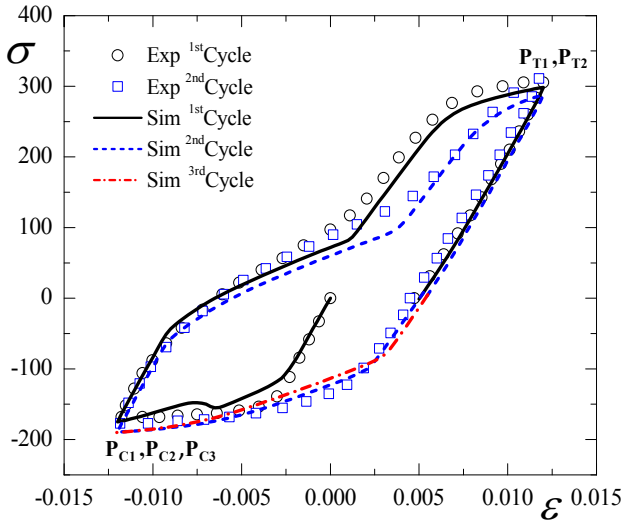

Figure 3.7 Comparison of the measured (symbols, after Wu et al., 2008b) and predicted (curves) stress-strain responses under cyclic loading along the extrusion direction.

Figure 3.8 presents a comparison between the evolution of the normalized diffracted intensity of the {00.2} diffraction peak and the *predicted* volume fraction of grains that satisfy the corresponding Bragg condition. Because the intensity of the {00.2} diffraction peak is proportional to the volume fraction of twins, this comparison may be viewed as a validation of the approach. The model parameters were not adjusted to achieve these predictions. However, it must be admitted that "twinning is kinematically-driven" (Eisenlohr, 2013). Note the linear relationship between twin volume fraction and twinning strain (e.g. Eqs. 3.2.8, 3.2.10, & 3.2.12). Similarly, previous publications have also emphasized that achieving a good prediction of twin volume fraction does not depend strongly upon model details (Clausen et al., 2008). Figure 3.9 shows the complete texture evolution due to twinning and detwinning. Note that each alternate pole figure looks similar, after twinning and detwinning, respectively. Although such a collage has

not been experimentally measured for alloy ZK60A, these simulation results compare well with similar compilations produced by x-ray or neutron diffraction of AZ31 (Lou et al. 2007; Wu et al., 2010). During the initial compressive quarter-cycle, twin initiation (operation A) dominates the evolution. During the compressive unload, tensile-reload cycle Operation C (reverse boundary motion or "ungrowth") dominates the response. It is reassuring that this correlates so well with the acoustic emission data of Lou et al. (2007) which suggested that twinning required nucleation events detectable with AE, while detwinning was not accompanied by a significant AE signal.

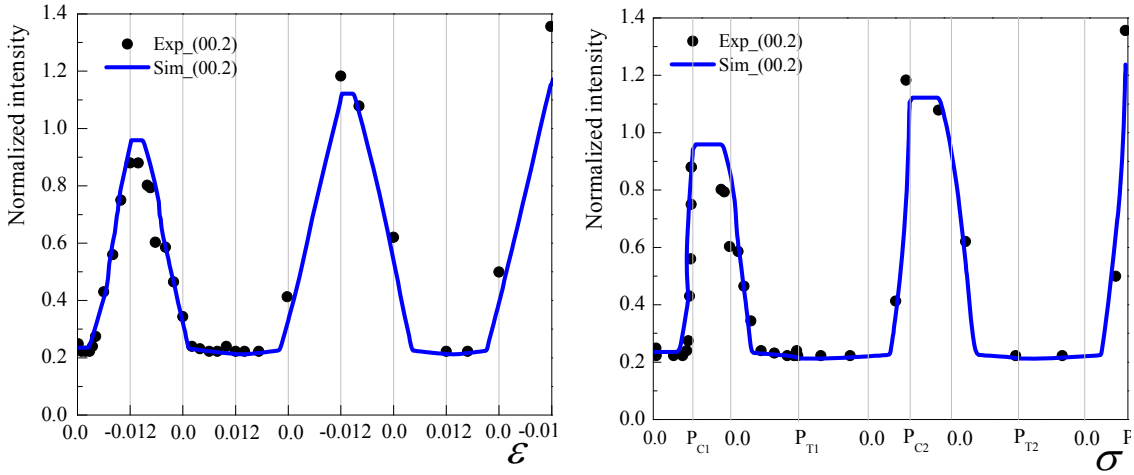

(a) **(b)**

Figure 3.8 Normalized intensity of the {00.2} diffraction peak along longitudinal direction (after Wu et al., 2008a) as a function of macroscopic strain (a), and applied stress (b) under cyclic loading along the ED.

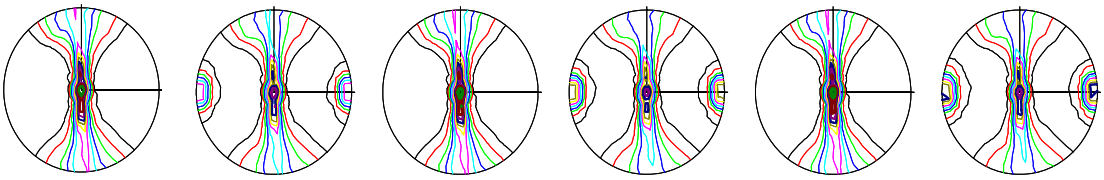

Figure 3.9 Basal {00.2} pole figures for (read left to right): the initial texture, that after -1.2% (first quarter cycle), +1.2% (first cycle), -1.2% (early second cycle), +1.2% (late second cycle), and -1.2% (early third cycle). Note that each alternate pole figure looks similar, after twinning and detwinning, respectively. The pole figures are oriented such that ED is horizontal, ND is vertical, and TD is out of the page.

The measured and simulated internal strains may be plotted as functions of the macroscopic applied strain or stress (as they were in Figure 3.4). The latter has been more conventional in the literature even though the independent variable in the present tests was the applied strain. The overall trends of the predictions well match those observed experimentally (Figure 3.10). For example, the lattice strain decreases within all grain orientations along the longitudinal direction during compressive loading and increases during tensile loading. As shown earlier, the {10.0}, {10.1}, and {11.0} predictions for the longitudinal direction are qualitatively good. Only the {00.2} subset of grains shows gross variation from the experiment and this is related to the fact that the present model does not adequately account for the relaxation that occurs within the twins (Clausen et al., 2008), despite the fact that there is some relaxation associated with the decrease in critical stress between twin initiation and growth (Table 3.1).

During the subsequent unload and reload in the tensile direction, there is good agreement, up until the point where detwinning is exhausted (i.e., all the twins are gone, about 1/3 of the way from 0 to P_{T1} in Figure 3.10). At this point, the experimental data for {10.1} and {11.0} grains, in particular, exhibit a slowing evolution in the lattice strain,

which is not evidenced by the model predictions. The disagreement with the {10.0} grains is not so strong and the {00.2} grains have "disappeared" due to detwinning, so the model {00.2} predictions at this stage are somewhat meaningless (indeed the volume fraction of grains with this orientation is only 0.0014, relative to ~ 0.02-0.068 in the other orientations). It is not immediately obvious how all of these grain orientations are predicted to show higher lattice strains than the experimental, while the overall stress strain curve (Figure 3.7) and intensity (twin volume fraction) variations (Figure 3.8) match so well. During the subsequent unload, reload in compression, unload and reload in tension, the agreement between the experimental and predicted lattice strain is regained. Only after detwinning is nearing completion the second time does the variance reappear again, most strongly in the {10.1} oriented grains.

Predicting the lattice strains in the transverse direction is notoriously difficult. Neil et al. (2010) recently showed that grains which belong to a single {*hk.l*} subset can have very different responses to the applied loads and develop very different lattice strains. In fact, they noted that the range of lattice strains within a single subset of grains which satisfy a Bragg condition was greater than the range of lattice strains observed experimentally across all possible diffraction conditions. Nevertheless, we present the predictions of the model for comparison with data that Wu et al. (2008b) made available. As with the longitudinal direction, it can be stated that the major trends are captured, even if quantitative agreement between the experiment and predictions are not observed. Again, the reason the {00.2} predictions look erratic is because the intensity associated with this direction is coming and going throughout the simulations. (When there is {00.2} intensity

in the longitudinal bank, there is low intensity in the transverse bank, etc.) The strongest mismatch between model and experiment in the transverse lattice strain data again appears in the {10.1} and {11.0} grain sets. The mismatch occurs during the unloading from compressive loading. During subsequent tensile reload, the agreement is regained.

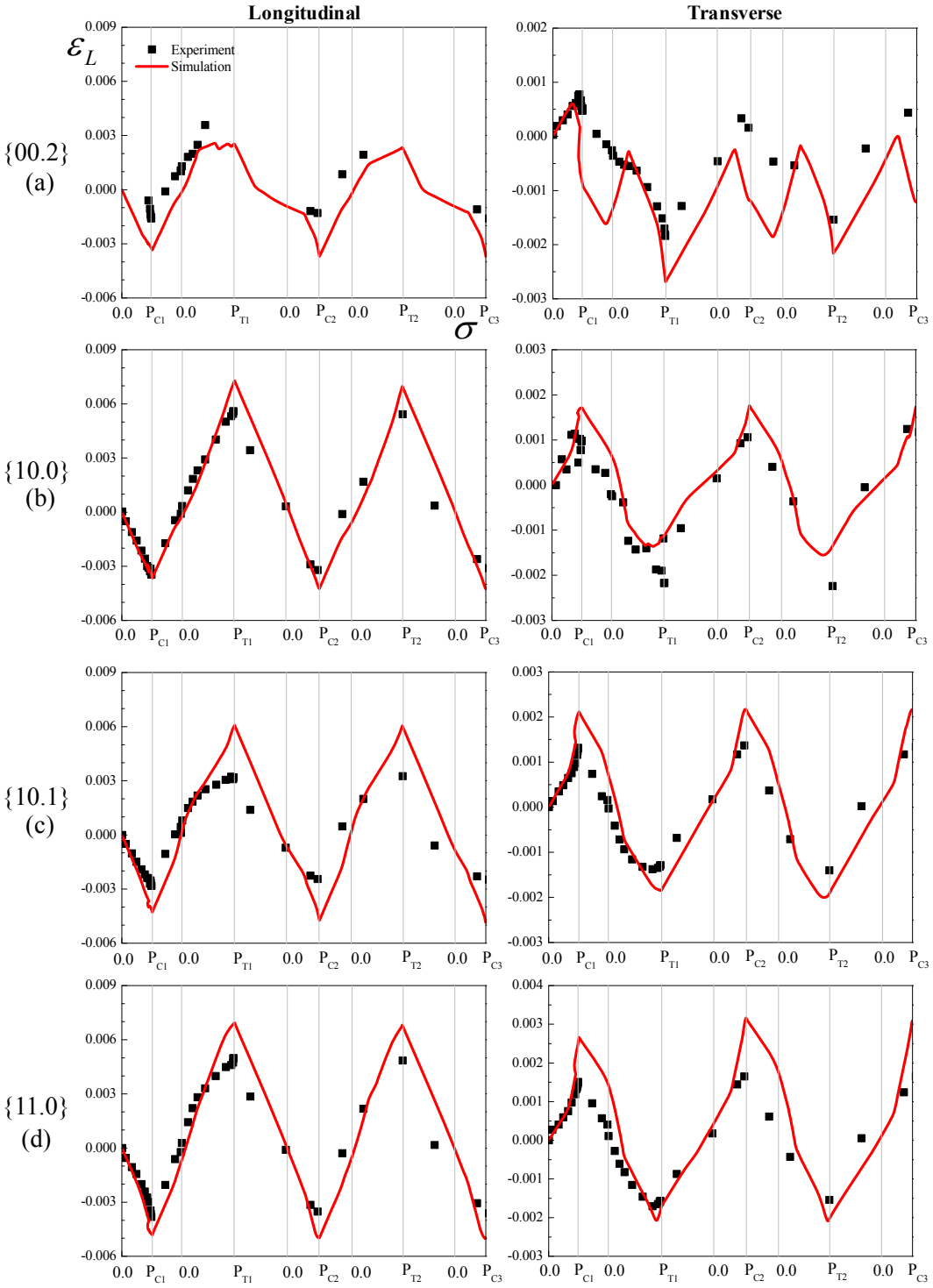

Figure 3.10 Lattice strains of the {00.2} family (a),{10.0} family (b), and {10.1} family (c), {11.0} family (d) as a function of applied stress under cyclic loading along the ED.

3.3.3 Predictions of monotonic straining along the TD and ND

Wu (2009) also published monotonic tension and compression curves obtained from the transverse (TD) and normal (ND) directions. The results of simulations of TD and ND deformation performed using parameters obtained after fitting the model to ED tension, compression, and cyclic data are presented in Figures 3.11 and 3.12. The results of these predictions are quite encouraging. They show that the model can correctly predict the level of strength anisotropy and asymmetry, as well as the strain hardening behavior. It is admitted that the strength of the ND compression curve is a bit high, relative to the experimentally observed. However, subtle variations in the local texture are known to exist and it is not known how closely the position of the extracted test samples matched that of the sample on which the texture measurement was made. Note that changes to even the least constrained fit parameters obtained from the ED testing (e.g. the strength of the <c+a> slip system) lead to degradation of these predictions. It is also interesting that twinning process may be different during tension along *c*-axis from that during compression perpendicular to c-axis. Twinning is equally favored in both cases, but the former leads to much more twin intersection than the latter (Hong et al., 2010a). Further, based on the EBSD analyses of two distinct grains deforming within the same extruded AM30 alloy, it has been shown by El Kadiri et al. (2013b) that twin intersection does lead to greater incidence of nucleation, but the overall amount of twinning may remain the same.

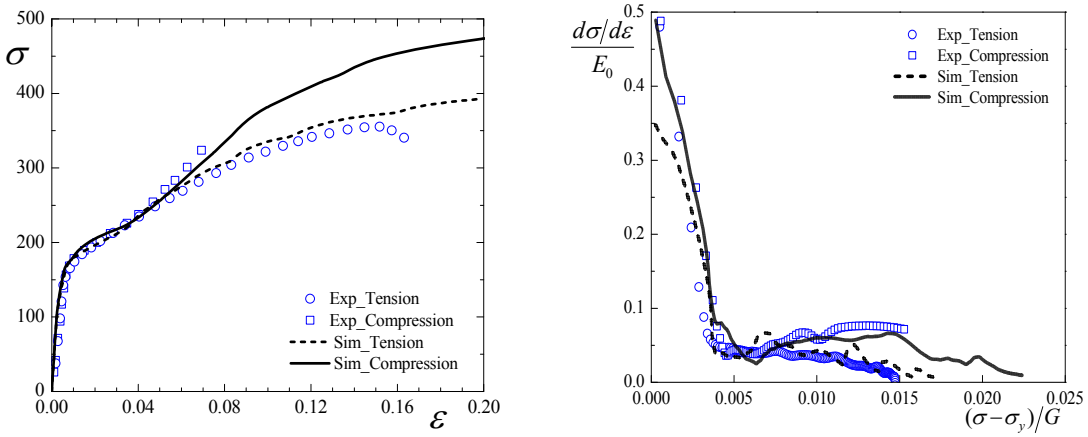

(a) (b)

Figure 3.11 (a) Measured and simulated stress-strain responses in monotonic, uniaxial tension/compression along the TD and (b) the Kocks-Mecking plot of the normalized strain hardening rate versus the flow stress minus the yield stress, where E_0 (45GPa) and G (16.3GPa) arethe Young's modulus and shear modulus, respectively.

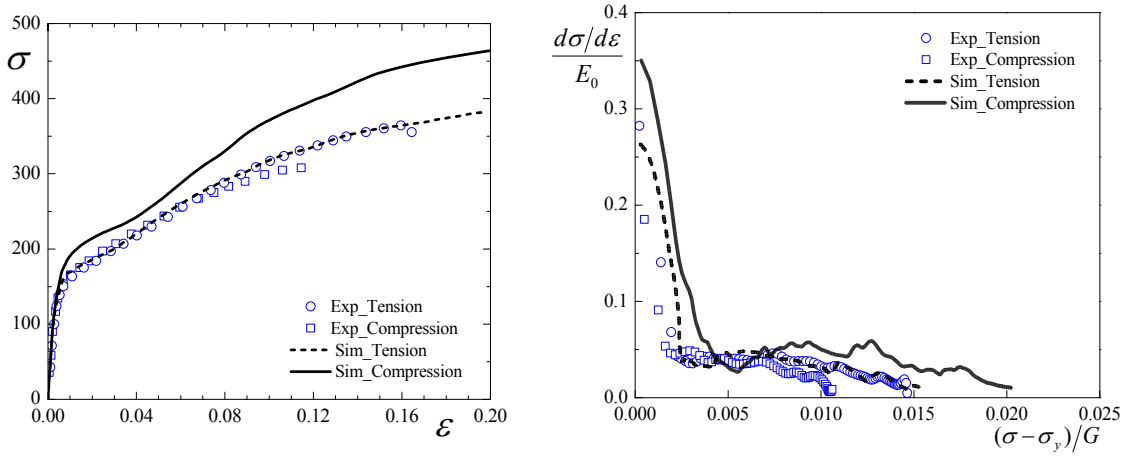

(a) (b)

Figure 3.12 (a) Measured and simulated stress-strain responses in monotonic, uniaxial tension/compression along the ND, and (b) the Kocks-Mecking plot of the normalized strain hardening rate versus the flow stress minus the yield stress, where E_0 (45GPa) and G (16.3GPa) arethe Young's modulus and shear modulus, respectively.

The deformation mode activity which is predicted to be responsible for the observed behavior is a natural output of the model (Figures 3.13 & 3.14). The results show that basal slip is much more active during compression testing along these straining directions

than either of the ED tests. Twinning exhibits an intermediate level of activity ($f^{tw} = 0.3 \sim 0.5$) relative to that observed during tension (0.05) and compression (0.8) along the extrusion direction. This is noteworthy, because previous authors have commented on the difficulty of predicting the stress strain response for cases involving intermediate levels of twinning, even when the cases of dominant twinning and minimal twinning were well-described (Oppedal et al., 2013). The texture which results from twinning has a significant impact upon secondary slip mode operation. The twinning places c-axes parallel to the loading axis during compression testing and they reorient orthogonal to the loading axis during tension. This results in more <c+a> slip during compression and more prismatic slip during tension. A comparison of the predicted normalized intensity evolution with that observed in situ, during TD tension, is presented in Figure 3.15. It shows a good overall agreement with the {00.2} and {10.0} normalized intensities observed parallel and orthogonal to the loading direction. In particular, this suggests that the predicted level of twinning is correct, since twinning produces the most rapid texture evolution responsible for intensity change.

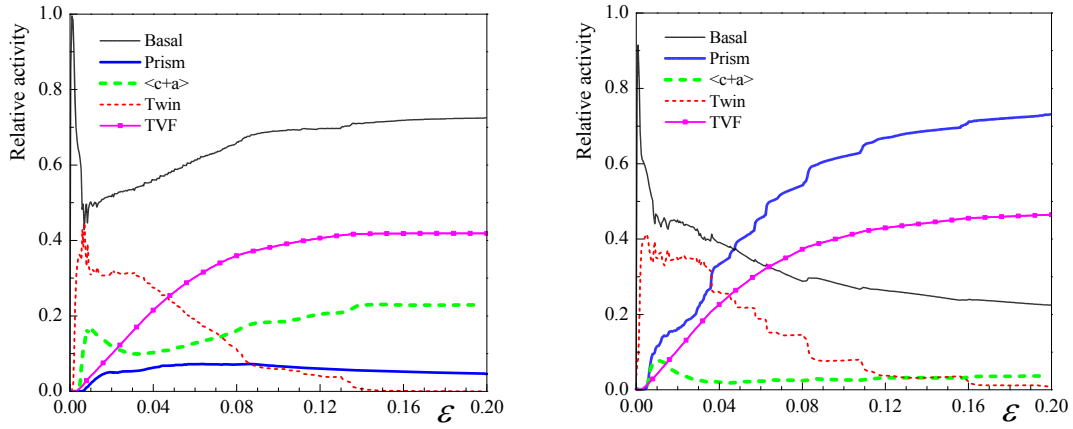

Figure 3.13 The relative deformation mode activities under uniaxial (a) compression and (b) tension along the TD.

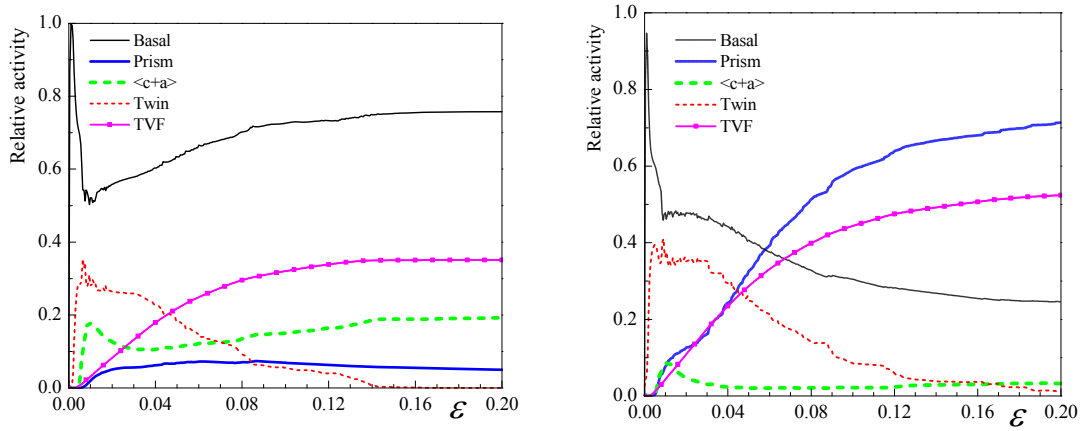

Figure 3.14 The relative deformation mode activities under uniaxial (a) compression and (b) tension along the ND.

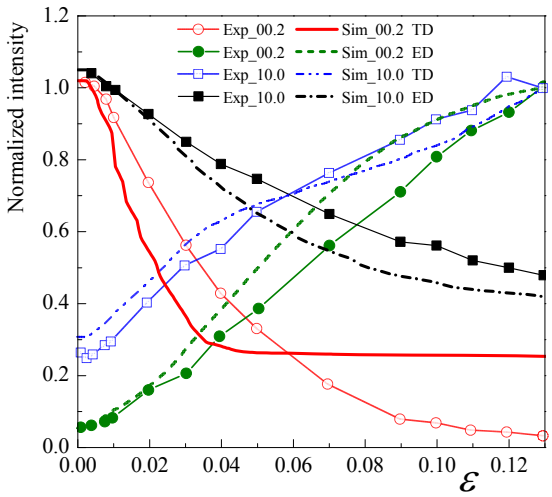

Figure 3.15 Comparison of the measured (symbols, after Wu, 2009) and predicted normalized intensity evolutions under monotonic tension along the TD.

3.3.4 Predictions of cyclic straining along the TD

Samples from the TD were tested at the same strain amplitude (1.2%) as the ED presented above. The predictions are (not surprisingly) less impressive than the fits to ED behavior shown earlier (Figure 3.16). However, the shapes of the hysteresis loops look similar to experimental hysteresis loops obtained at higher levels of cycles. The hysteresis loops obtained at higher strain amplitudes (3.0%) show similar deficiencies, whether they are compression first (Figure 3.17) or tension first (Figure 3.18) cycling experiments. Namely, the twinning and detwinning plateau behaviors complete in the case of the simulations, leading to rapid hardening at the tips of the hysteresis loops.

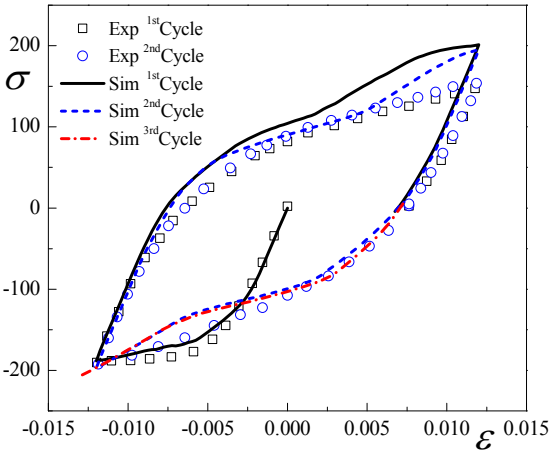

Figure 3.16 Comparison of the measured (symbols, after Wu, 2009) and predicted (curves) stress-strain responses under cyclic loading along the TD.

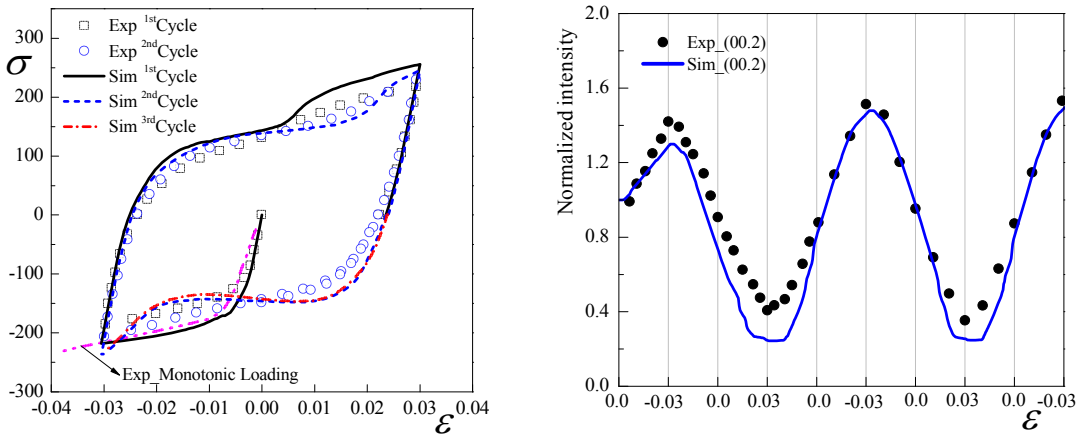

(a) (b)

Figure 3.17 Comparison of the measured (symbols, after Wu, 2009) and predicted (curves) (a) stress-strain responses under cyclic loading along the TD and (b) normalized intensity of the {00.2} diffraction peak along stress axis direction during cyclic loading along the TD beginning with compression. The dash-dot-dot line shown in (a) is the experimental data during monotonic compression along the TD.

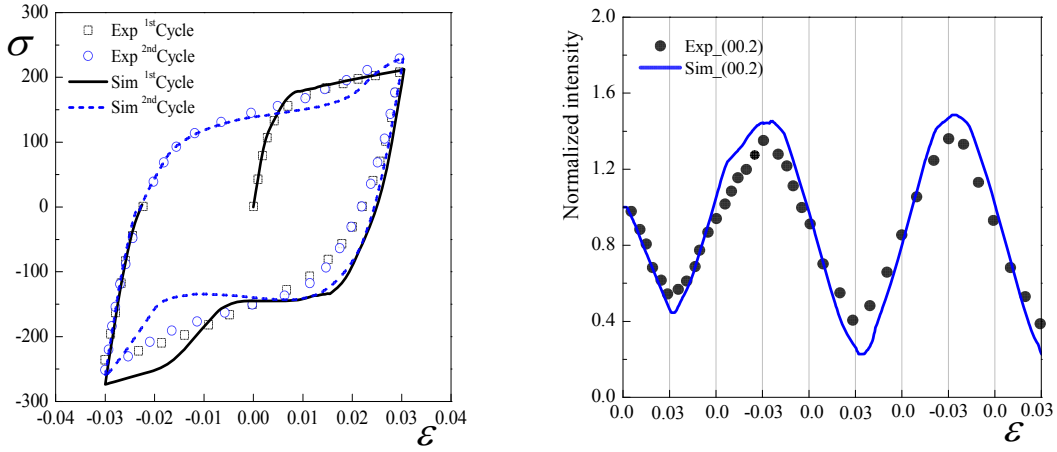

(a) (b)

Figure 3.18 Comparison of the measured (symbols, after Wu, 2009) and predicted (curves) (a) stress-strain responses under cyclic loading along the TD and (b) normalized intensity of the {00.2} diffraction peak along stress axis direction during cyclic loading along the TD beginning with tension.

3.4 Discussion

3.4.1 Modeling of twinning/detwinning

The concept of discriminating between the stress required to initiate twins τ_A and that required to grow them τ_B was introduced previously by Wang et al. (2012b, 2013a). However, it was not to this point exploited. Here, we show that the concept makes it possible to describe the sudden yielding and the yield plateau observed in materials where twinning is the main strain accommodation mechanism responsible for yield. In this initial example, a yield point peak results because of the way the formalism is introduced. Very simply, τ_A controls twin activation until the volume fraction of each twin system α reaches a threshold value (recall, f_{cr}^{tw} = 0.035). Henceforth, the code requires the stress only reaches τ_B for continued growth of the twin. Then, when the volume fraction of

twins exceeds the threshold value, V^{th}, the parent grain is no longer permitted to twin. The evolution of the critical stress with respect to the twin volume fraction of each grain is schematically shown in Figure 3.19 for clarity. More work needs to be done to fully develop this model and describe mechanistically how (and under what circumstances) the critical stress should undergo these transitions. As mentioned above, the presently employed values result in a sort of yield point peak, which is sometimes experimentally observed in Mg alloys (e.g., Clausen et al., 2008; Barnett et al., 2012), but is not clearly observed in the present case. It is suggested that the values for twin initiation and twin growth will likely have distinct grain size dependencies, which would enable modeling the effects observed by Barnett et al. (2012).

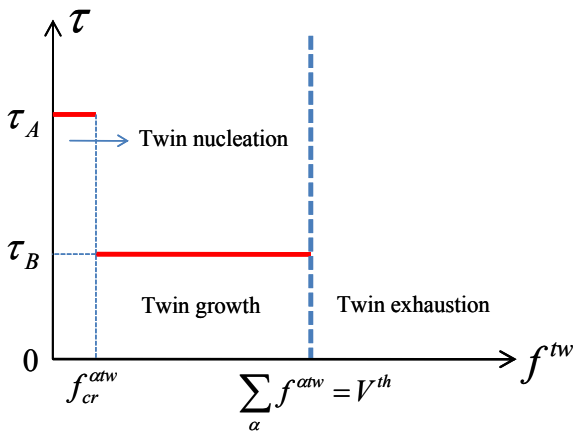

Figure 3.19 Schematic illustration of the model concept for twinning in each grain showing τ_A, τ_B and the threshold twin volume fraction.

One of the clear failures of the present model is the inability to capture the experimentally observed relaxation, which occurs upon twinning (see the discrepancy in Figure 3.4 between the predicted and observed {00.2} internal strains). There is an outstanding question pertaining to the internal strain state within twins when they are

born, based upon discrepancies between experiments and predictions originally highlighted by Clausen et al. (2008) and taken up by others in the meantime (Aydiner et al., 2009; Abdolvand and Daymond, 2012; Juan et al., 2014). It is suggested that the present transition between τ_A and τ_B and the threshold twin volume fraction f_{cr}^{tw} are related to the relaxation effect introduced by Zhang et al. (2008) and Clausen et al. (2008). A future work will explore this connection in more detail and introduce a means of including this relaxation effect within the present TDT modeling scheme. Another aspect that previous authors have emphasized, with respect to the nucleation phase is the stochastic nature of it, as revealed by analyses of electron back-scattered diffraction data (Capolungo et al., 2009; Beyerlein et al., 2010). This is not accounted for in the present model, as it does not seem to help the main shortcoming identified above.

As mentioned earlier in the paper, no discrimination is made between the CRSS values of twin growth τ_B and twin shrinkage τ_C; i.e., it is imagined that the twin boundaries can move with equal ease in the forward and reverse directions. At this point, it is considered why Lou et al. (2007) concluded that twinning is somewhat more difficult than detwinning. First of all, they employed the VPSC modeling approach for assessing the impact of texture upon the flow strength. As we have tried to emphasize throughout this paper, the texture evolution due to twinning does not immediately impact the flow strength as one might suppose (and as the VPSC modeling in the paper by Lou et al. predicts). Rather, it is only after the twinning (or detwinning) mechanism is exhausted that the orientation of the grains vis a vis other deformation mechanisms (e.g. slip) begins to impact the flow strength. Until that point, the grains which are undergoing the

relatively soft mechanism of twinning (or detwinning) will control the flow strength. Thus, it is not possible/correct to assess the impact of texture on the slip mechanism (as in App. B, Lou et al., 2007) without also accounting for the twinning mechanism. The authors concluded that the material was softened with respect to slip since they measured the texture at a point prior to the completion of twinning. In reality, the texture evolution explored in that paper (and the present) ultimately leads to significant *hardening* since grains are reoriented to the hardest orientation possible, where the c-axes are essentially parallel with the compression axis.

The other aspect overlooked by that prior analysis was the role of intergranular backstress. The EVPSC strategy presently employed naturally accounts for the internal stresses between grains. This stress has the effect of "pushing back" on the twins thereby making detwinning appear easier than twinning, from a macroscopic perspective. The results show that employing an equal stress for twinning and detwinning at the grain level well-represents the observed phenomenon. In particular, the gradual yielding behavior which is observed during unloading and reloading in the opposite direction (here tension) to the initial straining direction (here compression) is well-captured by the model. This more gradual yielding behavior in detwinning is not because it is easier that twin growth, but because there is no requirement for twin initiation, which does require a higher stress level.

3.4.2 Strengthening mechanisms

Stanford and Barnett (2013) have just performed a rather exhaustive study of the effect of Zn solid solution strengthening (and softening) of basal and non-basal slip of <a> type dislocations and deformation twinning. If we assume that the Zn content in the alloy is close to the equilibrium solubility limit (~0.2 wt %) at the aging temperature, we can compare the present results with those of Stanford and Barnett. The grain size extruded Mg alloy, ZK60A, is in the range of ~10-30 μm (this is not a precise number as extruded Mg alloy, ZK60A, typically exhibits a heterogeneous microstructure consisting of fine and coarse grains, see for example Agnew et al., 2014a.) Considering first basal slip, Stanford and Barnett (2013) report $\tau_{basal} = 0.9 + 1.55 \cdot d^{-1/2}$ (with d given in mm) which yields a range $\tau_{basal} \sim$ 10-16 MPa. For non-basal (prismatic) slip, they show a value of $\tau_{prism} \sim$ 45-55 MPa for the present grain size range. For the initiation of {10.2} twinning, they show a critical resolved shear strength of $\tau_A \sim$ 17-28 MPa.

Stanford and Barnett (2009), Rosalie et al. (2012), and Rosalie and Pauw (2014) all recently published rather complete analyses of the precipitate microstructure within binary Mg-Zn alloys. Each of these analyses have shown that the particle aspect ratios are in the range of 10:1 (5:1 – 30:1). Employing precipitate geometries relevant to the present study (i.e. yielding comparable macroscopic yield strengths for aging conditions similar to those employed commercially), Stanford and Barnett (2009) employ the Ashby-Orowan equation to predict a strengthening increment of 40 and 70 MPa for basal and prismatic slip, respectively. Finally, the work of Robson et al. (2011, 2013) sought to

determine the strengthening increment provided by precipitation to deformation twinning. If we add these values to the ranges given above, for the combined effect of solute strengthening and grain size strengthening, we can make a comparison with the values obtained in the present EVPSC modeling study of in-situ neutron diffraction data (Table 3.2).

Table 3.2 List of critical resolved shear stress values derived from experimental assessments of solid solution and grain size effects (Stanford and Barnett, 2013), strengthening due to Orowan bowing (Stanford and Barnett, 2009; Robson et al., 2011), the sum of these strengthening contributions, and the values derived in the present EVPSC study.

Mode	Solid solution and grain size strengthening (MPa)	Precipitate strengthening (MPa)	Total predicted strength (MPa)	EVPSC critical strength, τ_0 (MPa)	EVPSC saturation stress, $\tau_0 + \tau_1$(MPa)
Basal	10-16	~40	50-56	40	55
Prismatic	45-55	~70	115-125	115	130
<c+a>	-	-	-	125	285
Twinning	17-28	7-15	24-43	50-70/ 32	32

The results are encouraging, since we appear close to the point of being able to predict the response of the individual slip modes. It is noted that the basal slip system strength predicted (by the sum of the solid solution and precipitation strengthening) is higher than the critical stress inferred by EVPSC modeling of the in-situ neutron diffraction data and more in line with the saturation stress. This may be a result of the manner in which Stanford and Barnett (2013) determined the basal slip strength from simple shear tests. Alternatively, it is cautiously suggested that there may be an upper limit on the degree of precipitation strengthening which the basal slip system can undergo. Perhaps the stress at which basal screw dislocations can cross-slip onto prismatic planes

(presumably in the range of 45-55 MPa for the present Mg-Zn alloy composition and grain size) governs the basal slip system strengthening limit, since such a cross-slip event could enable dislocations to avoid having to immediately bow around an obstacle. The notion that cross-slip may limit the precipitation strengthening potential was already hinted at by Rosalie et al. (2012), and it merits further investigation. The predictions for the prismatic slip strength are very similar the present "observations," and there have been not yet been and predictions of the effect of solute on <c+a> dislocation slip strength, although there is presently work on the mentioned in a recent paper by Ghazisaeidi et al. (2014).

Regarding the effect on twinning, the results are quite interesting. Robson et al. (2011) made careful considerations of the effect of precipitation on twinning. They show that, due to the small Burgers vector of the partial dislocations responsible for twinning, the Orowan strengthening contribution is predicted to be quite small. (It is the value of 7 MPa shown in Table 3.2.) They predict a larger contribution to be due to the requirement for slip accommodation (this is the larger value of 15 MPa presented in Table 3.2.) However, even when this value is added to the solid solution and grain size strengthening effect, the total falls short (by at least 25 MPa or ~60%) of the value observed in the present study, for the activation of twinning τ_A ~ 56-70 MPa. Robson et al. (2011) implicitly acknowledge that their model is missing some aspect, since the level of tension-compression asymmetry is over predicted. (They predict $\sigma_C/\sigma_T = 0.22$, while they observe 0.53 experimentally, and we observe σ_C/σ_T ~ 0.63 in the present study.) Interestingly, the range of strength that they predict overlaps the range presently observed

for twin growth τ_B ~ 32 MPa. It seems plausible that the strengthening concepts employed by Robson et al. (2011) are appropriate for the growth of {10.2} twins, but do not relate specifically to twin nucleation.

3.4.3 Cyclic deformation

The hysteresis loops simulated for ED compare well with the experimentally measured data. However, the loops predicted for TD cycling show some characteristic distinctions from those observed experimentally. The predictions show a rapid hardening toward the tips of the hysteresis loops, which is associated with the exhaustion of twinning or detwinning. An element which is missing from the present model, which may be able to account for the observed early twin exhaustion is a back-stress (kinematic hardening) implemented at the slip system level. Such a back-stress, which is commonly employed in crystal plasticity models of fatigue deformation (McDowell, 2008; Wollmershauser et al., 2012), including a recent attempt to model a Mg alloy (Guillemer et al., 2011). The absence of such a back-stress could also explain the general failure of the present model to capture the gradual yielding of the polycrystal during unload and reload along the TD, except for the case of transition from compression to tension in the tension first case. Interestingly, the predicted hysteresis loops look more like those obtained experimentally after a large number of cycles (Wu, 2009). This experimental result suggests that there is some slow, cyclic hardening of the slip systems, which forces the twinning/detwinning mechanisms to accommodate more strain after cycling, which then leads to more rapid exhaustion of twinning/detwinning followed by rapid hardening.

This observation also supports the notion that the model of slip-based deformation would benefit from combined "kinematic" and "isotropic" hardening. However, this is beyond the scope of the present work, which shows good agreement for the monotonic deformation cases, and illuminates some specific opportunities for more work on the cyclic.

3.4.4 Load sharing of the second phase

The load sharing effect of the strengthening precipitates in heat treatable alloys is often ignored because the volume fractions are often low. In the present case, however, a load sharing effect of the precipitates is suggested by the presence of a lower than expected level of internal strains within the matrix phase. In a previous study, including an appropriate phase fraction of elastic second phase inclusions provided a sufficient level of load sharing to explain the observation (Agnew et al., 2013). In the present study, that was not the case. It was insufficient to account for the interaction between properly oriented precipitates with the homogenous effective medium of the self-consistent approach. Even though the strengthening phase is stiffer than the matrix, including an appropriate volume fraction of second phase particles has only a nominal effect on the level of internal strains predicted. One reason for the distinction between the two cases is the different level of strain hardening observed between the two cases. The present material does not begin to flow appreciably until a stress level of about 150 MPa and the highest stress level observed during the cyclic is 175 MPa. In contrast, the age-hardened

material in the previous study yielded at about 150 MPa and was observed up to a stress level greater than 250 MPa.

One hypothesis for further study is the use of a truly multi-scale approach which considers the interaction between precipitates and the individual grains in which those precipitates reside. This could help overcome the present problem of loading the precipitates insufficiently (as also noted previously by Oliver et al., 2004) because rather than interacting with the mean field, the precipitate would be interacting with a very compliant matrix grain. A larger strain mismatch between the grains and the elastic inclusions within them is anticipated, which would improve predictions by lowering the internal strain within the matrix grains.

3.5 Conclusions

A recently developed crystal plasticity model (denoted TDT, Wang et al., 2012b, 2013a, 2013c) for describing twinning and detwinning behavior is employed to simulate the cyclic deformation behavior of extruded Mg alloy, ZK60A. The results of the modeling effort permit the following conclusions to be drawn:

1. Unlike other crystal plasticity models to date, the TDT model permits simulation of the yield strain plateau often observed in strongly textured Mg alloys without resorting to *ad hoc* approximations which have been misproven since their introduction.
2. The rapid strain hardening which follows the strain hardening plateau is simulated using an empirical model which determines the exhaustion of the twinning

mechanism (i.e. describes the point when grains can no longer undergo twinning.) This model requires future work to develop a physical/mechanistic basis.

3. As suggested in the recent literature, it is necessary to discriminate between the stress required to initiate twinning and that required to grow (thicken) previously existing twins. In the present context, the stress for twin nucleation (operation A) is significantly higher than twin growth and twin shrinkage (operations B & C) (see Tables 3.1 and 3.2).
4. The resulting model is able to simulate the unusual stress-strain hysteresis behavior during twinning (e.g., sharp yielding behavior) as well as that of detwinning (characterized by quite gradual yielding).
5. The diffracted intensity evolution, which is indicative of the volume fraction of twinning compares well with the experimental data. This reflects the fact that twinning (and detwinning) is largely "kinematically driven" (i.e. the strains imposed dictate the amount of twinning observed).
6. Lattice strain evolutions during cyclic loading (and involving twinning and detwinning) are predicted. Most features of the experimentally observed internal strain evolution are well-described. In particular, the inflections which may be associated with the initiation of particular deformation mechanisms: basal and non-basal slips, as well as deformation twinning are predicted.
7. The model is able to predict the texture-induced strength anisotropy and asymmetry as well as anisotropic strain hardening behavior without requiring a

complex, dislocation density based latent hardening approach, though complex strain path change simulations may require such an approach.

8. Careful comparison of the simulated and measure lattice strains reveals greater expected load sharing by the precipitate phase and modeling shows that precipitate shape and orientation strongly influence the tension-compression asymmetry of the strain hardening response.
9. On two points, the lattice strain predictions are viewed as requiring more work: (i) the experimental results show a stronger twin relaxation than that predicted by the current model and (ii) once detwinning is complete, certain grain orientations are predicted to undergo more rapid lattice strain evolution than was observed experimentally. Perhaps these two shortcomings are related.
10. Aspects for future work include: (i) accounting for the strain rate independence (i.e. the athermal character) of twinning in the rate and temperature range of interest; (ii) accounting for the relaxation due to twin initiation, taking cues from the partially successful concepts of Clausen et al. (2008); (iii) developing a physically based model for exhaustion of the twinning and detwinning mechanisms; (iv) incorporating a back-stress which affects slip system hardening; and (v) accounting for load sharing of the precipitates by directly modeling the interaction between individual grains and the precipitate microstructure within them.

Chapter 4. A new empirical equation for termination of twinning in magnesium alloys

Plastic deformation in Magnesium (Mg) and its alloys is accommodated by both slip and twinning. The most commonly observed twinning mode is the $\{10\bar{1}2\}<10\bar{1}1>$ extension twinning. Intensive research has been recently focused on the role of twinning in plastic deformation of Mg alloys (Bohlen et al., 2006; Barnett, 2007; Lou et al., 2007; Muránsky et al., 2010a; Hong et al., 2010a; Jager et al, 2011; Jain et al., 2011; Wang et al., 2012b, 2013a; Abdolvand and Daymond, 2013a; Wu et al., 2015; Mathis et al., 2015; Barnett et al., 2015). Based upon acoustic emission data (Bohlen et al., 2006; Lou et al., 2007; Muránsky et al., 2010a; Mathis et al., 2015), it has been generally accepted that under twinning dominated conditions, the yielding and immediate post-yielding plasticity is governed largely by twin nucleation, whereas plastic deformation at higher strains is governed by twin growth and dislocation slip. After a region of low stress and low strain hardening, the material hardens rapidly resulting in an S-shaped flow curve. This is associated with two aspects: the radical texture evolution due to extensive extension twinning and the exhaustion of twinning as a strain accommodation mechanism. Therefore, to perform accurate deformation process modeling, it is important to develop constitutive models which properly account for reorientation due to twinning and twinning exhaustion. Different schemes for modeling the effect of twinning have been proposed, including the widely used predominant twin reorientation (PTR) scheme (Tomé et al., 1991) and the recently developed twinning and de-twinning (TDT) model (Wang et al., 2012b, 2013a)

In both the PTR and TDT models, a threshold twin volume fraction is defined to terminate twinning because it is rare that a grain can be fully twinned. Correspondingly, the models introduce two statistical variables: accumulated twin fraction V_{acc} and effective twinned fraction V_{eff}, with V_{acc} and V_{eff} being respectively the weighted volume fraction of the twinned region and volume fraction of grain in which twinning is exhausted. The threshold volume fraction V_{th} is defined as

$$V_{th} = \min\left(1.0,\ A_1 + A_2 \frac{V_{eff}}{V_{acc}}\right) \tag{4.1}$$

where A_1 and A_2 are two parameters. It has been demonstrated that the above equation is able to simulate experimental flow curves for Mg alloys by carefully calibrating the two parameters. However, it has been noticed that values of the fitted A_1 and A_2 adopt a wide range of values, are difficult to be determined, and have no clear connection with a physical process. It is important to point out that the PTR model considers only the twin variant with the maximum Schmid Factor (SF), while the TDT model considers all possible twin variants. Furthermore, the TDT model considers a twin as a new grain. The orientation of the new grain is initially related to that of the parent through the crystallographic twin relation, and the volume fraction associated with the new grain is updated at the end of the first straining step in which the twin variant is activated. Therefore, even considering only the $\{10\bar{1}2\}$ extension twinning mode, a parent grain could potentially become seven grains (parent plus six twins). In the PTR model, the

number of grains remains fixed throughout the simulation, which gives it a computational advantage, though there is a compromise in the fidelity of the results.

After carefully reviewing recent crystal plasticity based modeling of plastic deformations of Mg alloys, a new empirical equation to terminate twinning is proposed. For a given grain *g*, assume that f_g^α is the twin volume fraction of extension twinning system α ($\alpha = 1,6$), and $V_{th,g}^\alpha$ is its threshold value. Consequently, twinning is terminated by $f_g^\alpha = V_{th,g}^\alpha$ or $\sum_\alpha f_g^\alpha = 1$, where the latter condition corresponds to the point where the entire parent grain has been consumed. We define $V_{th,g}^\alpha$ as

$$V_{th,g}^\alpha = \begin{cases} A\left(\dfrac{m_g^\alpha}{m_g^{\alpha_{max}}}\right)^5 & \alpha \neq \alpha_{max} \\ A + \dfrac{m_g^{\alpha_{max}}}{0.5}\dfrac{\overline{V}_{eff}}{V_{acc}} & \alpha = \alpha_{max} \end{cases} \tag{4.2}$$

Here, m_g^α denotes the Schmid Factor (SF) of twinning system α at the beginning of loading, α_{max} is the twinning system with the maximum value of the SF, $m_g^{\alpha_{max}}$. Same as in Eq. (4.1) V_{acc} is the accumulated twin fraction in the aggregate and is written as $V_{acc} = \sum_g (w_g \sum_\alpha f_g^\alpha)$, with w_g being the weight or volume fraction of the grain g in the aggregate. In (4.2) $\overline{V}_{eff}$ is the effective twinned fraction defined by $\overline{V}_{eff} = \sum_g \left(w_g \sum_\alpha f_g^{\alpha,T} \right)$, with $f_g^{\alpha,T}$ denoting the twin volume fraction of the twinning system α in which twinning has been terminated. It is noted that in Eq. (4.1) used in the PTR and TDT approaches,

$V_{eff} = \sum_g w_g$ for those grains in which twinning has been terminated. This implies that if $\sum_\alpha f_g^{\alpha,T} = 1$ is assumed, $\overline{V}_{eff}$ in Eq. (4.2) reduces to V_{eff} in Eq. (4.1).

It is important to point out that the popular empirical equation, Eq. (4.1), is applied at the grain level, while the proposed new empirical equation is at the twinning system level. According to the proposed empirical formulation, for a given grain *g*, twinning system α is terminated when $f_g^\alpha = V_{th,g}^\alpha$. However, the other twinning systems in the grain can be still active if $\sum_\alpha f_g^\alpha < 1$. Therefore, for a given grain, while twinning exhaustion is a sudden event according to Eq. (4.1), twinning exhaustion described by Eq. (4.2) is a gradual process, which more closely approximates what is observed physically. It is also important to note that since the proposed new empirical equation is at the twinning system level, the new empirical equation can be applied only to the TDT model.

For the twinning system having the maximum SF, $\left(\frac{m_g^{\alpha_{max}}}{0.5} \right)$ is used in Eq. (4.2). This is rationalized that the threshold volume fraction should scale with the SF. It is important to note that the term $\left(\frac{m_g^\alpha}{m_g^{\alpha_{max}}} \right)^5$ is used in Eq. (4.2) for the twinning systems other than the one with the maximum SF. This implies that a twinning system with a very low SF should not still be active at large strains. It is also important to mention that in the early stage of the development of the proposed empirical equation (4.2), the power of

$\left(\frac{m_g^{\alpha}}{m_g^{\alpha_{max}}} \right)$ was a free parameter. We have carried out a detailed parametrical study to assess effects of the power on the calculated stress-strain response and twin volume fraction. For example, for an extruded AZ31 cylinder under uniaxial compression along the extrusion direction (this materials will be studied in Fig. 4.2), it was found that at small strains the power has a negligible effect. At strains larger than 0.06, the predicted twin volume fraction decreases with increasing the power, while the predicted stress-strain curve is not very sensitive to the power. This implies that a high power will significantly reduce the non-maximum system contribution. It is noted that Pei et al. (2012) investigated activities of the extension twin variants in a commercially available AZ31 sheet under uniaxial compression along the RD. They found that at a strain of 5% approximately 30% of the examined grains contain twins corresponding to twin variants with the third or lower ranked SF. This figure increases to 40% for samples deformed to 10% compression. Probabilistic meaningful statistics, such as the one reported by Beyerlein et al. (2010) for Mg, show results consistent with those reported by Pei et al. (2012). Eq. (4.2) suppresses twin variants with very low SF but allows the other twin variants, those with their SFs not being significantly lower than the highest SF, to be active at large strains. Surprisingly, fixing the value of the power at 5 and employing A as a fitting parameter, Eq. (4.2), could accurately simulate the mechanical behavior of all the Mg alloys examined.

The proposed new empirical equation, Eq. (4.2), has been implemented in the elastic visco-plastic self-consistent (EVPSC) model (Wang et al., 2010a), with the recently developed twinning and detwinning (TDT) description (Wang et al., 2012b, 2013a). In addition, it has been shown that, among the popular self-consistent schemes examined, the Affine self-consistent scheme gives the best overall performance for Mg alloys (Wang et al., 2010b), while both the Affine and M_{eff} schemes are suitable for Zr alloys (Qiao et al., 2015a). Therefore, the Affine self-consistent scheme is applied in the present study.

The proposed empirical equation is validated by applying it to (4.1) three typical wrought Mg alloys: a rolled AZ31B plate, an extruded AZ31 cylinder and an extruded ZK60 sheet; and to (4.2) a cast Mg alloy AZ80. The three Mg alloys have previously been studied based on the EVPSC-TDT model, with Eq. (4.1) being used for termination of twinning. On the other hand, the behaviour of cast Mg alloy AZ80 has been studied previously using the VPSC-PTR model by Jain et al. (2012). In all the simulations reported in the present paper, we consider slip in the Basal $\{0001\}<11\bar{2}0>$, Prismatic $\{10\bar{1}0\}<11\bar{2}0>$, and Pyramidal $\{\bar{1}\,\bar{1}22\}<\bar{1}\,\bar{1}23>$ slip systems, and twinning in the $\{10\bar{1}2\}<\bar{1}011>$ extension twinning system.

We start by applying the model to a rolled AZ31B plate with a H24-temper, which has been investigated by Guo et al. (2013) and Wu et al. (2014). Figure 4.1a presents the measured and simulated true stress and true strain curves under uniaxial tension and compression along the rolling direction (RD). In the simulations based on Eq. (4.1), the values of the hardening parameters for various slip systems and twinning are the same as

the ones used in the simulations reported previously by Guo et al. (2013), with parameters $A_1 = 0.65$ and $A_2 = 0.75$. In the simulations based on Eq. (4.2), the values of the hardening parameters for various slip systems and twinning system are the same as in the simulations using Eq. (4.1), and the single parameter of Eq. (4.2), $A = 0.36$. It is clear that the proposed new empirical equation with a single fitting parameter can numerically reproduce both tension and compression behavior simultaneously and precisely for the H24-temper AZ31B. Figure 4.1b demonstrates that by adjusting value of the parameter A the proposed empirical equation is able to cover a range of different hardening behaviour associated with the termination of twinning.

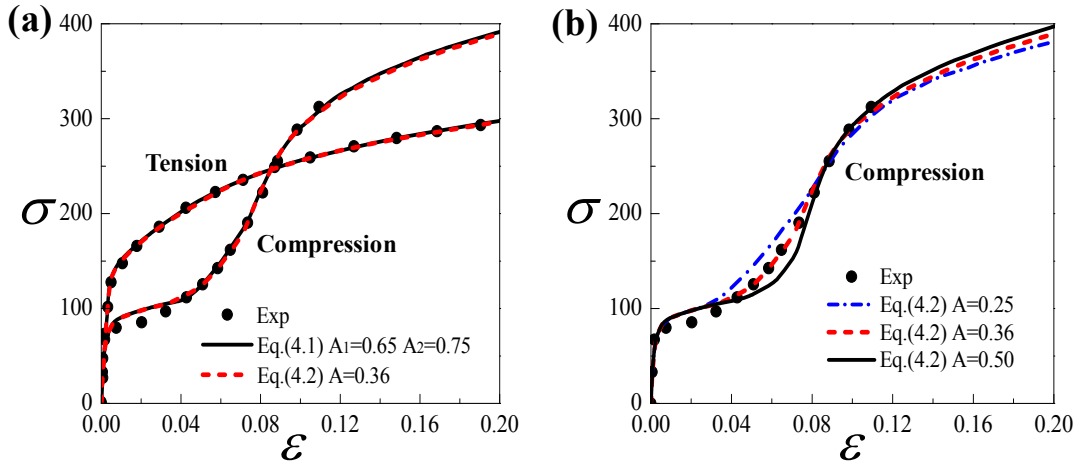

Figure 4.1 Measured (symbols) and simulated (solid lines are based on Eq. (4.1) with $A_1 = 0.65$ and $A_2 = 0.75$, and dashed lines are according to Eq.(4.2) with $A = 0.36$) true stress and true strain curves under uniaxial tension and compression along the RD (a), and predicted effect of parameter A on flow curve of uniaxial compression along the RD (b) for a H24-temper AZ31B sheet. The experimental data are taken from Guo et al. (2013).

We proceed by investigating an extruded AZ31 bar already studied by Clausen et al. (2008) and Wu et al. (2015). Figure 4.2 shows the measured and simulated true stress and true strain curves under uniaxial tension and compression along the extrusion direction (ED) (Figure 4.2a), and the measured and simulated twin volume fraction under uniaxial compression along the ED (Figure 4.2b). In the simulations, based on the EVPSC-TDT model with the termination of twinning described by the popular empirical equation (4.1), the values of the hardening parameters are the same as those listed in Wu et al. (2015). It is found that using these values of the hardening parameters, together with $A = 0.25$, the EVPSC-TDT model with Eq. (4.2) can reproduce both tension and compression behavior for the extruded AZ31 bar.

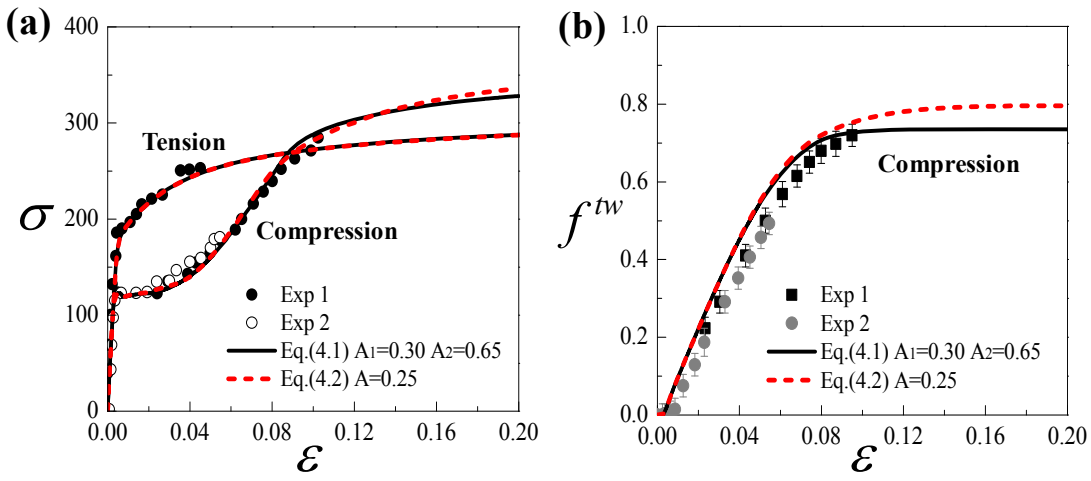

Figure 4.2 Measured (symbols) and simulated (solid and dashed lines) true stress and true strain curves under uniaxial tension and compression along the ED (a), and twin volume fraction under uniaxial compression along the ED (b) for an extruded AZ31 cylinder. Solid lines are based on Eq. (4.1) with $A_1 = 0.30$ and $A_2 = 0.65$, and dashed lines are according to Eq. (4.2) with $A = 0.25$. The experimental data are taken from Clausen et al. (2008).

Figure 4.3 shows the measured and simulated true stress and true strain curves under uniaxial tension and compression along the ED (Fig. 4.3a) and the transverse direction (TD) (Fig. 4.3b), as well as the measured and predicted normalized {0002} diffraction peak intensity for the diffraction vector parallel to the stress axis during uniaxial tension along the TD (Fig. 4.3c) for an extruded ZK60 sheet, which has been investigated experimentally by Wu et al. (2009) and numerically by Qiao et al. (2015b). The values of the hardening parameters involved in the EVPSC-TDT model with the popular empirical equation (4.1) are the same as those listed in Qiao et al. (2015b). It is found that using these values of the hardening parameters, together with $A = 0.35$, the EVPSC-TDT model with Eq. (4.2) can reproduce both tension and compression behavior along the ED. Significantly, the EVPSC-TDT model with $A_1 = 0.56$ and $A_2 = 0.70$ in Eq. (4.1) or $A = 0.35$ in Eq. (4.2) can accurately predict uniaxial tension and compression along the TD where twinning neither dominates nor is strongly suppressed, but exhibits an intermediate level of twinning and a intermediate hardening response. More significantly, Fig. 4.3c clearly indicates that the EVPSC-TDT model with Eq. (4.1) greatly overestimates the experimental data after the strain of ~0.04 since twinning in most of the grains which contribute to the {0002} diffraction peak is suddenly terminated when the total twin volume fraction reaches the threshold value. The EVPSC-TDT model with Eq. (4.2) provides a much better prediction. This is due to the fact that although one twinning system in a grain has been terminated, the proposed empirical equation allows the other twinning systems in the grain to be still active and to continue accommodating

plastic deformation. Incidentally, although it is not shown in Fig 4.3c, it was found that the predicted intensity is not sensitive to the value of the power used in Eq. (4.2).

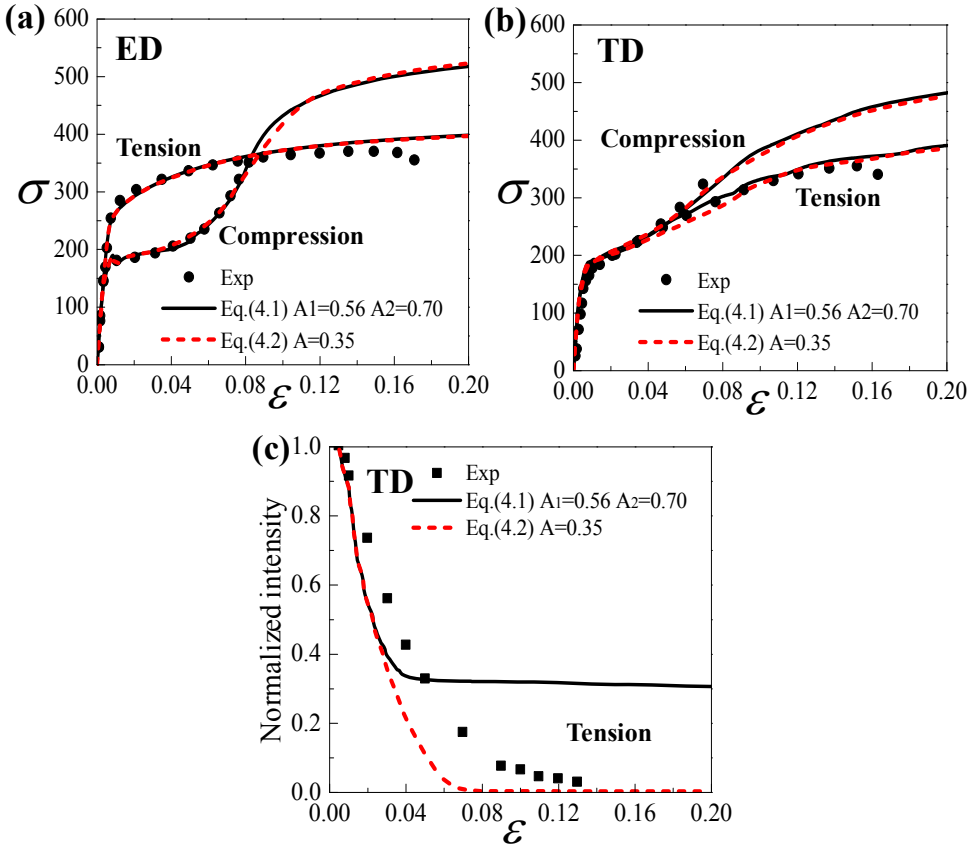

Figure 4.3 Measured (symbols) and simulated (solid and dashed lines) true stress and true strain curves under uniaxial tension and compression along the ED (a), and TD (b), as well as the measured and predicted normalized {0002} diffraction peak intensity for the diffraction vector parallel to the stress axis during uniaxial tension along the TD (c) for an extruded ZK60 sheet. Solid lines are based on Eq. (4.1) with $A_1 = 0.56$ and $A_2 = 0.70$, and dashed lines are according to Eq. (4.2) with $A = 0.35$. The experimental data are taken from Wu et al. (2009).

Although the results are not shown in the present paper, we have also validated the proposed equation by investigating other wrought Mg alloys we have access to their experimental data necessary for carrying out numerical simulations. For example, it was

found that $A_1 = 0.50$ and $A_2 = 0.60$ in Eq. (4.1) or $A = 0.24$ in Eq. (4.2) reproduced the mechanical behaviour of an extruded AM30 tube experimentally investigated by Jiang et al. (2007) and numerically studied by Levesque et al. (2010) and Guo et al. (2015b). It was also revealed that both Eq. (4.1) with $A_1 = 0.60$ and $A_2 = 0.80$ and Eq. (4.2) with $A = 0.30$ predicted well the anisotropic and twinning behaviour in a hot-rolled AZ31 sheet under uniaxial compression (Chapuis et al. 2014b; Guo et al., 2015a). For a cold-rolled AZ31B sheet already studied experimentally by Lou et al. (2007) and numerically by Wu et al. (2015), Eq. (4.1) with $A_1 = 0.65$ and $A_2 = 0.80$ and Eq. (4.2) with $A = 0.40$ reproduced well the experimentally observed mechanical behavior.

While the cases presented above are all for the wrought Mg alloys with strong basal textures, it is very interesting to see if the proposed empirical equation can model cast Mg alloys with weak textures. Figure 4.4 presents the measured and simulated true stress and true strain curves under uniaxial tension and compression along the cast direction (CD) for a cast Mg alloy AZ80, which has been studied by Jain et al. (2012) and Tomlinson et al. (2013). It is found that, using same values of the hardening parameters, the EVPSC-TDT model with $A_1 = 0.20$ and $A_2 = 0.75$ in Eq. (4.1) or $A = 0.20$ in Eq. (4.2) can reproduce both tension and compression behavior for the cast AZ80.

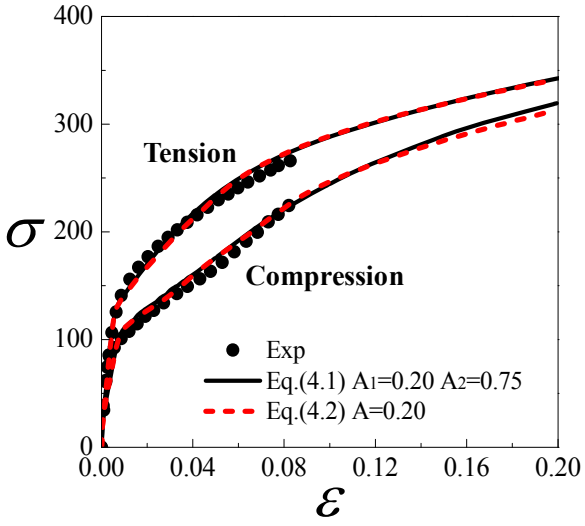

Figure 4.4 Measured (symbols) and simulated (solid and dashed lines) true stress and true strain curves under uniaxial tension and compression along the cast direction for a cast AZ80. Solid lines are based on Eq. (4.1) with $A_1 = 0.20$ and $A_2 = 0.75$, and dashed lines are according to Eq. (4.2) with $A = 0.20$. The experimental data are taken from Tomlinson et al. (2013).

Finally, it is worth mentioning that although fixing the power of $\left(\frac{m_g^{\alpha}}{m_g^{\alpha_{max}}}\right)$ at 5 can accurately simulate the mechanical behavior of all the Mg alloys examined, with a very wide range of initial textures, it could be better or even necessary to consider the power as an adjustable parameter when the proposed empirical equation is applied to other metals like Ti and Zr alloys. Furthermore, although the proposed empirical model can be applied only to the TDT model in the currently form, it could be slightly modified for using in the PTR model. All these are in progress and will be reported elsewhere.

In summary, we have developed a new empirical equation (4.2) for termination of twinning in Mg alloys. In contrast with the popular two parameter empirical equation (4.1) widely used in the PTR and TDT twinning schemes, the new empirical equation involves

only a single parameter. The proposed equation has been implemented in the EVPSC-TDT model, and it has demonstrated that the EVPSC-TDT model with the proposed empirical equation is able to capture key macroscopic features associated with twinning and its termination experimentally observed in a variety of magnesium alloys with different textures, including a nearly randomly textured casting.

Chapter 5. General conclusions and future work

This study aims to investigate the deformation mechanisms in HCP metals. Twinning and detwinning play important roles in accommodating plastic deformation in HCP metals due to the limited number of independent slip systems. A better understanding of the mechanisms associated with twinning and detwinning will assist further industrial applications of HCP metals.

This study first focuses on the study of the deformation behavior of a Zircaloy-2 slab under different deformation processes. In order to take into account the effects of thermal residual strains generated during the cooling process (from 898 K to 298 K) on the subsequent mechanical loading, the EVPSC model (Wang et al., 2010a) is extended by including the thermal strain effect. It is known that the predicted overall response of a polycrystal closely depends on the activated slip and twinning systems during the loading process and should be sensitive to the homogenization method employed in polycrystal models. Therefore, various self-consistent schemes used in the modified EVPSC model have been evaluated in terms of the quality of predictions of the macroscopic (flow curves and R-values) and microscopic behaviors (lattice strain and texture coefficients). It is demonstrated by numerical results that among the models examined, the EVPSC model with the Affine and Meff=0.1 self-consistent schemes give much better performance for the Zircaloy-2 slab than the Secant and Tangent SCSs.

Detwinning is twinning in the twinned region which reorients the orientation of a twin back into its parent orientation. Detwinning occurs after twinning during reverse

loading. Twinning and detwinning alternatively appear during cyclic loading. This study has investigated the twinning and detwinning behavior of Mg alloy ZK60A during monotonic and cyclic loading based on the EVPSC-TDT model (Wang et al., 2012b, 2013a). Notably, accounting for the initial texture and calibrating the model using tension and compression along one direction permits prediction of the strength anisotropy, strength asymmetry, and strain hardening behavior along other directions, for cases in which the contribution of twinning is large, small and intermediate. The model discriminates between the stress required to initiate twinning and that required to grow (thicken) previously existing twins. This enables the model to simulate the unusual stress-strain hysteresis behavior during twinning (sharp yielding behavior) as well as that of detwinning characterized by quite gradual yielding. The strain hardening plateau which occurs during both twinning and detwinning are captured, as are the rapid hardening induced by the exhaustion of these mechanisms. Finally, the modeling is validated using previously published in-situ neutron diffraction data. The predicted diffracted intensity evolution, which is indicative of the volume fraction of twinning compares well with the experimental data. For the first time, the lattice strain evolutions during cyclic loading (involving twinning and detwinning) of an extruded magnesium alloy are predicted. Most features of the experimentally observed internal strain evolution are well-described. In particular, the inflections which may be associated with the initiation of particular deformation mechanisms: basal and non-basal slips, as well as deformation twinning are predicted. Careful analysis of the lattice strains reveals a greater than expected load sharing by the precipitate phase.

To perform accurate deformation process modeling for a polycrystal, it is important to develop constitutive models which properly account for twinning induced reorientation and twinning exhaustion. In all existing polycrystal models, an empirical equation for the termination of twinning in a grain is often needed. A new empirical equation for describing the termination of twinning in magnesium alloys has been developed in this study. It is important to point out that the popular empirical equation currently used in all polycrystal models is applied at the grain level, while the proposed new empirical equation is at the twinning system level. According to the proposed empirical formulation, a twinning system will be terminated when the twin volume fraction of the twinning system reaches a threshold value. However, the other twinning systems in the grain can be still active if the total twin volume fraction of all twinning systems in the grain is still less than 1.0. According to the widely used empirical equation, twinning exhaustion is a sudden event within a given grain. In contrast, the twinning exhaustion described by the new proposed empirical equation is a gradual process, which is more representative of what is observed physically. In addition, the new description introduces only a single parameter, while the widely used empirical equation involves two parameters. It is demonstrated that it is easy to calibrate the single parameter and the proposed empirical equation is able to accurately simulate the experimentally observed rapid hardening associated with twinning exhaustion.

As mentioned in the general introduction, crystal plasticity finite element method (CPFEM) is another important alternative modeling method to investigate the deformation mechanisms of HCP metals, where both equilibrium and compatibility

throughout the polycrystalline aggregate can be naturally accommodated in a weak finite element sense. Wu et al. (2015) have developed a new twin nucleation, propagation and growth (TNPG) model for HCP materials. The TNPG model explicitly takes into account the stress relaxation associated with twin nucleation and it has been implemented into the EVPSC-TDT model (Wang et al., 2012b, 2013a). The authors mentioned that the EVPSC-TNPG model is still not able to explicitly show how a twin nucleates and propagates due to the nature of homogenized polycrystal plasticity models. However, the finite element model combined with the TNPG model is expected to visually describe the spatially inhomogeneous deformation process of twin nucleation, propagation and growth. In order to investigate the idea, a crystal plastic finite element method with implementation of the TNPG model has been developed to simulate the deformation behavior of a Mg single crystal under compression perpendicular to the *c*-axis. Preliminary numerical results show a successful modeling on how a twin nucleates, propagates and grows in a matrix. However, further validation of the code and careful analyses of numerical results are still needed in the future.

List of references

Abdolvand H., Daymond M.R., Mareau C., 2011. Incorporation of twinning into a crystal plasticity finite element model: evolution of lattice strains and texture in Zircaloy-2. International Journal of Plasticity 27, 1721-1738.

Abdolvand H., Daymond M.R., 2012. Internal strain and texture development during twinning: comparing neutron diffraction measurement with crystal plasticity finite element approaches. Acta Mater 60, 2240-2248.

Abdolvand H., Daymond M.R., 2013a. Multi-scale modeling and experimental study of twin inception and propagation in hexagonal closed packed materials using crystal plasticity finite element approach-Part I: average behavior. Journal of the Mechanics and Physics of Solids 61, 783-802.

Abdolvand H., Daymond M.R., 2013b. Multi-scale modeling and experimental study of twin inception and propagation in hexagonal closed packed materials using crystal plasticity finite element approach-Part II: local behavior. Journal of the Mechanics and Physics of Solids 61, 803-818.

Abdolvand H., Majkut M., Oddershede J., Wright J.P., Daymond M.R., 2015. Study of 3-D stress development in parent and twin pairs of a hexagonal close-packed polycrystal: Part II-crystal plasticity finite element modeling. Acta Materialia 93, 235-245.

Agnew S. R., Yoo M. H., Tomé C.N., 2001. Application of texture simulation to understanding mechanical behavior of Mg and solid solution alloys containing Li or Y. Acta Materialia 49, 4277-4289.

Agnew S.R., 2002. Plastic anisotropy of magnesium alloy AZ31B sheet. TMS Annual Meeting, Magnesium Technology, 169-174.

Agnew S.R., Tomé C.N., Brown D.W., Holden T.M., Vogel S.C., 2003. Study of slip mechanisms in a magnesium alloy by neutron diffraction and modeling. Scripta Materialia 48, 1003-1008.

Agnew S.R., Horton J.A., Lillo T.M., Brown D.W., 2004. Enhanced ductility in strongly textured magnesium produced by equal channel angular processing. Scripta Materialia 50, 377-381.

Agnew S.R., Duygulu O., 2005. Plastic anisotropy and the role of non-basal slip in magnesium alloy AZ31B. International Journal of Plasticity 21, 1161-1193.

Agnew S.R., Senn J.W., Horton J.A., 2006a. Mg sheet metal forming: Lessons learned from deep drawing Li and Y solid-solution alloys. Jom 58, 62-69.

Agnew S.R., Brown D.W., Tomé C.N., 2006b. Validating a polycrystal model for the elastoplastic response of magnesium alloy AZ31 using in situ neutron diffraction. Acta Materialia 54, 4841-4852.

Agnew S.R., Mulay R.P., Polesak F.J., Calhoun C.A., Bhattacharyya J.J., Clausen B., 2013. In situ neutron diffraction and polycrystal plasticity modeling of a Mg-Y-Nd-Zr alloy: Effects of precipitation on individual deformation mechanisms. Acta Materialia 61, 3769-3780.

Agnew S.R., Calhoun C.A., Clausen B., 2014a. In-situ Neutron diffraction study of aging in alloy ZK60A. Magnesium Technology, 389-393.

Agnew S.R., Wittington W., Oppedal A., El Kadiri H., Shaeffer M., Ramesh K.T., Bhattacharyya J.J., DeLorme R., Davis B., 2014b. Dynamic behavior of a rare earth containing Mg alloy, WE43B-T5, plate with comparison to conventional alloy, AM30-F. Journal of Metals 66, 277-290.

Akhtar A., 1975. Prismatic slip in zirconium single crystals at elevated temperatures. Metallurgical Transactions A 6, 1217-1222.

Alharbi H.F., Kalidindi S.R., 2015. Crystal plasticity finite element simulations using a database of discrete Fourier transforms. International Journal of Plasticity 66, 71-84.

Anand L., Kalidindi S.R., 1994. The process of shear band formation in plane strain compression of fcc metals: Effects of crystallographic texture. Mechanics of Materials 17, 223-243.

Asaro R.J., Rice J.R., 1977. Strain localization in ductile single crystals. Journal of the Mechanics and Physics of Solids 25, 309-338.

Asaro R.J., Needleman A., 1985. Texture development and strain hardening in rate dependent polycrystals. Acta Metallurgica 33, 923-953.

Askari H., Young J., Field D., Kridli G., Li D., Zbib H., 2013. A study of the hot and cold deformation of twin-roll cast magnesium alloy AZ31. Philosophical Magazine 94, 381-403.

Aydıner C.C., Bernier J.V., Clausen B., Lienert U., Tomé C.N., Brown D.W., 2009. Evolution of stress in individual grains and twins in a magnesium alloy aggregate. Physical Review B 80, 024113.

Bakarian P.W., Mathewson C.H., 1943. Slip and twinning in magnesium single crystals at elevated temperatures. Transactions of the Metallurgical Society of AIME 152, 226-254.

Ballinger R.G., Lucas G.E., Pelloux R.M., 1984. The effects of plastic strain on the evolution of crystallographic texture in zircaloy-2. Journal of Nuclear Materials 126, 53-69.

Barlat F., Lege D.J., Brem J.C., 1991. A six-component yield function for anisotropic materials. International Journal of Plasticity 7, 693-712.

Barlat F., Maeda Y., Chung K., Yanagawa M., Brem J.C., Hayashida Y., Lege D.J., Matsui K., Murtha S.J., Hattori S., Becker R.C., Makosey S., 1997. Yield function development for aluminum alloy sheets. Journal of the Mechanics and Physics of Solids 45, 1727-1763.

Barnett M.R., Keshavarz Z., Beer A.G., Atwell D., 2004. Influence of grain size on the compressive deformation of wrought Mg-3Al-1Zn. Acta Materialia 52, 5093-5103.

Barnett M.R., 2007. Twinning and the ductility of magnesium alloys: Part I: "Tension" twins. Materials Science and Engineering A464, 1-7.

Barnett M.R., Nave M.D., Ghaderi A., 2012. Yield point elongation due to twinning in a magnesium alloy. Acta Materialia 60, 1433-1443.

Barnett M.R., Stanford N., Ghaderi A., Siska F., 2013. Plastic relaxation of the internal stress induced by twinning. Acta Materialia 61,7859-7867.

Barnett M.R., Bouaziz O., Toth L.S., 2015. A microstructure based analytical model for tensile twinning in a rod textured Mg alloy. International Journal of Plasticity 72, 151-167.

Bauschinger J., 1886. On the Change of the Position of the Elastic Limit of Iron and Steel Under Cyclic Variations of Stress. Mitt. Mech. Tech. Lab., Munich, 13(8), 1-115.

Bell R.L., Cahn R.W., 1957. The dynamics of twinning and the interrelation of slip and twinning in zinc crystals. Proceedings of the Royal Society of London A 239, 494-521.

Bertin N., Tomé C.N., Beyerlein I.J., Capolungo L., 2014. On the strength of dislocation interactions and their effect on latent hardening in pure magnesium. International Journal of Plasticity 62, 72-92.

Beyerlein I.J., Tomé C.N., 2008. A dislocation-based constitutive law for pure Zr including temperature effects. International Journal of Plasticity 24, 867-895.

Beyerlein I.J., Tomé C.N., 2010. A probabilistic twin nucleation model for HCP polycrystalline metals. Proceedings of the Royal Society A 466, 2517-2544.

Beyerlein I.J., Capolungo L., Marshall P.E., McCabe R.J., Tomé C.N., 2010. Statistical analyses of deformation twinning in magnesium, Philosophical Magazine 90, 2161-2190.

Bohlen J., Chmelik F., Dobron P., Letzig D., Lukac P., Kainer K.U., 2004. Acoustic emission during tensile testing of magesium AZ alloys. Journal of Alloys and Compounds 378, 214–219.

Bohlen J., Dobron P., Meza Garcia E., Chmelík F., Lukáč P., Letzig D., Kainer K.U., 2006. The Effect of Grain Size on the Deformation Behaviour of Magnesium Alloys Investigated by the Acoustic Emission Technique. Advanced Engineering Materials 8,422-427.

Boger R.K., Wagoner R.H., Barlat F., Lee M.G., Chung K., 2005. Continuous, large strain, tension/compression testing of sheet material. International Journal of Plasticity 21, 2319-2343.

Bourke M.A.M., Dunand D.C., Üstündag E., 2002. SMARTS–a spectrometer for strain measurement in engineering materials, Applied Physics A, A 74 [Suppl.], S1707–S1709.

Bronkhorst C.A., Kalidindi S.R., Anand L., 1992. Polycrystalline plasticity and the evolution of crystallographic texture in FCC metals. Philosophical Transactions of the Royal Society A 341, 443-477.

Brown D.W., Agnew S.R., Bourke M.A.M., Holden T.M., Vogel S.C., Tomé C.N., 2005. Internal strain and texture evolution during deformation twinning in magnesium. Materials Science and Engineering A 399, 1-12.

Brown D.W., Jain A., Agnew S.R., Clausen B., 2007. Twinning and Detwinning during Cyclic Deformation of Mg Alloy AZ31B. Materials Science Forum, 539-543, 3407-3413.

Burke E.C., Hibbard W.R., 1952. Plastic deformation of magnesium single crystals. Transactions of AIME 194, 295-303.

Cáceres C.H., Sumitomo T., Veidt M., 2003. Pseudoelastic behavior of cast magnesium AZ91 alloy under cyclic loading-unloading. Acta Materialia 51, 6211-6218.

Camposilvan E., Torrents O., Anglada M., 2014. Small-scale mechanical behavior of zirconia. Acta Materialia 80, 239-249.

Capolungo L., Marshall P.E., McCabe R.J., Beyerlein I.J., Tomé C.N., 2009. Nucleation and growth of twins in Zr: A statistical study. Acta Materialia 57, 6047-6056.

Capolungo L., Beyerlein I.J., Wang Z.Q., 2010. The role of elastic anisotropy on plasticity in hcp metals: a three-dimensional dislocation dynamics study. Modelling and Simulation in Materials Science and Engineering 8, 085002 (16pp).

Castelnau O., Francillette H., Bacroix B., Lebensohn R.A., 2001. Texture dependent plastic behavior of Zr 702 at large strain. Journal of Nuclear Materials 297, 14-26.

Cazacu O., Barlat F., 2001. Generalization of Drucker's yield criterion to orthotropy. Math. Mech. Solids 6, 613-630.

Cazacu O., Barlat F., 2003. Application of representation theory to describe yielding of anisotropic aluminum alloys. International Journal of Engineering Science 41, 1367-1385.

Cazacu O., Barlat F., 2004. A criterion for description of anisotropy and yield differential effects in pressure insensitive metal. International Journal of Plasticity 20, 2027-2045.

Cazacu O., Plunkett B., Barlat F., 2006. Orthotropic yield criterion for hexagonal closed packed metals. International Journal of Plasticity 22, 1171-1194.

Chapuis A, Xin Y, Zhou X, Liu Q., 2014a. {10-12} Twin variants selection mechanisms during twinning, re-twinning and detwinning. Materials Science and Engineering A 612, 431-439.

Chapuis A., Wang B., Liu Q., 2014b. A comparative study between uniaxial compression and plane strain compression of Mg–3Al–1Zn alloy using experiments and simulations. Materials Science and Engineering A 597, 349-358.

Chin G.Y., Hosford W.F., Mendorf D.R., 1969. Accommodation of constrained deformation in f.c.c. metals by slip and twinning. Proceedings of the Royal Society of London A 309, 433-456.

Chmelik F., Lukac P., Janecek M., Moll F., Mordike B.L., Kainer K.U., Langdon T.G., 2002. An evaluation of the creep characteristics of an AZ91 magnesium alloy composite using acoustic emission. Materials Science and Engineering A 338,1-7.

Christian J.W., 2002. The theory of transformations in metals and alloys. 3rd ed. New York: Pergamon Press.

Christian J.W., Mahajan S., 1995. Deformation twinning. Progress in Materials Science 39, 1-157.

Clausen B., Tomé C. N., Brown D. W., Agnew S. R., 2008. Reorientation and stress relaxation due to twinning: Modeling and experimental characterization for Mg. Acta Materialia 56, 2456-2468.

Choi S.H., Kim D.W., Seong B.S., Rollett A.D., 2011. 3D simulation of spatial stress distribution in an AZ31 Mg alloy sheet under in-plane compression. International Journal of Plasticity 27, 1702-1720.

Conrad H., Robertson W.D., 1957. Effect of temperature on the flow stress and strain-hardening coefficient of magnesium single crystals. Transactions of AIME 209, 503-513.

Cooper R.E., 1962. Kinetics of elastic twinning in calcite. Proceedings of the Royal Society of London A 270, 525-537.

Cox B., 2005. Some thoughts on the mechanisms of in-reactor corrosion of zirconium alloys. Journal of Nuclear Materials 336, 331-368.

Daymond M.R., Priesmeyer H.G., 2002. Elastoplastic deformation of ferritic steel and cementite studied by neutron diffraction and self-consistent modelling. Acta Materialia 50, 1613-1626.

Duesbery M.S., Vitek V., 1998. Plastic anisotropy in b.c.c. transition metals. Acta Materialia 46, 1481-1492.

Eisenlohr, P., 2013. Private communication.

El Kadiri H., Baird J.C., Kapil J, Oppedal A.L., 2013a. Flow asymmetry and nucleation stresses of twinning and non-basal slip in magnesium. International Journal of Plasticity 44, 111-120.

El Kadiri, H., Kapil J., Oppedal A.L., Hector Jr, L.G., Agnew S.R., Cherkaoui M., Vogel S.C., 2013b. The effect of twin-twin interactions on the nucleation and propagation of {10-12} twinning in magnesium. Acta Materialia 61, 3549-3563.

Eshelby J.D., 1957. The determination of the elastic field of an ellipsoidal inclusion, and related problems. Proceedings of the Royal Society of London A241, 376-396.

Fernandez A., Perez-Prado M.T., Yei W., Jerusalem A., 2011. Continuum modeling of the response of a Mg alloy AZ31 rolled sheet during uniaxial deformation. International Journal of Plasticity 27, 1739-1957.

Foley D.C., Al-Maharbi M., Hartwig K.T., Karaman I., Kecskes L.J., Mathaudhu S.N., 2011. Grain refinement vs. crystallographic texture: Mechanical anisotropy in a magnesium alloy. Scripta Materialia 64, 193-196.

Francillette H., Bacroix B., Gasperini M., Bechade J.L., 1998. Grain orientation effects in Zr702 a polycrystalline samples deformed in channel die compression at room temperature. Acta Materialia 46, 4131-4142.

Ghazisaeidi M., Hector Jr, L.G., Curtin W.A., 2014. First-principles core structures of <c+a> edge and screw dislocations in Mg. Scripta Materialia 75, 42-45.

Gharghouri M.A., 1997. Study of the mechanical properties of magnesium-8.5wt% aluminum by in-situ neutron diffraction. Ph.D Thesis. Department of Materials Science and Engineering. McMaster University, Hamilton, Canada.

Gharghouri M. A., Weatherly G. C., Embury J. D., Root J., 1999. Study of the mechanical properties of Mg7.7at.% Al by in-situ neutron diffraction. Philosophical Magazine A 79, 1671-1695.

Ghosh S., Anahid M., 2013. Homogenized constitutive and fatigue nucleation models from crystal plasticity FE simulations of Ti alloys, Part 1: Macroscopic anisotropic yield function. International Journal of Plasticity 47, 182-201.

Gloaguen D., Fajoui J., Girault B., 2014. Residual stress fields analysis in rolled Zircaloy-4 plates: Grazing incidence diffraction and elastoplastic self-consistent model. Acta Materialia 71, 136-144.

Graff S., Brocks W., Steglich D., 2007. Yielding of magnesium: From single crystal to polycrystalline aggregates. International Journal of Plasticity 23, 1957-1978.

Gröger R., Vitek V., 2005. Breakdown of the Schmid law in bcc molybdenum related to the effect of shear stress perpendicular to the slip direction. Materials Science Forum Vol. 482,123-126.

Griffiths M., 1988. A review of microstructure evolution in zirconium alloys during irradiation. Journal of Nuclear Materials 159, 190-218.

Griffiths M, Holt RA, Rogerson A., 1995. Microstructural aspects of accelerated deformation of Zircaloy nuclear reactor components during service. Journal of Nuclear Materials 225, 245-258.

Gu C.F., Toth L.S., Hoffman M., 2014. Twinning effects in a polycrystalline magnesium alloy under cyclic deformation. Acta materialia 62, 212-224.

Guillemer C., Clavel M., Cailletaud G., 2011. Cyclic behavior of extruded magnesium: Experimental, microstructural and numerical approach. International Journal of Plasticity 27, 2068-2084.

Guo X.Q., Wu W., Wu P.D., Qiao H., An K., Liaw P.K., 2013. On the Swift effect and twinning in a rolled magnesium alloy under free-end torsion. Scripta Materialia 69, 319-322.

Guo X.Q., Chapuis A., Wu P.D., Agnew S.R., 2015a. On twinning and anisotropy in rolled Mg alloy AZ31 under uniaxial compression. International Journal of Solids and Structures 64-65, 42-50.

Guo X.Q., Wang H., Qiao H., Mao X.B., 2015b. Numerical study of the large strain behavior of extruded magnesium alloy AM30 tube by elastic viscoplastic self-consistent model. Materials and Design 79, 99-105.

Gurao N.P., Akhiani H., Azpunar J.A., 2014. Pilgering of Zircaloy-4: Experiments and simulations. Journal of Nuclear Materials 453, 158-168.

Hama T., Takuda H., 2011. Crystal-plasticity finite-element analysis of inelastic behavior during unloading in a magnesium alloy sheet. International Journal of Plasticity 27, 1072-1092.

Hama T., Takuda H., 2012. Crystal plasticity finite-element simulation of deformation behavior in a magnesium alloy sheet considering detwinning. Steel Research International, Special Edition, 1115-1118.

Hama T., Kuchinomachi Y., Hosokawa N., Fujimoto H., Takuda H., 2012. Work-hardening behaviors of magnesium alloy sheet during in-plane cyclic loading. Materials Science and Engineering A551, 209-217.

Hama T, Kitamura N, Takuda H., 2013. Effect of twinning and detwinning on inelastic behavior during unloading in a magnesium alloy sheet. Materials Science and Engineering A 583, 232-241.

Hama T., Nagao H., Kuchinomachi Y., Takuda H., 2014. Effect of pre-strain on work-hardening behavior of magnesium alloy sheets upon cyclic loading. Materials Science and Engineering A591, 69-77.

Herrera-Solaz V., LLorca J., Dogan E., Karaman I., Segurado J., 2014. An inverse optimization strategy to determine single crystal mechanical behavior from polycrystal tests: Application to AZ31 Mg alloy. International Journal of Plasticity 57, 1-15.

Hill R., 1948. A theory of the yielding and plastic flow of anisotropic metals. Proceedings of the Royal Society of London A 193, 281-297.

Hill R., 1965. Continuum micro-mechanics of elastoplastic polycrystals. Journal of the Mechanics and Physics of Solids 13, 89-101.

Hiura F., 2010. Latent Hardening in Pure Magnesium Single Crystals, M.S. Thesis, McMaster University.

Hong S.G., Park S.H., Lee C.S., 2010a. Role of {10-12} twinning characteristics in the deformation behavior of a polycrystalline magnesium alloy. Acta Materialia 58, 5873-5885.

Hong S.G., Park S.H., Lee C.S., 2010b. Enhancing the fatigue property of rolled AZ31 magnesium alloy by controlling {10-12} twinning-detwinning characteristics. Journal of Materials Research 25, 784-792.

Hosford W.F., 1993. The Mechanics of Crystal and Textured Polycrystals. New York: Oxford University Press.

Hosford W.F., 1966. Texture strengthening. Metals Engineering Quarterly 6, 13-19.

Hsu S.S., Cullity B.D., 1954. On the torsional deformation and recovery of single crystals. Transactions of AIME 200, 305-312.

Hutchinson B., Jain J., Barnett M.R., 2012. A minimum parameter approach to crystal plasticity modeling. Acta Materialia 60, 5391-5398.

Hutchinson J.W., 1976. Bounds and self-consistent estimates for creep of polycrystalline materials. Proceedings of the Royal Society of London A348, 101-127.

Ito K., 2001. Atomistic study of non-Schmid effects in the plastic yielding of bcc metals. Philosophical Magazine A, 2001, 81, 1387-1407.

Jager A., Ostapovets A., Molnar P., Lejcek P., 2011. {10-12}-{10-12} double twinning in magnesium. Philosophical Magazine Letters 91, 537-544.

Jain A., Agnew S.R., 2007. Modeling the temperature dependent effect of twinning on the behavior of magnesium alloy AZ31B sheet. Materials Science and Engineering A 462, 29-36.

Jain A., Brown D.W., Agnew S.R., Clausen B., 2007. Twinning and Detwinning Cyclic Deformation of Mg Alloy AZ31B. Materials Science Forum 539-543, 3407-3413.

Jain J., Zhou J., Sinclair C.W., Poole W.J., 2011. Double tensile twinning in a Mg-8Al-0.5Zn alloy. Journal of Microscopy 242, 26-36.

Jain J., Poole W.J., Sinclair C.W., 2012. The deformation behaviour of the magnesium alloy AZ80 at 77 and 293 K. Materials Science and Engineering A 547, 128-137.

Jiang L., Jonas J.J., Mishra R.K., Luo A.A., Sachdev A.K., Godet S., 2007. Twinning and texture development in two Mg alloys subjected to loading along three different strain paths. Acta Materialia 55, 3899-3910.

Juan P.-A., Berbenni S., Barnett M.R., Tomé C.N., Capolungo L. 2014. A double inclusion homogenization scheme for polycrystals with hierarchal topologies: application to twinning in Mg alloys, International Journal of Plasticity 60, 182-196.

Kabirian F , Khan A.S., Gnäupel-Herlod T., 2015. Visco-plastic modeling of mechanical responses and texture evolution in extruded AZ31 magnesium alloy for various loading conditions. International Journal of Plasticity 68, 1-20.

Kalidindi S.R., 1998. Incorporation of deformation twinning in crystal plasticity models. Journal of the Mechanics and Physics of Solids 46, 267-290.

Kanjarla A.K., Van Houtte P., Delannay L., 2010. Assessment of plastic heterogeneity in grain interaction models using crystal plasticity finite element method. International Journal of Plasticity 26, 1220-1233.

Kapoor R., Sarkar A., Singh J., Samajdar I., Raabe D., 2014. Effect of strain rate on twinning in a Zr alloy. Scripta Materialia 74, 72-75.

Keskar N., Mukherjee S., Mani Krishna K.V., Srivastava D., Dey G.K., Pant P., Doherty R.D., Samajdar I., 2014. Quantifying the mesoscopic shear strains in plane strain compressed polycrystalline zirconium. Acta Materialia 69, 266-274.

Kim J.H., Kim D., Lee Y.S., Lee M.G., Chung K., Kim H.Y., Wagoner R.H., 2013. A temperature-dependent elasto-plastic constitutive model for magnesium alloy AZ31sheets. International Journal of Plasticity 50, 66-93.

Kleiner S., Uggowitzer P.J., 2004. Mechanical anisotropy of extruded Mg-6% Al-1% Zn alloy. Materials Science and Engineering A 379, 258-263.

Knezevic M., Beyerlein I.J., Nizolek T., Mara N.A., Pollock T.M., 2013. Anomalous basal slip activity in zirconium under high-strain deformation. Materials Research Letters 1, 133-140.

Kocks U.F., Mecking H., 2003. Physics and phenomenology of strain hardening: the FCC case. Progress in Materials Science 48,171-273.

Kok S., Beaudoin A.J., Tortorelli D.A., 2002. A polycrystal plasticity model based on the mechanical threshold. International Journal of Plasticity 18, 715-741.

Koike J., Kobayashi T., Mukai T., Watanabe H., Suzuki M., Maruyama K., Higashi K., 2003. The activity of non-basal slip systems and dynamic recovery at room temperature in fine-grained AZ31B magnesium alloys. Acta Materialia 51, 2055-2065.

Koike J., Ohyama R., 2005. Geometrical criterion for the activation of prismatic slip in AZ61 Mg alloy sheets deformed at room temperature. Acta Materialia 53, 1963-1972.

Kouddane R., Molinari A., Canova G.R., 1993. Self-consistent modeling of heterogeneous viscoelastici and elastic-viscoplastic materials. In: Teodosiu, C., Raphanel, J.L., Sidoroff, F. (Eds), Large Plastic Deformations, Fundamentals and Applications to Metal Forming. Balkerma, Rotterdam, The Netherlands, pp. 121-141.

Kroner E., 1958. Berechnug der elastischen konstanten des vielkristalls aus den konstanten des einnkristalls. Zeitschrift Fur Physik 151, 504-518.

Kubota K., Mabuchi M., Higashi K., 1999. Processing and mechanical properties of fine-grained magnesium alloys. Journal of Materials Science 34, 2255-2262.

Kulekci M.K., 2008. Magnesium and its alloys applications in automotive industry. The international Journal of Advanced Manufacturing Technology 39, 851-865.

Kumar N. , Choudhuri D. , Banerjee R. , Mishra R.S. , 2015. Strength and ductility optimization of Mg–Y–Nd–Zr alloy by microstructural design. Internation Journal of Plasticity 68, 77-97.

Lamark T.T., Chmelik F., Estrin Y., Lukac P., 2004. Cyclic deformation of a magnesium alloy investigated by the acoustic emission technique. Journal of Alloys and Compounds 378, 202–206.

Lavrentev F.F., Pokhil Yu.A., 1975. Relation of dislocation density in different slip systems to work hardening parameters for magnesium crystals. Materials Science and Engineering 18, 261-270.

Lebensohn R.A., Tomé C.N., 1993. A Self-Consistent Anisotropic Approach for the Simulation of Plastic-Deformation and Texture Development of Polycrystals - Application to Zirconium Alloys. Acta Metallurgica et Materialia 41, 2611-2624.

Lebensohn R.A., González M.I., Tomé C.N., Pochettino A.A., 1996. Measurement and prediction of texture development during a rolling sequence of Zircaloy-4 tubes. Journal of Nuclear Materials 229, 57-64.

Lebensohn R.A., Tomé C.N., Maudlin P.J., 2004. A selfconsistent formulation for the prediction of the anisotropic behavior of viscoplastic polycrystals with voids. Journal of the Mechanics and Physics of Solids 52, 249-278.

Lebensohn R.A., Tomé C.N., Castaneda P.P., 2007. Self-consistent modelling of the mechanical behaviour of viscoplastic polycrystals incorporating intragranular field fluctuations. Philosophical Magazine 87, 4287-4322.

Lee K.W , Kim S.K , Kim K.T , Hong S.I , 2001. Ductility and strain rate sensitivity of Zircaloy-4 nuclear fuel claddings. Journal of Nuclear Materials 295, 21-26.

Lee M.G., Wagoner R.H., Lee J.K., Chung K., Kim H.Y., 2008. Constitutive modeling for anisotropic/asymmetric hardening behavior of magnesium alloy sheets. International Journal of Plasticity 24, 545-582.

Lee S.Y., Wang H., Gharghouri M.A., Nayyeri G., Woo Wu., Shin E., Wu P.D., Poole W.J., Wu W., An K., 2014. Deformation behavior of solid-solution-strengthened Mg-9 wt.% Al alloy: In situ neutron diffraction and elastic-viscoplastic self-consistent modeling. Acta Materialia 73, 139-148.

Levesque J., Inak K., Neale K.W., Mishra R.K., 2010. Numerical modeling of formability of extruded magnesium alloy tubes. International Journal of Plasticity 26, 65-83.

Li H., Sun G., Woo W., Gong J., Chen B., Wang Y., Fu Y.Q., Huang C., Xie L., Peng S., 2014. Tensile deformation behaviors of Zircaloy-4 alloy at ambient and elevated temperatures: In situ neutron diffraction and simulation study. Journal of Nuclear Materials 446, 134-141.

Li J., Weng G.J., 1997. A secant-viscosity approach to the time-dependent creep of an elastic-viscoplastic composite. Journal of the Mechanics and Physics of Solids 45, 1069-1083.

Li J., Weng G.J., 1998a. A unified approach from elasticity to viscoelasticity to viscoplasticity of particle-reinforced solids. International Journal of Plasticity 14, 193-208.

Li J., Weng G.J., 1998b. Time-dependent creep of a dual-phase viscoplastic material with lamellar structure. International Journal of Plasticity 14, 755-770.

Li M., 2006. Constitutive Modeling of Slip, Twinning, and Untwining in AZ31B Magnesium. Ph.D. Thesis, Ohio State University, USA.

Li M., Lou X.Y., Kim J.H., Wagoner R.H., 2010. An efficient constitutive model for room-temperature, low-rate plasticity of annealed Mg AZ31B sheet. International Journal of Plasticity 26, 820-858.

Liu Y., Xie Z.L., 2003. Twinning and detwinning of <011> type II twin in shape memory alloy. Acta Materialia, 51, 5529-5543.

Livescu V., Cady C.M., Ceretta E.K., Henrie B.L., Gray G.T., 2006. The high strain rate deformation behavior of high purity magnesium and AZ31B magnesium alloy. Magesium Technology, Eds. Luo A.A., Neelameggham N. and Beals R. (TMS: Warrendale, PA), 153-158.

Lim H., Carroll J.D., Battaile C.C., Buchheit T.E., Boyce B.L., Weinberger C.R., 2014. Grain-scale experimental validation of crystal plasticity finite element simulations of tantalum oligocrystals. International Journal of Plasticity 60, 1-18.

Lou X.Y., Li M., Boger R.K., Agnew S.R., Wagoner R.H., 2007. Hardening evolution of AZ31B Mg sheet, International Journal of Plasticity 23, 44-86.

Lu Y., Gharghouri M.A., Taheri F., 2008. Effect of Texture on Acoustic Emission Produced by Slip and Twinning in AZ31B Magnesium Alloy-Part I: Experimental. Nondestructive Testing And Evaluation 23, 141-161.

Mathewson C.H., Phillips A.J., 1928. Twinning in beryllium, magnesium, zinc and cadmium. Proceedings of the Institute Of Metals Division - AIME 78.

Mayama T., Aizawa K., Tadano Y., Kuroda M., 2009. Influence of twinning deformation and lattice rotation on strength differential effect in polycrystalline pure magnesium with rolling texture. Computational Materials Science 47, 448-455.

MacEwen S. R., Faber J., Turner A.P.L., 1983. The use of time-of-flight neutron-diffraction to study grain interaction stresses. Acta Metallurgica 31, 657-676.

MacEwen S.R., Tomé C.N., Faber J., 1989. Residual stresses in annealed zircaloy. Acta Metallurgica 37, 979-989.

Mareau C., Daymond M.R., 2010. Study of internal strain evolution in Zicaloy-2 using polycrystalline models: Comparison between a rate-dependent and a rate-independent formulation. Acta Materialia 58, 3313-3325.

Martin J.L., Reed-Hill R.E., 1964. A study of basal slip kink bands in polycrystalline zirconium. Transactions of the Metallurgical Society of AIME 230, 780-785.

Masson R., Bornert M., Suquet P, and Zaoui A., 2000. An affine formulation for the prediction of the effective properties of nonlinear composites and polycrystals. Journal of the Mechanics and Physics of Solids 48, 1203-1227.

Mathis K., Csiszar G., Capek J., Gubicza J., Clausen B., Lukas P., Vinogradov A., Agnew S.R., 2015. Effect of the loading mode on the evolution of the deformation mechanisms in randomly textured magnesium polycrystals – Comparison of experimental and modeling results. International Journal of Plasticity 72,127-150.

McDowell D. 2008. Viscoplasticity of heterogeneous metallic materials, Materials Science and Engineering: R: Reports 62, 67-123.

Mercier S., Molinari A., 2009. Homogenization of elastic-viscoplastic heterogeneous materials: Self-consistent and Mori-Tanaka schemes. International Journal of Plasticity 25, 1024-1048.

Miura S., 2004. Unpublished research. Hokkaido University, Hokkaido, Japan.

Miyazaki S., Otsuka K., Wayman C.M., 1989a. The shape memory mechanism associated with the martensitic transformation in Ti Ni alloys--I. Self-accommodation. Acta Metallurgica 37, 1873-1884.

Miyazaki S., Otsuka K., Wayman C.M., 1989b. The shape memory mechanism associated with the martensitic transformation in Ti Ni alloys--II. Variant coalescence and shape recovery.Acta Metallurgica 37, 1885-1890.

Molinari A., Ahzi S., Kouddane R., 1997. On the self-consistent modeling of elastic-plastic behavior of polycrystals. Mechanics of Materials 26, 43-62.

Molinari A., Canova G.R., Ahzi S., 1987. A self-consistent approach of the large deformation polycrystal viscoplasticity. Acta Metallurgica 35, 2983-2994.

Molinari A., Toth L.S., 1994. Tuning a self-consistent viscoplastic model by finite-element results .1. modeling. Acta Metallurgica Et Materialia 42, 2453-2458.

Mordike B.L., Ebert T., 2001. Magnesium- Properties- applications- potential. Materials Science and Engineering A 302, 37-45.

Morrow B.M., McCabe R.J., Cerreta E.K., Tome C.N., 2014a. In-situ TEM observation of twinning and detwinning during cyclic loading in Mg. Materials Transactions A 45, 36-40.

Morrow B.M., McCabe R.J., Cerreta E.K., Tomé C.N., 2014b. Observations of the atomic structure of tensile and compressive twin boundaries and twin–twin interactions in Zirconium. Metallurgical and Materials Transactions A 45A, 5891-5897.

Mozzani N., Auzoux Q., Le Boulch D., Andrieu E., Blanc C., Scott C.P., Barnel N., 2014. Mechanical behavior of recrystallized Zircaloy-4 under monotonic loading at room temperature: Tests and simplified anisotropic modeling. Journal of Nuclear Materials 447, 94-106.

Mu S., Tang F., Gottstein G., 2014. A cluster-type grain interaction deformation texture model accounting for twinning-induced texture and strain-hardening evolution: Application to magnesium alloys. Acta Materialia 68, 310-324.

Muhammad W., Mohammadi M., Kang J., Mishra R.K., Inal K., 2015. An elasto-plastic constitutive model for evolving asymmetric/anisotropic hardening behavior of AZ31B and ZEK100 magnesium alloy sheets considering monotonic and reverse loading paths. International Journal of Plasticity 70, 30-59.

Mukai T., Yamanoi M., Watanabe H., Higashi K., 2001. Ductility enhancement in AZ31 magnesium alloy by controlling its grain structure. Scripta Materialia 45, 89-94.

Muránsky O., Carr D.G., Barnett M.R., Oliver E.C., Sittner P., 2008. Investigation of deformation mechanisms involved in the plasticity of AZ31 Mg alloy: In situ neutron diffraction and EPSC modelling. Materials Science and Engineering A 496, 14-24.

Muránsky O., Carr D.G., Sittner P., Oliver E.C., 2009. In situ neutron diffraction investigation of deformation twinning and pseudoelastic-like behavior of extruded AZ31 magnesium alloy. International Journal of Plasticity 25, 1107-1127.

Muránsky O., Barnett M.R., Carr D.G., Vogel S.C., Oliver E.C., 2010a. Investigation of deformation twinning in a fine-grained and coarse-grained ZM20 Mg alloy: Combined in situ neutron diffraction and acoustic emission. Acta Materialia 58, 1503-1517.

Muránsky O., Barnett M.R., Luzin V., Vogel S.C., 2010b. On the correlation between deformation twinning and Luders-like deformation in an extruded Mg alloy: in situ neutron diffraction and EPSC.4 modelling. Materials science and Engineering A 527, 1383-1394.

Muránsky O., Daymond M.R., Bhattacharyya D., Zanellato O., Vogel S.C., Edwards L., 2014. Load partitioning and evidence of deformation twinning in dual-phase fine-grained Zr-2.5%Nb alloy. Materials science and Engineering A564, 548-558.

Murty K.L., Charit I., 2006. Texture development and anisotropic deformation of zircaloys. Progress in Nuclear Energy 48, 325-359.

Neil C.J., Agnew S.R., 2009. Crystal plasticity-based forming limit prediction for non-cubic metals: application to Mg alloy AZ31B. International Journal of Plasticity 25, 379-398.

Neil C.J., Wollmershauser J.A., Clausen B., Tomé C.N., Agnew S.R., 2010. Modeling lattice strain evolution at finite strains and experimental verification for copper and stainless steel using in situ neutron diffraction. International Journal of Plasticity 26, 1772-1791.

Nemat-Nasser S., Obata M., 1986. Rate-dependent, finite elastoplastic deformation of polycrystals. Proceedings of the Royal Society of London A 407, 343-375.

Nguyen N.T., Lee M.G., Kim J.H., Kim H.Y., 2013. A practical constitutive model for AZ31B Mg alloy sheets with unusual stress strain response. Finite Elements in Analysis and Design 76, 39-49.

Niezgoda S.R., Kanjarla A.K., Beyerlein I.J., Tomé C.N., 2014. Stochastic modeling of twin nucleation in polycrystals: An application in hexagonal close-packed metals. International Journal of Plasticity 56, 119-138.

Niewczas M., 2010. Lattice correspondence during twinning in hexagonal close-packed crystals. Acta Materialia 58, 5848-5857.

Northwood D.O. , London I.M. , Bähen L.E., 1975. Elastic constants of zirconium alloys. Journal of Nuclear Materials 55, 299-310.

Nomura N., 2015. Zirconium Alloys for orthopedic applications. Advances in Metallic Biomaterials, Springer, 3, 215-221.

Numakura H., Minonushi Y., Koiwa M.,1991. 〈11-23〉 {10-11} slip in zirconium, Philosophical Magazine A 63, 1077-1084.

Obreimov V., Startsev V.I., 1959. Work of formation of an elastic twin in calcite. Soviet Physics-JETP 35, 743-748.

Oliver E.C., Daymond M.R., Withers P.J., 2004. Interphase and intergranular stress generation in carbon steels. Acta Materialia 52, 1937-1951.

Oppedal A.L., El Kadiri H., Tomé C.N., Kaschner G.C., Vogel S.C., Baird J.C., Horstemeyer M.F., 2012. Effect of dislocation transmutation on modeling hardening mechanisms by twinning in magnesium. International Journal of Plasticity 30-31, 41-61.

Oppedal A. L., El Kadiri H., Tomé C.N., Vogel S.C., Horstemeyer M., 2013. Anisotropy in Hexagonal Close-packed Structures: Improvements to Crystal Plasticity Approaches Applied to Magnesium Alloy. Philosophical Magazine 9, 4311-4330.

Padilla H.A., Lambros J., Beaudoin A.J., Robertson I.M., 2012. Relating inhomogeneous deformation to local texture in zirconium through grain-scale digital image correlation strain mapping experiments. International Journal of Solids and Structures 49, 18-31.

Partridge P.G., 1965. Cyclic twinning in fatigued close-packed hexagonal metals. Philosophical Magazine 12, 1043-1054.

Partridge P.G., 1967. The crystallography and deformation modes of hexagonal close packed metals. Metallurgical Reviews 12, 169-194.

Philippe M.J., Wagner F., Esling C., 1988. Proceedings of the 8th International Conference on Textures of Material (ICOTOM-8), The Metallurgical Society, p. 837.

Plunkett B., Cazacu O., Barlat F., 2008. Orthotropic yield criteria for description of the anisotropy in tension and compression of sheet metals. International Journal of Plasticity 24, 847-866.

Proust G., Tomé C.N., Kaschner G.C., 2007. Modeling texture, twinning and hardening evolution during deformation of hexagonal materials. Acta Materialia 55, 2137-2148.

Proust G., Tomé C.N., Jain A., Agnew S.R., 2009. Modeling the effect of twinning and detwinning during strain-path changes of magnesium alloy AZ31. International Journal of Plasticity 25, 861-880.

Proust G., Kaschner G.C., Beyerlein I.J., Clausen B., Brown D.W., McCabe R.J., Tomé, C.N., 2010. Detwinning of high-purity zirconium: in-situ neutron diffraction experiments. Experimental Mechanics 50,125-133.

Qiao H., Agnew S.R., Wu P.D., 2015b. Modeling twinning and detwinning behavior of Mg alloy ZK60A during monotonic and cyclic loading. International Journal of Plasticity 65, 61-84.

Qiao H., Wu P.D., Gharghouri M.A., Daymond M.R., 2015a. Evaluation of elastic-viscoplastic self-consistent polycrystal plasticity models for zirconium alloys. International Journal of Solids and Structures 71, 308-322.

Rampton T. Khosravani A., Fullwood D., Miles M., Mishra R.K., 2012. Twin Prediction in AZ31 Via Machine Learning Applied To EBSD Data, Presented at the 9th International Conference on Magnesium Alloys and their Applications in Vancouver, B.C., Canada.

Rapperport E.J., Hartley C.S., 1960. Deformation modes of zirconium at 77, 575, and 1075 K. Transactions of the Metallurgical Society of AIME 218, 869-876.

Reed-Hill R.E., Robertson W.D., 1957a. Addtional modes of deformation twinning in magensium. Acta Metallurgica 5, 717-727.

Reed-Hill R.E., Robertson W.D., 1957b. Deformation of magnesium single crystals by nonbasal slip. Transactions of AIME 209, 496-502.

Robson J.D., Stanford N., Barnett M.R., 2011. Effect of precipitate shape on slip and twinning in magnesium alloys. Acta Materialia 59, 1945-1956.

Robson J.D., Stanford N., Barnett M.R., 2013. Effect of Precipitate Shape and Habit on Mechanical Asymmetry in Magnesium Alloys. Metallurgical and Materials Transactions A 44, 2984-2995.

Rosalie J.M., Somekawa H., Singh A., Mukai T., 2012. The effect of size and distribution of rod-shaped β_1' precipitates on the strength and ductility of a Mg–Zn alloy, Materials Science and Engineering A 539, 230-237.

Rosalie J.M., Pauw B.R., 2014. Form-free size distributions from complementary stereological TEM/SAXS on precipitates in a Mg-Zn alloy. Acta Materialia 66, 150-162.

Sachs G., 1928. Plasticity problems in metals. Zeitschrift Verein Deutcher Ingenieur 72, 734-736.

Sandlöbes S. , Pei Z. , Friák M. , Zhu L.F. , Wang F. , Zaefferer S., Raabe D., Neugebauer J., 2014. Ductility improvement of Mg alloys by solid solution: Ab initio modeling, synthesis and mechanical properties. Acta Materialia 70, 92-104.

Sarkar A., Boopathy K., Eapen J., Murty K.L., 2014. Creep Behavior of Hydrogenated Zirconium Alloys. Journal of Materials Engineering and Performance 23, 3649-3656.

Sarker D, Chen D.L., 2014. Dependence of compressive deformation on pre-strain and loading direction in an extruded magnesium alloy: Texture, twinning and de-twinning. Materials Science and Engineering A 596, 134-144.

Sattari M., Holt R.A., Daymond M.R., 2014. Variant selection and transformation texture in zirconium alloy Excel. Journal of Nuclear Materials 453, 120-123.

Schmid E., 1931. Beitrage zur physik und metallographie des magnesium. Zeitschrift fur Elektrochemie 37, 447-459.

Segurado J., Lebensohn R.A., LLorca J., Tomé C. N., 2012. Multiscale modeling of plasticity based on embedding the viscoplastic self-consistent formulation in implicit finite elements. International Journal of Plasticity 28, 124-140.

Simmons G., Wang H., 1971. Single crystal elastic constants and calculated polycrystal properties MIT Press.

Stanford N., Barnett M.R., 2009. Effect of particles on the formation of deformation twins in a magnesium-based alloy. Materials Science and Engineering A 516, 226-234.

Stanford N., Barnett M.R., 2013. Solute strengthening of prismatic slip, basal slip and {10-12} twinning in Mg and Mg–Zn binary alloys. International Journal of Plasticity 47, 165-181.

Staroselsky A., Anand L., 1998. Inelastic Deformation of F.C.C. Materials by Slip and Twinning. Journal of the Mechanics and Physics of Solids 46, 671-696.

Staroselsky A.., 1998. Crystal plasticity due to slip and twinning, in: Mechanical Engineering, Ph.D Thesis, Massachusetts Institute of Technology, Cambridge, MA.

Steglich D. , Jeong Y. , Andar M.O. , Kuwabara T., 2012. Biaxial deformation behaviour of AZ31 magnesium alloy: Crystal-plasticity-based prediction and experimental validation. International Journal of Solids and Structures 49, 3551-3561.

Straumal B.B. , Gornakova A.S. , Mazilkin A.A. , Fabrichnaya O.B. , Kriegel M.J. , Baretzky B. , Jiang J.Z., Dobatkin S.V. , 2012. Phase transformations in the severely plastically deformed Zr–Nb alloys. Material Letters 81, 225-228.

Styczynski A., Hartig C., Bohlen J., Letzig D., 2004. Cold rolling textures in AZ31 wrought magnesium alloy. Scripta Materialia 50, 943-947.

Taylor G.I., 1938. Plastic strain in metals. Journal Institute of Metals 62, 307-324.

Tenckhoff E., 1988. Deformation Mechanisms, Texture and Anisotropy in Zirconium and Zircaloy, ASTM STP 966. American Society for Testing and Materials. Philadelphia.

Thompson N., Millard D.J., 1952. Twin formation, in cadmium. Philosophical Magazine 43, 422-440.

Tomé C.N., Lebensohn R.A., Kocks U.K., 1991. A model for texture development dominated by deformation twinning-application to zirconium alloys. Acta Metallurgica Et Materialia 39, 2667-2680.

Tomé C. N., Canova G. R., Kocks U. F., Christodoulou N., Jonas J. J., 1984. The relation between macroscopic and microscopic strain-hardening in FCC polycrystals. Acta Metallurgica 32, 1637-1653.

Tomé C.N., 1999. Self-consistent polycrystal models: a directional compliance criterion to describe grain interactions. Modelling and Simulation in Materials Science and Engineering 7, 723-738.

Tomé C.N., Maudlin P.J., Lebensohn R.A., Kaschner G.C., 2001. Mechanical response of Zirconium-I. Derivation of a polycrystal constitutive law and finite element analysis. Acta Materialia 49, 3085-3096.

Tomé C.N., 2007. Program Pole (version 8a), Los Alamos National Laboratory.

Tomlinson P., Azizi-Alizamini H., Poole W.J., Sinclair C.W., Gharghouri M.A., 2013. Biaxial deformation of the magnesium alloy AZ80. Metallurgical and Materials Transactions 44A, 2970-2983.

Trivedi P, Goel S, Das S, Jayaganthan R., Lahiri D., Roy P., 2015. Biocompatibility of ultrafine grained zircaloy-2 produced by cryorolling for medical applications. Materials Science and Engineering C 46, 309-315.

Tucker M.T., Horstemeyer M., Gullett P., El Kadiri H., Whittington W.R., 2009. Anisotropic Effects on the Strain Rate Dependence of a Wrought Magnesium Alloy. Scripta Materialia 60, 182-185.

Turner P.A., Tomé C.N., Woo C.H., 1994. Self-consistent modelling of nonlinear visco-elastic polycrystals: an approximate scheme. Philosophical Magazine A 70, 689-711.

Turner P. A., Tomé C.N., 1994. A study of residual-stresses in Zircaloy-2 with rod texture. Acta Metallurgica Et Materialia 42, 4143-4153.

Turner P. A., Christodoulou N., Tomé C. N., 1995. Modeling the mechanical response of rolled zircaloy-2. International journal of plasticity 11, 251-265.

Ulacia I., Salisbury C.P., Hurtado I., Worswick M.J., 2011. Tensile characterization and constitutive modeling of AZ31B magnesium alloy sheet over wide range of strain rates and temperatures. Journal of Materials Processing Technology 211, 830-839.

Van Houtte P., 1978. Simulation of the rolling and shear texture of Brass by the Taylor theory adapted for mechanical twinning. Acta Metallurgica 36, 591-604.

Venables J.A., 1964. In: Reed-Hill RE, Hirth JP, Rogers HC, editors. Deformation twinning. New York: Gordon & Breach, p.77.

Vitek V., Mroveca M., Bassani J.L., 2004. Influence of non-glide stresses on plastic flow: fromatomistic to continuum modeling. Materials Science and Engineering A365 , 31-37.

Ward-Flynn P., Mote J., Dorn J.E., 1961. On the thermally activated mechanism of prismatic slip in magnesium single crystals. Transactions of the Metallurgical Society of AIME 221, 1148-1154.

Wang H., Wu P. D., Tomé C. N., Huang Y., 2010a. A finite strain elastic-viscoplastic self-consistent model for polycrystalline materials. Journal of the Mechanics and Physics of Solids 58, 594-612.

Wang H., Raeisinia B., Wu P. D., Agnew S. R., Tomé C. N., 2010b. Evaluation of self-consistent crystal plasticity models for magnesium alloy AZ31B sheet. International Journal of Solids and Structures 47, 2905-2917.

Wang H., Wu P. D., Gharghouri M. A., 2010c. Effects of basal texture on mechanical behaviour of magnesium alloy AZ31B sheet. Materials Science and Engineering A527, 3588-3594.

Wang H, Wu Y., Wu P.D., Neale K.W., 2010d. Numerical analysis of large strain simple shear and fixed-end torsion of HCP polycrystals. CMC-Computers, Materials & Continua 19, 255-284.

Wang H., Wu P. D., Boyle K. P., Neale K.W., 2011. On crystal plasticity formability analysis for magnesium alloy sheets. International Journal of Solids and Structures 48, 1000-1010.

Wang H., Wu P.D., Tomé C.N., Wang J., 2012a. Study of lattice strains in magnesium alloy AZ31 based on a large strain elastic-viscoplastic self-consistent polycrystal model. International Journal of Solids and Structures 49, 2155-2167.

Wang H., Wu P.D., Tomé C. N., Wang J., 2012b. A constitutive model of twinning and detwinning for hexagonal close packed polycrystals. Material Science and Engineering A555, 93-98.

Wang H., Wu P.D., Wang J., Tomé C.N., 2013a. A physics-based crystal plasticity model for hexagonal close packed (HCP) crystals including both twinning and de-twinning mechanisms. International Journal of Plasticity 49, 36-52.

Wang H., Clausen B., Tomé C. N., Wu P.D., 2013b. Studying the effect of stress relaxation and creep on lattice strain evolution of stainless steel under tension. Acta Materialia 61, 1179-1188.

Wang H., Wu P.D., Wang J., 2013c. Modeling inelastic behavior of magnesium alloys during cyclic loading-unloading. International Journal of Plasticity 47, 49-64.

Wang, H., Wu, P.D., Wang, J., 2015. Modelling the role of slips and twins in magnesium alloys under cyclic shear. Computational Materials Science 96, 214-218.

Wollmershauser J.A., Clausen B., Agnew S.R., 2012. A slip system-based kinematic hardening model application to in-situ neutron diffraction of cyclic deformation of austenitic stainless steel. International Journal of Fatigue 36, 181-193.

Wu L., Agnew S.R., Brown D.W., Stoica G.M., Clausen B., Jain A., Fielden D.E., Liaw P.K., 2008a. Internal stress relaxation and load redistribution during the twinning-detwinning-dominated cyclic deformation of a wrought magnesium alloy, ZK60A. Acta Materialia 56, 3699-3707.

Wu L., Jain A., Brown D.W., Stoica G.M., Agnew S.R., Clausen B., Fielden D.E., Liaw P.K., 2008b. Twinning-detwinning behavior during the strain-controlled low-cycle fatigue testing of a wrought magnesium alloy, ZK60A. Acta Materialia 56, 688-695.

Wu L., 2009. Mechanical Behavior and the Role of Deformation Twinning in Wrought Magnesium Alloys Investigated Using Neutron and Synchrotron X-ray Diffraction. Ph.D Thesis, The University of Tennessee, Knoxville.

Wu L., Agnew S.R., Ren Y., Brown D.W., Clausen B., Stoica G.M., Wenk H.R., Liaw P.K., 2010. The effects of texture and extension twinning on the low-cycle fatigue behavior of a rolled magnesium alloy, AZ31B. Materials Science and Engineering A 527, 7057-7067.

Wu P.D., Lloyd D. J., 2004. Analysis of surface roughening in AA6111 automotive sheet. Acta Materialia 52, 1785-1798.

Wu P.D., Lloyd D. J., Jain M., Neale K.W., Huang Y., 2007. Effects of spatial grain orientation distribution and initial surface topography on sheet metal necking. International Journal of Plasticity 23, 1084-1104.

Wu P. D., MacEwen S. R., Lloyd D. J., Neale K. W., 2004. A mesoscopic approach for predicting sheet metal formability. Modelling and Simulation in Materials Science and Engineering 12, 511-527.

Wu P.D., Wang H., Neale K.W., 2012. On large strain torsion of HCP polycrystals. International Journal of Applied Mechanics 4, 1250024.

Wu P.D., Guo X.Q., Qiao H., Lloyd D.J., 2015. A constitutive model of twin nucleation, propagation and growth in magnesium crystals. Materials Science and Engineering A 625, 140-145.

Wu W , Lee SY, Paradowska AM, Gao Y, Liaw P.K., 2012. Twinning–detwinning behavior during fatigue-crack propagation in a wrought magnesium alloy AZ31B. Materials Science and Engineering A 556, 278-286.
Wu W., Qiao H., An K., Guo X.Q., Wu P.D., Liaw P.K., 2014. Investigation of deformation dynamics in a wrought magnesium alloy. International Journal of Plasticity 62, 105-120.

Xie Y.P., Wang Z.Y., Hou Z.F., 2013. The phase stability and elastic properties of MgZn2 and Mg4Zn7 in Mg–Zn alloys, Scripta Materialia 68, 495-498.

Xu F., 2007. Lattice strain and texture evolution during room-temperature deformation in Zircaloy-2. Ph.D thesis, Queen's University, Canada.

Xu F., Holt R.A., Daymond M.R., 2008a. Evidence for basal <a>-slip in Zircaloy-2 at room temperature from polycrystalline modeling. Journal of Nuclear Materials 373, 217-225.

Xu F., Holt R.A., Daymond M.R., 2008b. Modeling lattice strain evolution during uniaxial deformation of textured Zircaloy-2. Acta Materialia 56, 3672-3687.

Xu F., Holt R.A., Daymond M.R., Rogge R.B., Oliver E.C., 2008c. Development of internal strains in textured Zircaloy-2 during uniaxial deformation. Materials Science and Engineering: A 488, 172-185.

Xu F., Holt R.A., Daymond M.R., 2009. Modeling texture evolution during uniaxial deformation of Zircaloy-2. Journal of Nuclear Materials 394, 9-19.

Yapici G.G., Tomé C.N., Beyerlein I.J., Karaman I., Vogel S.C., Liu C., 2009. Plastic flow anisotropy of pure zirconium after severe plastic deformation at room temperature. Acta Materialia 57, 4855-4865.

Yoo M.H., 1981. Slip, twinning, and fracture in hexagonal close-packed metals. Metallurgical Transactions A 12, 409-418.

Yoon J.W., Barlat F., Chung K., 1998. Influence of initial back stress on the earing prediction of drawn cups for planar anisotropic aluminum sheets. Journal of Materials Processing Technology 80-81, 433-437.

Yu Q, Zhang J, Jiang Y., 2011. Direct observation of twinning–detwinning–retwinning on magnesium single crystal subjected to strain-controlled cyclic tension–compression in [0001] direction. Philosophical Magazine Letters 91, 757-765.

Yu Q, Zhang J, Jiang Y, Li Q, 2012. An experimental study on cyclic deformation and fatigue of extruded ZK60 magnesium alloy. International Journal of Fatigue 36, 47-58.

Yudin A.A., Ivanov V.I., 1985. Acoustic emission in plastic deformation of metals (review) Report 1. Strength of Materials 17, 842-851.

Zaimovskii A. S., 1978. Zirconium alloys in nuclear power. Soviet Atomic Energy 45, 1165-1168.

Zecevic M, Knezevic M., Beyerlein I.J., Tomé C.N., 2015. An elasto-plastic self-consistent model with hardening based on dislocation density, twinning and de-twinning: Application to strain path changes in HCP metals. Materials Science and Engineering A 638, 262-274.

Zhang J., Joshi S.P., 2012. Phenomenological Crystal Plasticity Modeling and Detailed Micromechanical Investigations of Pure Magnesium. Journal of the Mechanics and Physics of Solids 60, 945-972.

Zhang K., Holmedal B., Hopperstad O.S., Dumoulin S., Gawad J., Van Bael A., Van Houtte P., 2015. Multi-level modelling of mechanical anisotropy of commercial pure aluminium plate: Crystal plasticity models, advanced yield functions and parameter identification. International Journal of Plasticity 66, 3-30.

Zhang R.Y., Daymond M.R., Holt R.A., 2008. A finite element model of deformation twinning in zirconium. Materials Science and Engineering A 473, 139-146.